NASA
Reference
Publication
1219

November 1989

Introduction to Total- and Partial-Pressure Measurements in Vacuum Systems

R. A. Outlaw
and F. A. Kern

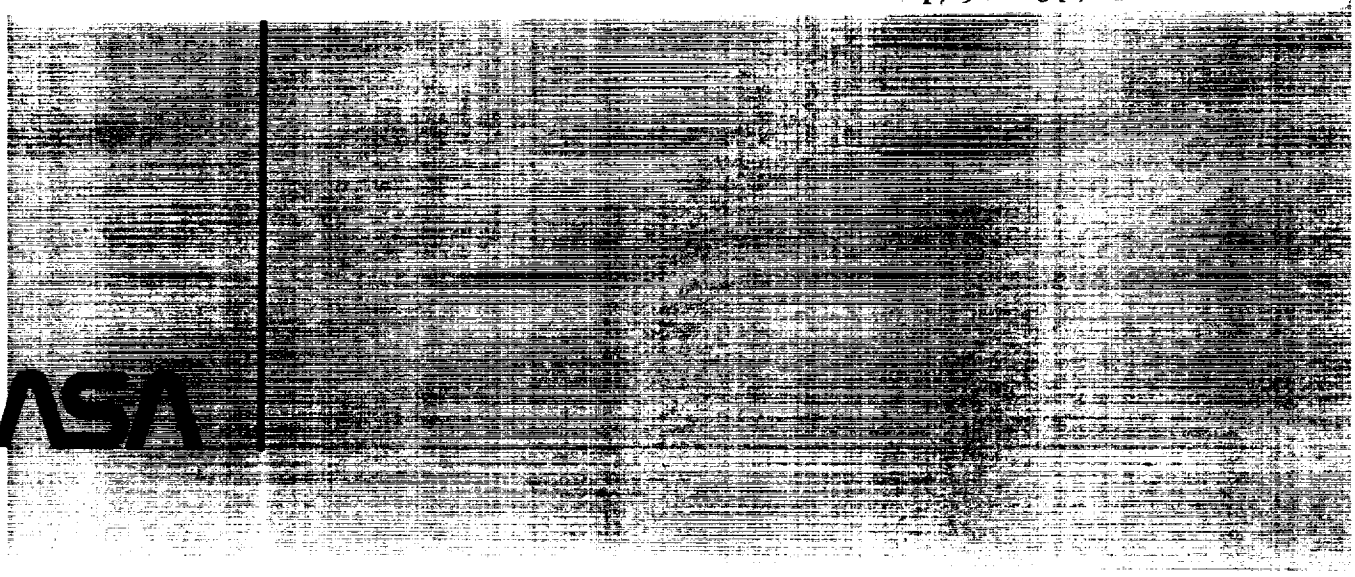

NASA

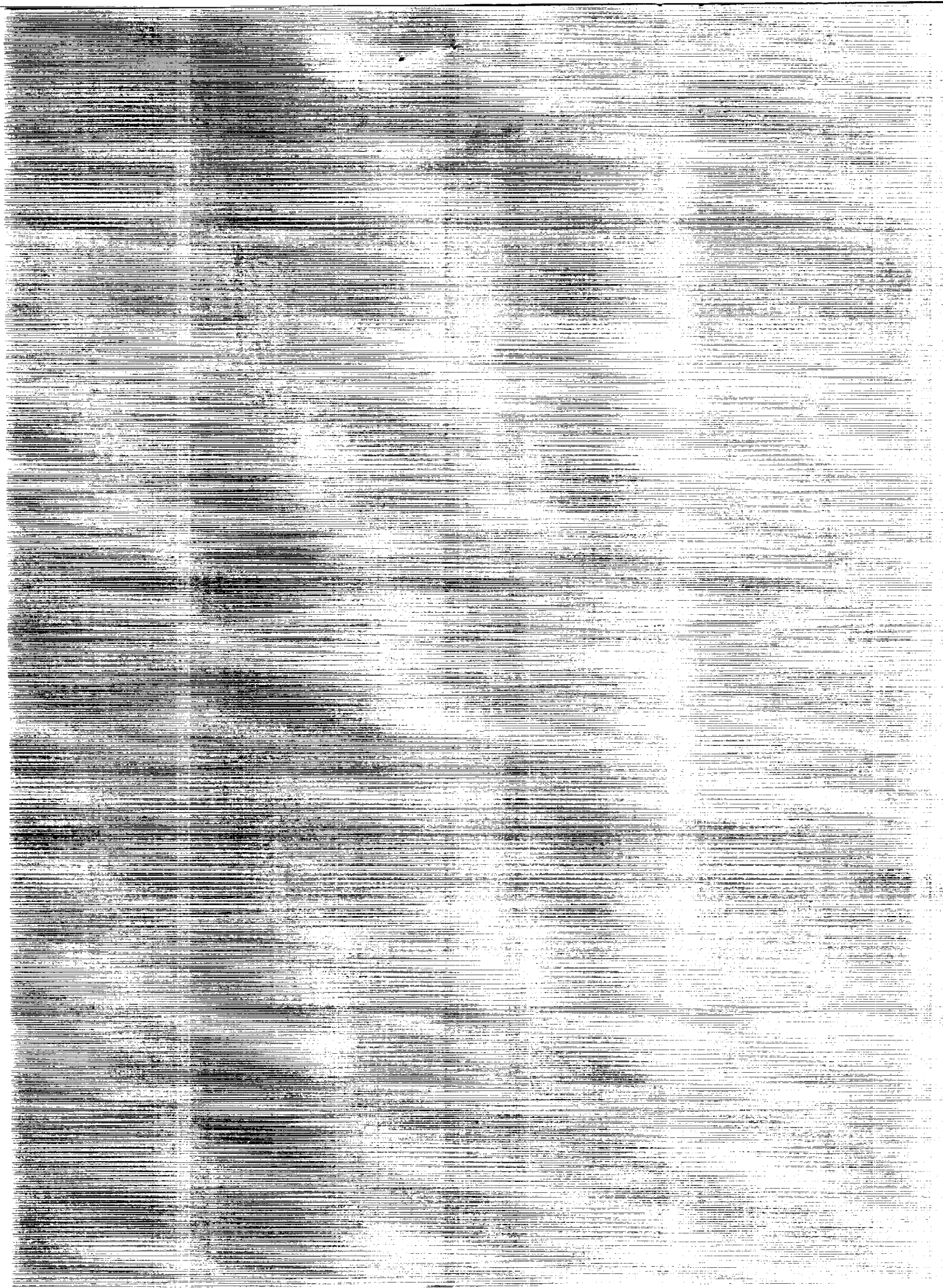

NASA Reference Publication 1219

1989

Introduction to Total- and Partial-Pressure Measurements in Vacuum Systems

R. A. Outlaw
and F. A. Kern
Langley Research Center
Hampton, Virginia

NASA
National Aeronautics and Space Administration
Office of Management
Scientific and Technical Information Division

Contents

Acknowledgment

The authors are very grateful to Dr. Leonard Beavis of Sandia National Laboratory for his many contributions to this manuscript.

Abstract

An introduction to the fundamentals of total- and partial-pressure measurement in the vacuum regime (760 to 10^{-16} torr (10^5 to 1.33×10^{-14} Pa)) is presented. The instruments most often used in scientific fields that require vacuum measurement are discussed, and special emphasis is placed on ionization-type gauges and quadrupole mass spectrometers. Some attention is also given to potential errors in measurement and to calibration techniques.

Introduction

History records that the first measurement of subatmospheric pressure was made by Robert Boyle, circa 1660. In 1654, Boyle modified the air pump that had been invented by Otto von Guericke and used it to evacuate the region above a mercury column (orricellian barometer) to study the characteristics of vacuum. The lowest pressure that he was able to study (ref. 1) was about 6 torr (8×10^2 Pa). Today, with the use of modern vacuum techniques, systems can be constructed which theoretically are capable of achieving 10^{-16} torr (1.33×10^{-14} Pa), which is only a few molecules per cm^3. While the measurement of such pressures is possible, it is primarily limited by the outgassing of the gauge materials. In a practical sense, however, most ultrahigh-vacuum systems used today have an ultimate pressure of about 10^{-11} torr (1.33×10^{-9} Pa), which is easily measured. The measurement of pressure has been and still is the most often used parameter to characterize a vacuum and to indicate the state of cleanliness of a given experimental system. Although mass spectrometers and surface diagnostics combined with pressure gauges are used to provide a much more thorough characterization of the system background level, the total pressure is still used as the main figure of merit.

Ideal-Gas Characteristics

The molecules of a gas can be considered hard rigid spheres with diameters on the order of 2×10^{-8} cm. At normal temperature and pressure (NTP is 20°C, 760 torr (10^5 Pa)), there are approximately 2.7×10^{19} molecules cm^{-3} at an average distance of 3×10^{-7} cm from each other. Their random velocities average about 4.7×10^4 $cm\text{-}sec^{-1}$ (N_2), and they collide each time they have traveled about 1000 diameters in a particular direction. The molecules also possess rotational and vibrational energies, and these energies are altered after each collision. The number of these collisions at NTP is about 10^{14} $cm^{-2}\text{-}sec^{-1}$.

Pressure p is defined simply as the normal (perpendicular) force F of a gas acting on a unit area A, or

$$p = \frac{F}{A} \tag{1}$$

In a molecular sense, this pressure is the force created by all the molecules colliding with a unit area in unit time. The total momentum exchange with the wall for a single molecule is $2mv_{xi}$, where m is its mass and v_{xi} is its perpendicular velocity. Assuming elastic collisions, the total number of molecules with v_{xi} going toward the wall is $n_i/2$, where n_i is the number per unit volume. In the vicinity of the wall, such molecules travel a distance of $v_{xi}\delta t$ in time δt without molecular collision. Thus, the number of molecules striking a unit area of the wall in time δt is $(1/2)n_i v_{xi} \times 2mv_{xi} = n_i m v_{xi}^2$. The total pressure of n molecules per unit volume requires summing over i for molecules of all values of v_x, or $p = nm\langle v_x^2 \rangle$.

Since $v^2 = v_x^2 + v_y^2 + v_z^2$, and since we average over all molecules, $\langle v^2 \rangle = \langle v_x^2 \rangle + \langle v_y^2 \rangle + \langle v_z^2 \rangle$; since all directions are equally probable, $\langle v_x^2 \rangle = \langle v_y^2 \rangle = \langle v_z^2 \rangle$, or $\langle v^2 \rangle = 3\langle v_x^2 \rangle$, and we have

$$p = (1/3)nm\langle v^2 \rangle \tag{2}$$

The average translational energy of a molecule can be written as $E = (1/2)m\langle v^2 \rangle$, which, by the equipartitioning of energy $(1/2)kT$ for each degree of freedom, is just $3/2kT$, where k is Boltzmann's constant and T is gas temperature. Thus,

$$m\langle v^2 \rangle = 3kT \tag{3}$$

Combining equation (3) with equation (2) gives a more recognizable form of the ideal gas law,

$$p = nkT = \frac{N}{\mathcal{V}}kT \tag{4}$$

where N is the total number of molecules in volume $\mathcal{V}$. Since Boltzmann's constant k is related to the gas constant R by $\frac{R}{k} = L_a$, where L_a is the Avogadro number, another form is

$$p = \left(\frac{N}{\mathcal{V}}\right)\frac{RT}{L_a} = \frac{\eta}{\mathcal{V}}RT \tag{5}$$

where η is the number of moles.

Although total pressure is the primary indicator of vacuum level, there are other parameters, such as the number density of the individual species that make up the pressure and the mean free path, the average distance a molecule travels before it has a collision. The number density is given by equation (4)

where

$$n = \frac{p}{kT} \tag{6}$$

and the mean-free path λ is given by

$$\lambda = \frac{kT}{\sqrt{2}(p\pi d^2)} \tag{7}$$

where d is the molecular diameter. A convenient approximation is

$$\lambda = \frac{5 \times 10^{-3}}{p} \tag{8}$$

where p is in torr and λ is in cm. At atmospheric pressure, there is a number density of 2.7×10^{19} molecules-cm^{-3}, and the molecules only travel about $\lambda = 6.6 \times 10^{-6}$ cm before a molecular collision occurs. As the pressure is lowered to around 1 torr (133 Pa), the number density decreases to 3.2×10^{16} molecules-cm^{-3} and $\lambda \approx 5 \times 10^{-3}$ cm. With further reduction to 10^{-3} torr (1.33×10^{-1} Pa), the number density decreases to 3.2×10^{13} molecules-cm^{-3}, and λ becomes about 5 cm, or begins to approach the size of the typical gauge envelope. Thus, the molecules are just as likely to hit the walls of the envelope as they are to colliding with each other. This change in collision characteristics represents the transition from viscous to molecular flow. Figure 1 is a plot of number density and mean-free path versus pressure. Note that λ is approaching 10^5 m when ultrahigh vacuum is attained.

Units

The units of pressure are consistent with the dimensional form

$$p = (m)(l)^{-1}(t)^{-2} \tag{9}$$

where m is the mass, l is the length, and t is the time. Table I gives a comparison and conversion factors for the pressure units most likely encountered in vacuum technology. Unfortunately, no single unit has been universally and exclusively adopted; therefore, one must become acquainted with several units to work comfortably in this field. Prior to the 1960's, most scientists, engineers, equipment manufacturers, and others in the field used mm of Hg as the basic pressure increment, but torr ultimately became the predominant unit (a comfortable conversion since 1 torr $\approx$ 1 mm of Hg). In 1954, the Conférence Générale des Poids et Mesures formally adopted the Systeme Internationale (SI) which is based on the MKSA system. Unfortunately, the pascal has not enjoyed much success as the primary unit, mainly because of tradition. As a result, many researchers in the United States have returned to the use of torr. Outside the U.S., the bar and submultiples, the millibar, and the microbar have become the most common units. As can be seen in table I, there is only a factor of 1.33 between torr and millibar, so in the future perhaps one of the two will be ultimately adopted to provide universal consistency. Another unit of pressure that should be mentioned is the micron (1 micron = 10^{-3} torr). Common practice is to express "roughing pump pressures" in this unit.

So that some degree of consistency can be maintained throughout this paper, the predominant unit presented is the torr. The unit of pascal is included in parentheses.

The span of many orders of magnitude of pressure can be characterized by generic labels which represent six ranges in increments of 10^3. Table II shows the specific ranges in units of Pa and torr. Often, one speaks of having a high-vacuum or ultrahigh-vacuum system. Note that ultrahigh vacuum is not achieved until the pressure is less than 7.5×10^{-10} torr (10^{-7} Pa).

Beginning with the 1950's and the revolution in vacuum technology, the measurement of pressure has undergone a tremendous development that has given rise to many instruments which span the pressure range from atmosphere to less than 10^{-16} torr (1.33×10^{-14} Pa). The following discussion represents an introductory treatment of this topic. Several excellent references exist which provide a much more thorough coverage and are highly recommended. (See refs. 2 through 5.)

Symbols

a, b	stability parameters
B	magnetic flux density ($\vec{B}$ used in figures)
m	mass
m/e	mass-to-charge ratio
p	pressure
t	time
U	dc voltage
V	RF voltage
$\mathcal{V}$	volume
v	velocity
y	peak height
Ω	resistance, ohms
ω	RF frequency

Total-Pressure Gauges

Reference Pressure Standards

Few pressure standards exist which are generally acceptable for vacuum calibration. Since pressure is force per unit area, a standard must measure this force directly. As the pressure decreases, it becomes more and more difficult to make a direct measurement of force. The small mechanical movement or stress which must be measured becomes subject to large perturbations by the environment of the gauge. Friction, hysteresis, nonelastic behavior, and cohesive and adhesive forces dominate measurements when pressures drop to about 10 to 100 torr (1.33×10^3 to 1.33×10^4 Pa).

A deadweight tester or rotating piston gauge is illustrated in figure 2 and is an example of a device which produces a very accurate pressure and is normally used as a reference standard. Lightweight, large-area, deadweight testers are capable of measuring pressures as low as 1 torr (133 Pa). A reference standard is the highest level measurement device in a laboratory that can provide traceability to national standards. A high vacuum is drawn on the upper chamber p_{HV}, and the weight, which has been accurately measured, is supported by the gas from the vacuum to be measured. To reduce the impact of friction, the weight is spun at several revolutions per minute. The gas flowing past the weight (tolerances are very close) into the high vacuum acts as a nearly frictionless bearing. Different pressure levels can be measured with the use of additional calibrated ring weights. The weight and rings are thus balanced according to

$$\frac{mg}{A} + p_{HV} = p \tag{10a}$$

where

A	area
g	acceleration due to gravity
m	mass
p	pressure

and since p_{HV} is small in comparison with $\frac{mg}{A}$, then

$$p \approx \frac{mg}{A} \tag{10b}$$

The other generally accepted standard for measuring low pressure is the U-tube manometer illustrated in figure 3. The working fluid in the U-tube manometer is normally mercury; however, mercury has toxicity problems so other fluids, such as low-vapor-pressure oils, are also used. The derivation of the archaic pressure-measurement terms "mm of Hg" and "micron of Hg" now becomes apparent (fig. 3(a)). When the left and right sides of the tube are at the same pressure ($p_L = p_R$), the heights are at the same level. If the right side of the manometer is reduced to a lower pressure (e.g., 160 torr (2.13×10^4 Pa)), the mercury column on that side is Δh mm higher than the mercury column on the left side, and a pressure difference exists which is capable of supporting that weight of mercury expressed as Δh in mm of Hg. The height of the column Δh times the density ρ of Hg times the acceleration due to gravity g plus the unknown pressure p must equal atmospheric pressure or

$$p_R + \rho g \Delta h = p_L \tag{11}$$

When measuring near the low-pressure limit of a U-tube manometer, the mercury column height differences are measured with a traveling telescope called a cathetometer. A cathetometer is capable of measuring height differences of 1 μm or less. The U-tubes must be uniform, exhibit identical wetting of the mercury, and not take any electrical charge for the most accurate measurements. Pressure as low as 10^{-2} torr (1.33 Pa) can be accurately measured in this fashion. Pressure that is an order of magnitude lower can be measured if the mercury column is replaced with one containing a uniform, low-density, low-vapor-pressure, organic fluid, such as dibutyl phthalate. Acoustic pulse reflections have been used to obtain an even more precise position of the manometer fluid surface.

The U-tube and deadweight tester are the only two instruments widely accepted as vacuum reference standards, although the McLeod gauge is sometimes considered to be a standard. Figures 4(a) and 4(b) illustrate the basic operation and parameters of a McLeod gauge. This gauge, which was invented in 1874, essentially uses the U-tube manometer and Boyle's law. Capillaries B and C act as the U-tube, and bulb A acts as the large volume from which the gas is compressed into the small-volume, closed capillary B. In figure 4(a), bulb A is in contact with the remainder of the vacuum system. The valve on the mercury reservoir is opened slowly to the atmosphere, and the mercury is forced up tube F. When the mercury reaches cutoff D, the volume associated with A and B is isolated from the vacuum system. Capillaries B and C must be identical and uniform in bore and inner-surface condition for the capillary depression in each to be the same during any measurement. As the mercury is allowed to continue to rise, the gas in $\mathcal{V}_A$ (volume of bulb A) and $\mathcal{V}_B$ (volume of capillary B) is compressed, and, as a

result of the smaller gas volume, the pressure must increase if the gas behaves ideally. The difference in levels of mercury in C and B is due to the difference in pressure over capillary C and the compressed gas in capillary B. (See fig. 4(b).) Application of Boyle's law relates the pressure in the vacuum system p_s by

$$p_s(\mathcal{V}_A + \mathcal{V}_B) = p'_B \mathcal{V}'_B \tag{12}$$

where

$\mathcal{V}'_B$	volume of closed capillary when mercury in capillary C is opposite the inner plug surface of capillary B
p'_B	pressure in closed capillary

Thus,

$$p_s = \frac{\pi \rho g d^2 h_c^2}{4(\mathcal{V}_A + \mathcal{V}_B) - h_c \pi d^2} \tag{13}$$

where ρ is the density of mercury (13.6 g/cm^3), h_c is the capillary height difference, d is the diameter of capillary B, and g is the acceleration due to gravity. McLeod gauges suffer from a number of difficulties. Such parameters as age of the gauge, exposure to contamination of various sources, and particularly, the Hg, glass charging, and gas entrainment in the mercury must be carefully managed to get accurate results from the McLeod gauge. Condensable vapors (e.g., mercury, water) will cause lower pressure readings in direct proportion to their partial pressure in the vacuum-system total gas pressure p_s to be measured.

In general, calibration is normally required for working gauges over their entire range of operation. The lower limits of standards discussed herein are 10^{-5} torr (1.33×10^{-3} Pa) for the best McLeod gauge, 10^{-3} torr (1.33×10^{-1} Pa) for the best U-tube manometer, and 1 torr (133 Pa) for the deadweight tester. Three procedures are normally used (although several others exist) for calibrations: volume expansion, linear pressure rise, and orifice flow. They are described in some detail in the section "Instrument Calibration."

Working Standards

Several instruments presently in use can be considered as working standards; that is, they are not directly traceable to basic principles, but have excellent measurement accuracy and repeatability. These instruments, after having been calibrated, can be used as convenient standards to which other gauges can be compared or calibrated.

One such instrument is the spinning-rotor gauge (SRG). (See refs. 6 and 7.) The concept for this gauge was introduced in the 1950's by Beams, but was perfected and marketed in the late 1970's. In figure 5, a cutaway shows the internal structure of the SRG. The steel spherical ball is magnetically levitated within the tube and then rotated to a frequency of about 400 Hz. At this point, the power that rotates the ball is removed and the ball is allowed to decelerate in the pressure environment by molecular drag. The ratio of change in angular velocity of a freely spinning rotor is proportional to the gas pressure and inversely proportional to the molecular velocity. The horizontal magnetic moment of the ball induces a voltage in the pickup coils which is applied to the digital counting circuitry and, as the ball decelerates, results in an increase in the interval counting time. The equation governing the frequency decrease is given by

$$\frac{-\dot{\omega}}{\omega} = \frac{\sigma_{\text{eff}} 10 \times p}{\pi a d \bar{c}} - \left(\frac{\dot{\omega}}{\omega}\right)_o \tag{14}$$

where

a	rotor-ball radius
$\bar{c}$	average molecular speed
d	density
o	initial condition
σ_{eff}	tangential momentum exchange coefficient
ω	angular frequency
$\dot{\omega}$	angular-frequency change

The value of σ_{eff} must be determined by calibration. The range of the SRG extends from 1 to 10^{-7} torr ($\approx$133 to 1.33×10^{-5} Pa). Although there are still some problems with the rotor-ball surface stability, over a 3-yr period, the repeatability of σ_{eff} was better than 1 percent. This exceptional repeatability provides a transfer standard capability with ionization gauges (and mass spectrometers) over 2 decades in pressure (10^{-5} to 10^{-7} torr (1.33×10^{-3} to 1.33×10^{-5} Pa)), and permits in situ calibration. This is an extremely useful capability where accurate high-vacuum and ultrahigh-vacuum measurements are required.

A second instrument which is more prevalent than the SRG and has been available for many years is the fused-quartz Bourdon tube. The pressure sensor is basically a fused-quartz tube in the shape of a helix with two wire-wound coils suspended from it in the configuration of a balance. (See fig. 6.) These coils are oriented in the field of permanent magnets which are anchored to the instrument body. The

unbalanced output of the coils is amplified and fed through the electromagnetic force-balancing coils, which establishes a torque equal and opposite to that caused by the pressure in the tube. This current is a measure of the applied vacuum. This instrument extends from 100 torr (1.33×10^4 Pa) full scale down to less than 10^{-2} torr (1.33 Pa) and has an accuracy of better than 10^{-2} torr (1.33 Pa) and a dynamic range of 10^5.

There are also several other instruments which come under the category of digital pressure transducers. This group includes different vibration elements such as diaphragms, cylinders, strings, tapes, and electronic oscillators employing inductive or capacitance sensors as part of a resonance circuit. One of the most popular instruments is the force-balance, quartz-pressure transducer, which employs a torque motor to restrain movement and gives fast response and negligible hysteresis. This instrument is useful from pressures exceeding 1 atm down to 4×10^{-2} torr (5.3 Pa). A second instrument of this type is the vibrating-cylinder pressure transducer. The inner cylinder of a concentric cylinder arrangement is a thin-wall, iron-nickel alloy which is actively excited by electromagnetic coils. The input pressure change produces a change in resonant frequency, and this change is detected by another set of pickup coils, whose amplified output drives the excitation coils. The resonant frequency of the cylinder varies directly with the mechanical stress exerted by the pressure differential across it. Although these instruments have an accuracy of ± 0.02 percent full scale, they are only able to measure an ultimate pressure of about 0.2 torr (26.6 Pa).

Direct-Force Instruments

All force-measuring gauges, including those described as standards in the previous sections, measure pressure directly and depend upon mechanical movement of a solid or liquid in their operation. Optical or electrical transducers of mechanical motion are capable of detecting movements as small as 1 Å (10^{-8} cm). The simplest diaphragm or Bourdon tube gauges depend upon displacement of an elastic material. The common wall barometer is an example of a simple-diaphragm gauge. Figures 7 and 8 are illustrations of simple Bourdon and diaphragm gauges. Many laboratory dial-type vacuum gauges that have been commonly used for decades are simple mechanical diaphragm gauges that act in an absolute or differential fashion. The reference side of the diaphragm is either a sealed high-vacuum chamber or is capable of being connected to a vacuum system, so that it can be evacuated to a very low reference pressure (e.g., 10^{-7} torr (1.33×10^{-5} Pa)). The pressure sensors can have many different configurations. Some are circular thin metal plates, with or without corrugations; others are flattened tubes bent to a C-shape; and others are corrugated bellows, twisted tubes, or helices. Metal gauges of this type have a dynamic range of about 10^3; that is, the maximum to minimum readable pressure ratio is about 1000. The minimum readable pressures are about 10^{-3} torr (1.33×10^{-1} Pa). The limitation in dynamic range is primarily imposed by the stiffness and elastic range of the material used. As previously discussed, a larger dynamic range (10^5) and lower minimum measurable pressure can be achieved through the use of quartz as the elastic material.

Since the late 1960's, with the improvements in materials and electronics, the capacitance manometer has become more available and is now widely used. (See ref. 8.) Deflections of a thin diaphragm (configured as one plate of the capacitor) as small as 10^{-8} cm can be detected; a deflection of this size corresponds to a pressure change of about 10^{-6} torr (1.33×10^{-4} Pa). The minimum useful pressure, however, is more than a decade higher. Thicker diaphragms allow the pressure range of such gauges to extend above 10^3 torr (1.33×10^5 Pa) with a constant dynamic range. The output of these gauges is displayed electrically in either analog or digital fashion. Figures 9 to 11 are schematic and pictorial examples of capacitance manometers in various configurations. The one-sided configuration shown in figure 11 is not as sensitive as those shown in figures 12 and 13 and is used when the nature of the measured atmosphere would be harmful to a capacitor electrode. The stationary capacitor plates consist of a ceramic insulating disk, upon which a thin metal film is deposited, and the active or deflecting membrane, which is a thin metal foil stretched and welded over the support frame. The electrodes are connected as a capacitor or capacitors in a bridge circuit that are excited with an ac voltage of 10 to 50 kHz. Any movement of the active element because of a pressure change is detected as unbalancing the bridge. This unbalance can be compensated for by adjusting the amplitude of the voltage applied to the capacitor. The amount of voltage required to rebalance the bridge is proportional to the pressure and is sensed and displayed as either an analog or digital signal. In this type of circuit, mechanical hysteresis effects are minimized because the diaphragm motion is minimized to small values well within the material elastic limit of the material. Some versions of the modern capacitance manometer are constructed of materials (conductors and insulators) which are compatible with ultrahigh-vacuum techniques. They have low-vapor pressure and are bakeable up to 400°C.

The most useful arrangement of instruments is the combined use of a 1000-torr (1.33×10^5 Pa) and 1-torr (1.33×10^2 Pa) transducer to cover a pressure range extending from 1 atm down to 10^{-4} torr (1.33×10^{-2} Pa). This arrangement allows a continuous pressure measurement from atmospheric pressure to where ion pumps and ion gauges can be started. In figure 12, a characteristic performance curve for a capacitance manometer (1000 torr (1.33×10^5 Pa) transducer) is shown. The useful dynamic range is about 10^4 where there is a 1-percent error.

Thermal-Conductivity Gauges

Thermal-conductivity gauges operate in the pressure range where the energy transport in the gas phase between two elements at different temperatures takes place by gaseous conduction. As shown in figure 13, convection becomes the dominant transport mechanism at higher pressures. Convection depends upon gas molecule-gas molecule interaction for energy transport. At pressures below the operating range of thermal-conductivity gauges, energy is primarily transported by radiation and possible conduction along elements. Heat loss in thermal-conductivity gauges is schematically illustrated in figure 14. Gaseous conduction depends upon a molecule gaining energy at the higher temperature surface and carrying it across the vacuum to a cold surface, where it loses this energy. Gases which move faster can obviously carry more energy per unit time than those which move slower, because of a higher collision frequency (e.g., hydrogen is a better conductor than oxygen). The other important parameter in gaseous conduction is the ability of the molecule to reach the temperature of the surface it is in contact with before it departs. The parameter that characterizes the energy absorption is called the accommodation coefficient α which is given by

$$\alpha = \frac{T_r - T_i}{T_s - T_i} \tag{15}$$

where

T_i incident molecular temperature

T_r reflected molecular temperature

T_s temperature of surface

As a general rule, more complex molecules accommodate better than less complex molecules, because they have more degrees of freedom to absorb energy. Therefore, carbon dioxide is a better transporter of energy than is argon. An indication of the relative power transmission efficiency of various gases is shown in figure 15. In this figure, it is shown that thermal-conductivity gauges do not measure pressure in the same direct sense that force gauges do. Each gas behaves differently, not necessarily linearly, as a function of pressure. Since these gauges are gas-composition sensitive, thermal-conductivity gauges must be calibrated for each gas or mixture of gases, and, in order to have accurate readings, the gas species being measured must be known. It is also important to know that this type of gauge is very temperature sensitive. A cold gas removes more heat from the wire, so the gauge must be calibrated for the gas temperature as well as its composition.

A Pirani gauge is the simplest of thermal-conductivity gauges. (See ref. 9.) Heat loss from a wire exposed to the vacuum is measured electrically as a resistance change in a Wheatstone bridge. The bridge circuit serves both to heat the metal wire and measure its resistance. Ideally, a metal wire which has a high-temperature coefficient of resistance, such as tungsten, nickel, molybdenum, or platinum, should be used. Pirani gauges have been used to detect pressures as low as 10^{-8} torr (1.33×10^{-6} Pa) with very sensitive circuitry, but the more practical lower limit is about 10^{-4} torr (1.33×10^{-2} Pa). A schematic of a bridge control circuit is shown in figure 16. The gauge R_g and the compensator R_s are as nearly identical as possible, and they also must be exposed to the same external temperature. The gauge element is open to the vacuum system to be measured, whereas the compensator has been evacuated to a very low pressure (10^{-7} torr (1.33×10^{-5} Pa) or less) and sealed off. The bridge circuit is operated as a constant-voltage (most often), constant-current, or constant-resistance bridge. Any change in pressure is reflected as a change in wire temperature, which is seen electrically as a change in resistance, current flow, or voltage drop in the metering circuit. Instead of a wire, a semiconducting material can be used as the resistance element. Semiconductors typically have larger (and negative) temperature coefficients of resistance (thermistors are examples of this type of instrument). They are used much in the same way as a metallic Pirani element, but because of slight nonuniformities in the materials used, they generally cannot be used to measure low pressures.

Thermocouple gauges are slightly more complex than Pirani gauges, in that the temperature of the heated wire is sensed by a small thermocouple attached to the center of the heated region. (The voltage output varies with the heat, which, in turn, varies with the pressure.) A popular form of thermocouple gauge is the thermopile, which employs two thermocouples in series and a third thermocouple in parallel that acts as a compensator for ambient

temperature variations (fig. 17). This gauge gives a larger output but has the same pressure range, about 10^3. Because of the aging phenomenon of the thermocouple junction (homogenization of the two wires by atomic diffusion), the minimum detectable pressure for thermocouple-type gauges is about 10^{-4} torr (1.33×10^{-2} Pa). The maximum pressure at which thermal-conductivity gauges are used depends on the gauge-element wall spacing; however, most commercial gauges are not useful above 1 torr (133 Pa). Primarily because of their simplicity, toughness, and low cost, these gauges are the most widely used indicators of "roughing" pressure. As can be seen in figure 15, however, large errors can result in the pressure measurement, since the gas composition changes continuously during initial pump-down. Thermocouple gauges, therefore, are devices that must be carefully calibrated and used only in the calibrated gas if they are to be reliable pressure gauges. Their most important utilization is that of roughing-pressure indicators, which are helpful in determining whether there are large leaks and/or whether the pressure is low enough to start a high-vacuum pump (e.g., an ion pump, turbo pump, cryopump, etc).

Ionization Gauges

Gauges normally used to sense the pressure of gas molecules well below 10^{-4} torr (1.33×10^{-2} Pa) are primarily ionization gauges. These all have a source for creating ions and a means for detecting these ions.

In the early part of the century, triode vacuum tubes were observed to be capable of detecting the presence of small quantities of a gas contained in tubes. Unfortunately, this observation led to the use of unsealed standard radio triodes as vacuum gauges. Figure 18 is a schematic of the conventional triode ionization gauge. (See ref. 10.) The source of ionization is a filament which is run at high enough temperatures to thermionically emit electrons. These electrons are accelerated to about 100 to 150 eV. At these energy levels, they produce ions by electron impact. The cross section for producing ions by electron bombardment for almost all gases peaks at approximately 70 to 80 eV. (See fig. 19.) Also, all gases show a threshold or appearance potential for ionization between 3 and 26 eV. All gases do not have the same ionization efficiency; therefore, it is again necessary to calibrate the gauge and to know what gases constitute the pressure in order to obtain the pressure from the output signal. After the ions are formed (near the grid), they are accelerated to the collector, where they are neutralized by electrons. The number of ions in the gauge is proportional to the pressure and to the number of electrons available for ionization. This number is computed as follows:

$$I_i = I_e S p \tag{16}$$

where

I_e	electron current
I_i	ion current
p	pressure
S	sensitivity

The sensitivity factor (sometimes called the gauge constant) must be determined for specific gauge and operating conditions (i.e., gas species, geometry, and electron energy). Table III is a list of relative sensitivities for a standard ionization gauge. If the sensitivity S of a gauge is known for a particular gas (e.g., $S(\mathrm{Ar})$), then the pressure for any other gas $p(x)$ can be estimated from its relative sensitivity. This relationship is simply

$$p(x) = \frac{S(\mathrm{Ar})p}{S(x)} \tag{17a}$$

where p is the indicated pressure.

Gauges are often calibrated in Ar, so if the gas is actually N_2 where $\frac{S(N_2)}{S(\mathrm{Ar})} = 0.8$ (table III) then equation (17a) becomes

$$p(N_2) = 1.25p \tag{17b}$$

A plot of ion current as a function of pressure for various gases is given in figure 20. It is important to understand that ion gauges do not measure pressure directly. The instrument detects ions which are proportional to the number density and, through calibration and the determination of the gauge sensitivity, can be related to pressure.

The conventional triode ion gauge was used to measure vacuum levels until about 30 years ago. From about 1930 to 1950, obvious improvements in vacuum technique did not result in any apparent reduction in pressure. In 1947, W. B. Nottingham of the Massachusetts Institute of Technology suggested the reason for this behavior. (See ref. 11.) He pointed out that electron collisions with the grid created soft X rays, which subsequently strike the collector and create a photoelectron. Since an electron leaving the collector appears like an ion arriving at the collector, a steady ion current (proportional to the emission current) would result in the so-called X-ray limit. This current was independent of pressure and of such a magnitude as to make the minimum detectable

pressure about 10^{-8} torr (1.33×10^{-6} Pa). This phenomenon is illustrated in figure 21.

As a result of this discovery, the hot-filament-gauge geometry was changed by Bayard and Alpert in 1950 to that shown in figure 22. (See ref. 12.) The collector was a 200-μm-diameter wire along the axis of the cylindrical geometry. The ionization and collection efficiencies of this gauge are nearly identical to those of the conventional ion gauge. Although the solid angle subtended by the collector has been greatly reduced, the sensitivity factors for gases are about the same as those for the conventional gauge. The X-ray limit for the Bayard-Alpert gauge is about 10^{-10} to 10^{-11} torr (1.33×10^{-8} to 1.33×10^{-9} Pa), depending on its configuration. A number of variations on the Bayard-Alpert gauge have been made which have substantially extended its low-pressure range. A more modern version of the ion gauge (nude version) is shown in figure 23. The primary difference in this geometry and that of the Bayard-Alpert gauge is the closed grid structure (which increases the instrument sensitivity). Figure 24 is a plot of indicated pressure versus true pressure for this gauge. The true-pressure data were obtained from a calibrated bent-beam gauge which is discussed subsequently. The dashed line represents the indicated pressure, which becomes nonlinear when the residual current begins to limit the pressure below 1.1×10^{-10} torr (1.5×10^{-8} Pa).

There are two major limitations for hot-filament ionization gauges at high pressures. Normal filament life decreases markedly at pressures above 10^{-5} torr (1.33×10^{-3} Pa) when the pressure is comprised of oxidizing gases. This shortcoming can be circumvented through the use of filaments which are not as sensitive to oxidation. Thoriated iridium or thoria-coated iridium are the filaments most often used, although tungsten has been recently shown to be more stable, even though it continues to oxidize. At 5×10^{-3} torr (0.67 Pa), the mean-free path for ions is about 1 cm, the typical electrode spacing in an ion gauge. At pressures higher than 5×10^{-3} torr (0.67 Pa), ions are increasingly likely to collide with gas atoms and be scattered and neutralized. The ion current collected may actually decrease as pressure increases in the nonmolecular flow regime. By reducing the spacing between electrodes, the upper pressure range of the ionization gauge can be extended, basically because ions can now be collected before being neutralized by molecular collision since $\frac{\lambda}{d} > 1$, where d is a characteristic distance for the geometry. The Shultz-Phelps gauge shown in figure 25 combines the high-pressure iridium filament with minimal spacing in an ionization-type gauge. (See ref. 13.) A useful upper range for this instrument is approximately 0.6 torr (80 Pa).

Another class of ionization-type instrument, a cold-cathode gauge, is also available for measurement of high vacuum. The first of these was invented by Penning and is described in reference 14. Figure 26 shows a Penning ionization gauge and its associated circuitry. Electrons to initiate the discharge are available from cosmic radiation or from field emission. The crossed electric and magnetic fields cause the electrons to describe helical paths confined by the anode ring, so that they make many excursions back and forth before they are collected by the anode. This long path length provides an increased probability of a collision with molecules and the creation of ions which ultimately terminate at the cathode where they are measured. Cold-cathode gauges do not have the problem with X rays that hot-filament gauges have, because the electron current is independent of pressure. They also do not have the hot-filament chemistry to distort the vacuum readings.

The magnetron discharge gauge is a significant refinement of the Penning gauge and was specifically designed for ultrahigh-vacuum service in the late 1950's by P. A. Redhead. (See ref. 15.) Figure 27(a) is a diagram of the Redhead magnetron gauge. The anode is a cylinder about 2 cm long and 3 cm in diameter and is perforated to improve access of the vacuum gases to the discharge volume. The cathode is spool shaped. The axial cylinder is joined to circular end disks, which are shielded from high electric fields by annular shield electrodes called auxiliary cathodes; these cathodes are operated at the cathode potential. Electron emission from the auxiliary cathodes is not measured in the ion-current detector circuit. The magnetron operates at 4.5 to 6 kV with a 1000-gauss magnetic field and has a linear operating pressure range of 10^{-4} to 10^{-10} torr (1.33×10^{-2} to 1.33×10^{-8} Pa). Below about 2×10^{-10} torr (2.66×10^{-8} Pa), the gauge becomes nonlinear, but, if calibrated, can be used to detect pressures down to 3×10^{-13} torr (4×10^{-11} Pa). Figure 27(b) shows a typical calibration curve that follows the power law below 2×10^{-10} torr (2.66×10^{-8} Pa) as follows:

$$I^+ = kp^n \tag{18}$$

where k and n are constants and I^+ is ion current.

Discharge extinction occurs at pressures below about 3×10^{-13} torr (4×10^{-11} Pa).

Less-Prominent Ionization Gauges

In figure 28, a modulation element (a collector wire located inside and very near the grid) has been added to a standard nude Bayard-Alpert instrument,

which allows the determination of the residual current and a pressure measurement (ref. 16) as low as 5×10^{-12} torr (6.7×10^{-10} Pa). If the modulator is at grid potential, then the collector current is

$$I_1 = I^+ + I_r \tag{19}$$

where I^+ is the gas-phase ion current and I_r is the residual current due to soft X-ray photoelectron emission. If the element is at ground potential, then it competes with the central collector for ions, so that only a fraction of the ions are collected; however, the residual current is virtually unchanged, so that

$$I_2 = \alpha I^+ + I_r$$

where α is the modulation factor. Solving equations (18) and (19) gives the true ion current (without the residual current) as

$$I^+ = \frac{I_1 - I_2}{1 - \alpha} \tag{20}$$

and the residual current as

$$I_r = \frac{I_2 - \alpha I_1}{1 - \alpha} \tag{21}$$

The modulation factor can be easily determined at high pressure, where $I^+ >> I_r$. This simple and inexpensive technique allows the measurement of pressure levels as low as most systems will attain.

A different approach to low-pressure measurement is the use of a suppressor electrode in front of the ion collector; this electrode suppresses the emission of electrons caused by the soft X rays. (See ref. 17 and fig. 29.) Although useful versions of this gauge were developed, the concept has not been widely used in practice. A further refinement to the hot-filament ionization gauge was published in 1966 by P. A. Redhead. (See ref. 18.) In this approach, the extractor gauge collector is fully removed from the ionization volume and is positioned behind an exit aperature as shown in figure 30. The ions are focused onto a fine collector wire that is surrounded by an ion reflector cup. The small area of the cross section of the wire further reduces the X-ray limit to less than 3×10^{-13} torr (4×10^{11} Pa). When the collector wire is replaced by an electron multiplier for ion detection, pressures as low as 10^{-15} torr (1.33×10^{-13} Pa) can be measured. Another type of extractor gauge is the bent-beam gauge, invented by J. C. Helmer in 1966, shown in figure 31. (See ref. 19.) This instrument extracted the ions and bent them 90° by using an electrostatic field, thus orienting the collector out of the line of sight of the X rays produced at the grid. Suppressor grids were also added to permit measurement of 10^{-14} torr (1.33×10^{-12} Pa) without the use of an electron multiplier. Figure 32 is a schematic of a hot-filament gauge that employs a magnetic field to improve sensitivity and suppress photoelectrons. This concept was developed by Conn and Daglish (ref. 20) and improved by Lafferty (ref. 21). If used with an electron multiplier, pressures as low as 3×10^{-18} torr (4×10^{-16} Pa) can theoretically be detected.

Other cold-cathode discharge gauges include the inverted magnetron, which has about the same low-pressure limit as the magnetron (ref. 22) and the orbitron gauge (ref. 23). Figure 33 shows the orbitron gauge, which sometimes has a hot filament to supply electrons that start the discharge (as opposed to field emission). The filament may be turned off after the gauge has started. The orbitron gauge also does not require a magnetic field to operate, since the central wire in the orbitron gauge is very small in diameter and the electrostatic field is adjusted to maximize the length of the orbiting electron trajectory.

Effects of Ionization Gauge

Each type of ion gauge includes its own set of anomalies, but there are effects that are somewhat common to all vacuum instruments. A few of the most significant effects are ion burial, gas-surface interactions, cracking anomalies, electron-stimulated desorption, floating elements, cross talk, thermal transpiration, gauge envelopes, and gauge degassing. These effects are discussed herein, but the discussion is not intended to be exhaustive. For more details, see reference 2.

All ionization-type gauges operate by ionizing the gas-phase atoms or molecules and subsequently accelerating these ions to a collector which ultimately counts them (usually in the form of a current). When the ion strikes the collector, there is some probability that it will be chemisorbed or driven into the lattice and effectively buried and, therefore, removed from the gas phase. In this way, ion gauges have a small, but nonnegligible, pumping speed. Reemission of the buried species can subsequently occur by diffusion to the surface and by desorption. However, for a grid at room temperature, this reemission does not occur readily. Table IV shows the pumping-speed values for several gauges and several gases. Degassing of the gauge by resistance heating or by electron bombardment raises the temperature of the elements to enhance desorption of chemisorbed species and to enhance diffusion of buried species to the surface. A good general rule is that, if a gauge is operated at maximum pressure for an extended length of time, the gauge must be degassed in order

to reliably measure pressures that are four decades less than the maximum exposure. A representative example would be an ultrahigh-vacuum (UHV) system that developed a leak which increased the system pressure to 10^{-5} torr (1.33×10^{-3} Pa). After locating the leak and repairing it, the system would pump back down to less than 10^{-9} torr (1.33×10^{-7} Pa), but the gauge would have to be thoroughly degassed for reliable measurement. The reason for this degassing is that the quantity of gas pumped by the gauge at much higher pressure provides sufficient outgassing from the gauge elements, so that the resulting gas density (from the outgassing) is competitive with the actual gas density. To ensure good measurements, proper degassing procedures should be followed on a regular basis. Although this is somewhat of a subjective procedure and very sensitive to the pressure level, one general rule is to degas the gauge once a day and allow at least an hour before taking data or conducting an experiment. If the experiment involves raising the pressure too high, additional degassing would be required.

Considering the hot filament that exists in some instruments, there are substantial reactions that can occur that alter the representative gas-phase constituents. These gases, such as CO_2, H_2, O_2, C_xH_y, and H_2O, can dissociate at the filament and react with other species adsorbed on the gauge elements or the vacuum envelope. Some of these reactions for a W filament and a ThO_2-coated Ir filament are shown in figure 34. Clearly, other filaments, such as Re, Ir, LaB_6, and those that are coated with low-work-function materials, yield different reaction products.

Since these gauges are gas-composition sensitive, an incorrect pressure would be indicated if the gas species were not known. Commercially supplied control units that read in units of pressure are usually adjusted for an average gauge sensitivity in a particular gas (e.g., $S = 0.1\text{A torr}^{-1}$, N_2, where $I_e = 4$ mA). Corrections must be made if a different gas or mixture of gases exists or if the emission current is changed.

Another effect that occurs because of the electron bombardment of the grid is electron stimulated desorption (ESD). At the higher pressures, especially in gas environments of CO, H_2, and O_2, the grid chemisorbs (and incorporates) quantities sufficient to be desorbed by ESD back into the gas phase at lower pressures, and again gives an incorrect pressure indication. (See fig. 35.) Highly reactive atomic hydrogen and atomic oxygen, which can substantially alter the true gas composition, are also effects of ESD. At pressures below 10^{-9} torr (1.33×10^{-7} Pa), errors due to ESD can exceed several hundred percent. Although degassing a gauge is necessary to obtain reliable measurements at low pressure, the gauge elements are very clean and the gauge pumping is at its highest rate (clean surfaces are highly reactive for chemisorption) immediately after this process (e.g., 100 mA for 5 min). Therefore, some time is needed to allow the elements to return to room temperature and for gauge pumping to reach a steady-state level before a stable reading can be obtained.

A major concern in making good pressure measurements is the type of enclosure (envelope) used. As shown in figure 36, many vacuum systems utilize gauges with a full envelope with the attachment to the system basically through a tube and flange. Such gauges are essentially little vacuum chambers themselves and, depending on the size and conductance of the tube, may measure very different pressures than those in the main system. They are not recommended for measurement of pressures less than 10^{-6} to 10^{-7} torr (1.33×10^{-4} to 1.33×10^{-5} Pa). Figure 37 represents a nude gauge in a short or long tubulation that is connected to the vacuum system. This arrangement provides a much larger conductance to the main system and gives a more accurate measurement. It is important to note that the gauge sensitivity (gauge constant) is very different for these two cases and may vary as much as 35 percent. A further discussion of this effect is contained in the section "Instrument Calibration."

Figure 38 is a schematic of a typical vacuum system containing a variety of gauges. It is preferable to equip systems with more than one ion gauge to increase the measurement reliability. Care must be taken, however, to ensure that there is no electronic or ionic interaction (cross talk) which can occur if the gauges are too close to each other or if they are oriented in a line of sight. The two ion gauges and the mass spectrometer may have a serious cross-talk problem. This consideration is important with regard to other instrumentation or charged elements as well; substantial errors in measurement can result. Also, measurements can be affected by temperature differential. As shown in figure 39, erroneous measurements can be made if taken at a different temperature than in the region of interest (e.g., the pressure measurements near a cryopanel or in a vacuum furnace). However, thermal transpiration corrections can be applied in certain geometries which permit this measurement. The pressure p_1 in volume $\mathcal{V}_1$ at T_1 is related to the pressure p_2 in $\mathcal{V}_2$ at T_2 by

$$p_1 = p_2 \left(\frac{T_1}{T_2} \right) \tag{22}$$

In those cases where a gauge can be added to the vicinity of interest, it is preferable to trying to estimate the pressure based on calculations.

Table V is a comparison of selected properties for some of the ionization gauges previously discussed. The low-pressure limit of some of the gauges, based on the use of an electron multiplier, is indicated by an asterisk.

Mass Spectrometers

The most severe deficiency of total-pressure instruments is that they provide virtually no chemical information concerning the gas environment in a vacuum system. The lack of identification of the partial pressures which make up the total pressure is such an enormous disadvantage that any good vacuum system should have a mass spectrometer. It provides, first of all, a built-in leak detector, which is absolutely necessary to confirm the vacuum integrity of a system. Secondly, it provides the state of cleanliness of a system by indicating the magnitude and type of the residual gases. Thirdly, it is a research tool that provides several diagnostic capabilities in addition to determining gas purity, gas desorption from elements of interest, and gas changes that occur during various processes.

The instruments discussed next are used in a support role on vacuum systems and are classified as partial-pressure analyzers, residual-gas analyzers, or mass spectrometers. The latter is probably the most common and most accurate designation of the instrument, since it can do much more than the first two labels indicate. Some users consider a mass spectrometer as a stand-alone analytical instrument for chemical analysis, perhaps with more sensitivity and resolution. It may also employ support apparatus like an inlet system or a unique ion source. In general, the vacuum-system instruments work the same way. A mass spectrometer is basically a three-stage instrument comprised of an ionization source, a mass separator, and an ion detector. All three stages can run the full extent of sophistication. As previously indicated for total-pressure instruments, the following is a discussion of only the more commonly used mass spectrometers and is not intended to be an exhaustive treatment.

Ionization Sources

The predominant mode of ionization that is used is electron impact as opposed to field or chemical ionization methods. Although the concerns for ionization gauges are also important for ionization sources, the primary differences between an ion gauge and a mass-spectrometer ion source are the ion extraction and focusing into the mass separator section required by the latter. The ultimate resolution of some mass spectrometers is quite sensitive to the energy and entrance angles of the incoming ions to the mass separator. Furthermore, ion sources are designed to minimize the X rays that might transit the separator to the detector and limit the detectability at low pressures. Figures 40 to 42 are schematics of three different types of ion sources used in mass spectrometers. The electron energy is usually set at about 70 eV, since that is near the maximum ion yield for most gases (fig. 19). This energy is adjustable on most instruments. The different ion yields for different species in the ion source give rise to the same relative sensitivity problem encountered in ion gauges, but it is shown subsequently that this problem can be accounted for in a calibration.

Mass Filters

As the ions enter the mass-separator section, they can be separated by a variety of methods, such as time of flight, magnetic fields, electrostatic fields, and electrodynamic fields (or a combination of the above).

Conventional magnetic deflection. The first mass spectrometers (refs. 24 and 25) were those using the well-known physical phenomenon that moving, charged particles are deflected from a straight line when traversing a magnetic field. (See fig. 43.) The radius of the path is determined from a force balance between the centrifugal force and the magnetic force, or

$$\frac{mv^2}{r} = BZev \text{ or } r = \frac{mv}{BZe} \tag{23}$$

where

B	magnetic field
e	elementary charge
m	mass of charged particle
v	velocity of charged particle
Z	charge number

Since the incoming kinetic energy is controlled by the accelerating voltage V into the mass separator, then

$$\frac{1}{2}mv^2 = ZeU \tag{24}$$

so that the radius described by the charged particle is

$$r = \frac{1}{B}\left(\frac{2mU}{Ze}\right)^{1/2} \tag{25}$$

The radius is thus sensitive to the square root of the mass-to-charge ratio m/e.

From equation (23), the magnetic-deflection instrument separates charged particles by momentum mv, by the electronic charge Ze, and by the strength of the magnetic field B. An ion being doubly charged

(two electrons removed from the molecule) follows the same path as the singly charged ion with half the mass. Instruments for vacuum measurements using simple magnetic deflection normally deflect the ion either 60° or 90°, but some systems utilize 180° separators. In general, greater angles give more separation and, therefore, more resolution.

The resolution of a magnetic-deflection mass spectrometer is controlled by (1) the width of the ion beam perpendicular to the magnetic field, (2) the ion-beam entrance angle into the magnetic-deflection region, (3) the variation of the ion energy, and (4) the variation in the magnetic field. The ion-energy variation is minimized by using a small electron bombardment ionization source and a stable ion-acceleration voltage. The homogeneity of the magnetic field is controlled by using a narrow magnetic gap, with the magnet and pole faces as large as possible. If an electromagnet is used, the power supply must be carefully regulated and stabilized. The entrance angle and beam width are controlled by beam-defining slits that are placed along the beam before it enters the magnet and occasionally at the exit of the magnetic field.

The use of narrow slits and a narrow magnet gap improves the resolution of the magnetic mass spectrometer at the expense of sensitivity. For any practical system, a compromise between resolution and sensitivity determines the slit opening. In addition to slit width and gap width, the sensitivity depends upon the efficiency of the ion source, the ion extraction efficiency, slit alignment, and, most importantly, the ion detector. Minimum detected partial pressures of 10^{-15} torr (1.33×10^{-13} Pa) have been reported. The mass-spectrometer parameters are adjusted to detect one mass-to-charge ratio at a time; therefore, a method of sweeping across the desired m/e range in some manner is required. This result may be accomplished by sweeping either the accelerating voltage or the magnetic field, although voltage sweeping is used most often because of its relative simplicity. The magnetic instruments have the advantage of a large useful amount of reference information on their operating characteristics. Also, very little electronic equipment is required (all of which is dc). Changes in resolution or sensitivity require removal of the analyzer from its envelope to adjust the slits.

Omegatron. The omegatron was first described by Sommer, Thomas, and Hipple (ref. 26), and later by Alpert and Buritz (ref. 27). It operates in a manner similar to the cyclotron; that is, ions move perpendicular to a magnetic field and are accelerated by a voltage, except that the resonant ions never drift in an electric-field-free region as in a cyclotron. They are instead continuously accelerated along an Archimedes spiral. Figure 44 is a schematic representation of the omegatron. The ions are formed along the axis parallel to the magnetic field and spiral out to the collector. The ions, with a frequency corresponding to resonance (i.e., always traveling toward an attracting electrode), have the following relationship to the applied RF frequency f_r in Hz:

$$f_r = \frac{1}{2\pi}\frac{eB}{m} \tag{26}$$

where

B	magnetic field
e	elementary charge
m	mass of charged particle

In this particular instrument, negative as well as positive ions can be collected.

Ions which are not in resonance follow closed paths of time-varying radius. Those farther from the resonant frequency deviate less from the region in which they were formed. Those ions which are so close to resonance that their radius exceeds the distance from the ionization axis to the collector contribute to the signal of the resonant ions. As before, the need for uniform electric and magnetic fields is an important consideration, and additional RF field-grading electrodes are generally added to the omegatron between the main RF electrodes. Resolution for the omegatron is about 40 at mass 40.

The omegatron is quite small but requires a large magnet and a variable-frequency, constant-amplitude voltage generator to sweep the mass range; unfortunately, the ion source cannot be mounted nude. Because of these reasons and the expense of the electronics, these instruments are no longer readily available.

Time-of-flight spectrometer. The time-of-flight (TOF) spectrometer (fig. 45) uses the simplest analyzer structure of any mass spectrometer. (See ref. 28.) Ions are formed in the source and are then injected into the drift region with a constant energy E_i. Since the ions are pulsed into the field-free drift tube of length L, the ion energy is given by

$$\frac{1}{2}m\left(\frac{dz}{dt}\right)^2 = E_i = eU_i \tag{27}$$

where

$\frac{dz}{dt}$	velocity down drift tube
m	mass of charged particle
U_i	injection voltage

When solved for the drift time Δt, equation (27) becomes

$$\Delta t = L\left(\frac{m}{2ZeU_i}\right)^{1/2} \tag{28}$$

where Ze is the extent of the charge.

Small injection voltages (e.g., 10 V) yield ion drift times for 1 m of about 10^{-5} sec; therefore, any detection system used with a TOF spectrometer must be very fast. It must also be very sensitive, because very few ions of any one m/e are transmitted in a pulse, which is typically 1 to 100 μsec in duration.

Resolution is proportional to the ratio of the ion transit time to the pulse duration. Also, resolution is adversely affected by nonenergetically, homogeneous ion bunches and by large ion-formation regions. Resolutions of over 100 units have been reported for 1-m drift regions. The sensitivity of the TOF spectrometer is directly proportional to the pulse duration. The lower partial-pressure detection limit using an electron multiplier is 10^{-12} torr (1.33×10^{-10} Pa). The upper operating pressure is defined by the mean free path of the ions in the drift region.

The TOF spectrometer is the only instrument capable of measuring reactions which take place in a few microseconds and is quite useful in determining the energy of ionic species. The instrument tends to be large, but has no magnet and is not heavy. The major problems involve the ion-formation region, which must be small and must generate monoenergetic ions, and the detector, which must be capable of resolving single ions separated in arrival times by tens of nanoseconds. Because the number of ions per pulse is small and the separation time per mass is small, an electron multiplier detector is required.

Quadrupole mass filter. One of the most recently developed techniques for mass separation was proposed by Paul (ref. 29) after an extensive mathematical study of the quadrupole field. In his original work, Paul proposed that the rods of the analyzer be of hyperbolic cross section. However, circular cross-section rods of radius $1.16r_o$ (r_o is the radius of the inscribed cross-sectional area of the quadrupole) have been found to work quite satisfactorily.

Ions are formed in the ion source and injected into the electrical quadrupole along the Z-axis of the quadrupole. (See fig. 46(a).) The rods of the quadrupole are energized with a constant dc potential U and an RF potential $V\cos\omega t$. The ions are subjected to a potential of the form

$$\phi = [U + V_o(\cos\omega t)]\frac{x^2 - y^2}{r_o^2} \tag{29}$$

where

U dc voltage

V_o RF voltage

x, y spatial coordinates of cross section

The equations of motion for the ions are

$$m\ddot{x} + 2g\,(U + r\cos\omega t)\frac{x}{r_o^2} = 0 \tag{30}$$

$$m\ddot{y} + 2g\,(U + r\cos\omega t)\frac{x}{r_o^2} = 0 \tag{31}$$

and

$$m\ddot{z} = 0 \tag{32}$$

where

m mass of charged particle

z axial coordinate

ω RF frequency

Equations (30) to (32) are Mathieu's differential equations.

A transformation of coordinates is introduced as follows:

$$\omega t = 2\xi \tag{33}$$

$$a = \frac{8\epsilon U}{mr_o^2\omega^2} \tag{34}$$

$$b = \frac{4\epsilon V_o}{mr_o^2\omega^2} \tag{35}$$

where

ϵ unit of electronic charge

ξ fitting parameter

The solutions of the differential equation in z are trivial. The solutions in x and y are infinite series of two types: the stable solution, for which x and y remain finite for all values of ξ, and the unstable solution, for which x and y become infinite as $\xi \to \infty$. The stability of the solutions depends on the values of a and b. Figure 46(b) shows two regions: (1) ions that fall outside the triangular-shaped area enter unstable oscillations and are collected at a quadrupole electrode, and (2) ions that fall inside the shaded area oscillate stably and pass through the analyzer.

The apex of the stability region occurs at $b = 0.706$, $a = 0.23699$, and $U/V_o \approx 0.17$. At this point,

only one mass, given by equation (37)

$$m = \frac{2.85\epsilon V_o}{w^2 r_o^2} \tag{36}$$

$$U \approx 0.17 V_o \tag{37}$$

will pass through the analyzer; the resolution is ∞. Of course, the intensity of such an ion beam would be nearly zero.

For any practical use, a lower value of U/V_o is selected. The mass range may be scanned either by varying the frequency (the RF and dc voltage remain constant, in which case the resolution remains constant) or by using a constant frequency and varying the RF and dc voltage level and keeping their ratio constant. In this case, the resolution varies as $1/m$. The latter method of mass scan is more commonly used. Certain boundary conditions on entrance aperture and entrance energy are required for optimum resolution.

Resolution of 100 at mass 100 with a sensitivity of 10^{-2} torr (1.33 Pa) is reported. (See section "Sensitivity and Resolution.") The instrument is capable of detecting partial pressures of less than 10^{-13} torr (1.33×10^{-11} Pa) and operating at maximum pressures above 10^{-4} torr (1.33×10^{-2} Pa).

A physical description of the mass separation (ref. 30) can be understood by referring to figure 47. If two of the rods opposite each other are at a positive dc potential $+U$, the potential is zero along the axis at the midpoint between the two rods. If an RF field of V of greater magnitude than the dc field is superimposed on the rods, then there is some interval where the potential on the rods becomes negative. If a positive ion is injected along the Z-axis, it experiences a repulsion from both rods and stays in the potential well as long as $U + V$ is positive; this is a stable condition. When the negative excursion of the RF drives the potential of the rods negative for a small fraction of the cycle, then the positive ions accelerate down the potential hill toward the rods; this is an unstable condition. Now the low-mass ions can react very rapidly to this attractive potential and oscillate back and forth. The amplitude increases with each negative excursion until it is finally captured by the rods and neutralized. The heavier ions are too slow to react significantly to the negative excursion, and their oscillations have small amplitudes. They would be controlled more by the positive repulsion, thereby keeping them in the stable condition. Eventually, their Z-axis momentum would allow them to transit the length of the rods and be collected. Thus, heavy positive ions pass through the mass filter, but light positive ions are neutralized by the rods. Now the other two rods have a negative potential $-U$ applied and represent the unstable condition, because the positive ions are accelerating toward the rods. However, when a superimposed RF field is applied with a magnitude greater than the dc field V, then there are small fractions of the cycle where the rods go positive, thereby providing the stable conditions. In this case, the low-mass positive ions can react to the positive excursion and maintain sufficiently small amplitudes to keep them from colliding with the rods. The low-mass ions can travel the full length of the mass filter and can be collected. The high-mass positive ions cannot react to the short positive excursion, therefore, they stay in the unstable condition. Ultimately, they collide with the rods and are neutralized. Thus, the light positive ions pass through the mass filter, and the heavy positive ions are lost to neutralization. These two combined conditions comprise the band-pass filter of the quadrupole and allow only a certain value of m/e ions to transit the full length of the quadrupole. The width of the passband is determined by the ratio of U to V_o, since that ratio controls the positive and negative excursion fractions as shown in figure 46(b). There is an upper limit to the magnitude of U/V_o as well, since it controls the amplitude of the stable ions. Too large an amplitude may exceed the physical dimensions of the rods. The mass of the ion and its velocity are also important considerations; slow ions (more massive) are in the quadrupole longer and experience many more oscillations than do the faster ions (less massive). Therefore, there is a higher probability of collection at the rods. Transmission through the quadrupole filter is therefore sensitive to the mass of the ion. Figure 48 shows the relative transmission as a function of mass. There is a substantial effect on ions which have masses in excess of 40 amu, but it can be accounted for by calibration. (See section "Instrument Calibration.")

The quadrupole has the advantages of rapid scanning (10 scans/sec of easily variable transmission and resolution), high operating pressure, and noncritical ion-injection requirements. Disadvantages are its requirement for stable high-voltage RF supplies and its asymmetrically and variably shaped mass peaks.

Ion Detectors

Faraday cup. The third section of the mass spectrometer is the ion detector. The Faraday cup shown in figure 49 is used when very stable signals are required and there is sufficient pressure to provide a detectable signal. The design is basically to retain secondary electrons, emitted by secondary emission or by photoemission, which effectively subtract from

the detected ion current. This, in part, can be accomplished by the small entrance aperture and/or a suppressor grid which is sufficiently negatively biased to deflect emitted electrons back to the cup. Currents to about 10^{-14} A are measurable with a sensitive electrometer, but, in general, 10^{-12} A is a practical limit. Considering the sensitivity of most mass spectrometers, this limit would translate to a pressure of 10^{-8} torr (1.33×10^{-6} Pa) or higher.

Discrete-stage electron multiplier. In order to measure partial pressures below 10^{-8} torr (1.33×10^{-6} Pa), a means of internal amplification is employed. Such an amplifier is the electron multiplier. The instrument is usually a discrete-stage or continuous-stage type. Figure 50(a) illustrates the discrete-dynode multiplier of the box and grid design. The discrete dynodes are a Cu 2-4% Be alloy which forms a BeO surface layer. These multipliers can have a gain greater than 10^6 at approximately 100 V per stage. (Gains of at least 10^5 are likely.) Ions exiting the mass separator are accelerated to the first dynode that is negatively biased 1 to 3 kV. Upon colliding with the dynode, the ions emit, on the average, several electrons per electron. These electrons are attracted to the next dynode with an accelerating potential of 100 to 300 V, where each electron emits, on the average, several more electrons. This process continues through each of the stages until 10^4 to 10^8 electrons from a single ion appear at the collector in a pulse of current. This pulse of current is orders of magnitude larger than that from a Faraday collector and is thus easier and quicker to detect in the external amplifier. The gain of a multiplier is

$$G = (I_e) \times (E_e)^{n-1} \tag{38}$$

where

E_e average electron-to-electron conversion (secondary emission) efficiency ($\approx$2.5)

I_e average ion-electron conversion (secondary emission) efficiency ($\approx$4 or 5)

n number of dynodes (10 to 16 in commercially available multipliers)

If the multipliers of this type are exposed to contaminating vapors such as halogens or pump oils (especially silicon based), the gain drops below 10^3. Rejuvenation of these instruments can be accomplished by appropriate degreasing of the dynodes and heating to 300°C to 400°C for a period of 1 to 8 hr, depending on the contamination, in flowing pure oxygen. The gain obtained is sensitive to these oxidation conditions. As long as these multipliers are exposed to controlled environments (e.g., Ar or N_2) when taken to atmosphere, a good vacuum bakeout of the system will also restore the gain.

Continuous-dynode electron multiplier. Figure 50(b) is a sketch of a continuous-dynode multiplier. It operates much like the discrete-dynode instrument, but the average electron conversion efficiency is only slightly greater than 1, and n is several thousand (eq. (38)). The design consists of a PbO-Bi_2O_3 tube typically with a 5-mm outside diameter and a 1-mm inside diameter. This multiplier behaves like a resistor chain and has electrons that describe a sawtooth cascade down the tube in the direction of the voltage gradient. There is usually a curvature to the tubes to prevent positive ions formed at the end of the tube from reversing their direction, moving back upstream, and colliding with a multiplier surface and creating secondary electrons that are not part of the actual signal. The channeltron (or spiraltron) is not as easily contaminated as the discrete-stage Cu-Be multiplier and does not seem to lose gain as readily after being exposed to atmosphere. However, it does have a limitation in that it becomes saturated at a lower current than Cu-Be multipliers and cannot be operated with a linear output at high pressures unless the operating voltage or the emission current is reduced.

The gain of multipliers is sensitive to many factors and is subject to change even when continuously exposed to a good vacuum. The gain should be initially measured before conducting experiments for masses of interest. The gain is ordinarily determined by comparing the ratio of the currents detected at the collector to that at the Faraday cup. This comparison usually requires backfilling the system to 10^{-8} torr (1.33×10^{-6} Pa) or higher with a particular gas (e.g., N_2). Periodically, the gain should be checked and the voltage adjusted to maintain a constant gain throughout an experiment. Electron multipliers should not be used in high-pressure applications, because the collector and dynodes can be destroyed if the average current to them exceeds a few microamperes. Another significant problem of multipliers is the gain dependence on the mass of the ion. Figure 51 shows the variation of gain with ion mass. This is obviously a function of the secondary emission of the particular ion striking the first dynode. The behavior is proportional to $\sqrt{m}$, so that the gain for H_2^+ ions is substantially greater than that for N_2^+ ions. (See refs. 31 and 32.)

Quadrupole Mass Spectrometer

Currently, the quadrupole is, by far, the most popular mass spectrometer. The primary reasons for this are its electrical (external) tuning of the resolution-sensitivity trade-off, its lack of a magnetic field, and its signal output with uniform mass increments. Figure 52 shows the three particular stages (ion source, mass separator, and electron multiplier) which comprise a quadrupole mass spectrometer. A typical spectrum from a clean, baked, ion-pumped, ultrahigh-vacuum system (total pressure of 1.5×10^{-10} torr (2×10^{-8} Pa)) taken with the quadrupole analyzer is shown in figure 53. The spectra seen for the gas species present in the vacuum system can be translated by first carefully labeling each mass peak present. The molecular mass can be determined by observing that the atomic weight of each molecule is the sum of the atomic weight of its constituent atoms. For example, a carbon dioxide molecule is 1 carbon plus 2 oxygen atoms, which is $12 + 2(16) = 44$. In figure 53, the ordinate is a log scale, so $m/e = 2$ is 10 times greater than $m/e = 16$. The spectrum in figure 53 shows that carbon dioxide ($m/e = 44$), argon ($m/e = 40$), and carbon monoxide ($m/e = 28$) are present. The $m/e = 28$ peak is greater than the $m/e = 44$ peak, although part of the 28 peak is a fragment of the 44 peak and no $m/e = 14$ caused by nitrogen is observed. Neon ($m/e = 20$) is also present. Mass 20 is greater than mass 40, so doubly charged argon ($m/e = 20$) cannot be the entire mass-20 peak. Water ($m/e = 18$) is barely detectable, since the system has been baked out. Mass 4 is caused by helium and mass 2 is caused by hydrogen. The particular spectrum displayed is common for an ion-pumped vacuum chamber, but it is by no means the most complicated spectrum that is likely to be encountered. Figure 54 shows a spectrum of a good pressure, 3.2×10^{-10} torr (4.27×10^{-8} Pa), but one where there is a very definite leak, as manifested by the large atomic nitrogen ($m/e = 14$) peak. When there is no significant methane signal ($m/e = 16, 15, 14$), the appearance of a large $m/e = 14$ peak indicates that N_2 ($m/e = 28$) is present in the system. If no N_2 is being admitted into the system, the signal usually means a leak.

The interpretation of spectra is normally straightforward, but can be quite complicated. It requires a certain level of understanding of the physics and chemistry that occur in a particular system. Figure 55 shows a computer-controlled, mass-spectrometer output of five gases being monitored when a Re filament of another instrument was turned on. The major peak desorbed was that of CO ($m/e = 28$), which went off the scale. The O_2 peak is 75 times smaller and represents a fragmentation peak of CO. The electron impact that produces the ions is also sufficiently energetic to cause dissociation (e.g., $CO_2 + \bar{e} \rightarrow CO_2^+ + CO^+ + O^+$, which is $m/e = 44$, $m/e = 28$, $m/e = 16$), so there are ionization fragmentation patterns for each multiatom molecule. Furthermore, atoms and molecules can be doubly ionized which means signals will be observed at $m/e = 40$ and $m/e = 20$ for Ar. Figure 56 shows the relative peak heights in spectral form for a few common gases and vapors. Table VI gives tabulated fractions for the fragments of a number of different gases detected by the quadrupole mass spectrometer of the type shown in figure 52. Computer programs are available that take into account these fractions (cracking patterns), analyze a complicated spectrum from the peak heights, and identify the kinds and percents of the gases that make up the vacuum environment being measured.

Sensitivity and Resolution

Sensitivity. The sensitivity of a mass spectrometer is defined as the change in response of the device divided by the change in input that caused the response. (See ref. 33.) In other words, the change in current output divided by the change in partial pressure of the gas causing the change is the usual way of determining the instrument sensitivity. The sensitivity may be constant over a range of operating pressures. The units of sensitivity are usually amperes per torr or some output increment per unit pressure. As an example, the modern quadrupole (with electron multiplier) might have a sensitivity of 100 A $torr^{-1}$. Another term which is closely associated with sensitivity is minimum detectable partial pressure (MDPP). A mass spectrometer has an MDPP when the signal-to-noise ratio for a specific gas is equal to one, which means that if the peak-to-peak noise is Y increments, the total peak-to-peak output (signal due to specific gas plus the noise) is $2Y$. The MDPP is equal to the noise multiplied by the reciprocal of the sensitivity. For example, the modern quadrupole (with electron multiplier) might have an MDPP of 10^{-14} torr (1.33×10^{-12} Pa). The determination of these parameters is accomplished by calibration. Although it is certainly possible to determine the sensitivity of the ion source, the transmission of the mass separator, and the gain of the multiplier for a particular gas, the calibration provides a sensitivity which encompasses all these factors. The operator must then assure that the identical emission current for the ion source and identical gain for the multiplier are used for this sensitivity to be applicable on a continuing basis.

Resolution. The resolution of a mass spectrometer is the ability to separate the peaks produced by ions of different mass-to-charge ratios. (See ref. 33.) It is basically a figure of merit of the mass-separator section of the instrument. There are several ways of describing resolving power; these methods are shown in figure 57 and are listed below:

1. Measurement on a single peak at mass number m. The resolution is given as $m/\Delta m$, where Δm is the width (in mass units) at a stated fraction x of peak height Y; x is usually 0.5.

2. Measurement on two peaks separated by one mass number. The mass number for the stated cross contribution is the highest mass number at which one peak contributes a percentage (usually 1 percent) to the height of the adjacent peak. It is usually assumed that both peaks are the same height.

3. Measurement on two peaks (Y_m and Y_{m+1}) separated by one mass number. The mass number for unit resolution is that mass number at which the height of the valley between peaks is a stated fraction x of the sum of two peak heights.

4. Measurement on two peaks of equal height. It is sometimes stated that the heights in method 3 are equal.

Since this is not very probable, method 3 is more general than method 4. Although all four of these methods have been used, method 1 is preferred. As $m/\Delta m$ remains relatively constant for magnetic, radio-frequency, or time-of-flight instruments, as well as some quadrupole instruments, the ability to separate adjacent peaks varies inversely with the mass. Resolution $m/\Delta m$ for omegatron instruments is not constant and varies inversely with the mass. Some quadrupole instruments have approximately constant Δm; therefore, the ability to separate peaks remains constant. Typical values of Δm for the quadrupoles range from 0.5 to 5 amu, and for constant Δm, the resolution R (resolving power) increases with the mass, so that

$$R = \frac{m}{\Delta m} \geq 2m \tag{39}$$

The basic relationship between sensitivity and resolution is

$$R \propto \frac{1}{S} \tag{40}$$

That is, adjusting the mass separator to provide an increase in sensitivity is accompanied by a decrease in resolution. Practically, the more the mass-separator parameters are adjusted to increase ion transmission through the separator, the less separation there is between peaks.

Instrument Calibration

Accurate pressure measurements for gas-composition-sensitive instruments such as the Pirani gauge, the spinning-rotor gauge, the ionization gauge, and the mass spectrometer are controlled by the quality of their calibration. In other words, the measurement is only as good as the calibration. Considering a high-accuracy calibration, the subsequent demounting of the instrument, exposure to the air, transfer from the calibration system to the operational system, remounting of the instrument, and finally, the bakeout and degassing required to reestablish calibration conditions, it is most difficult to maintain an actual sensitivity anywhere near the calibrated sensitivity. Ideally, the calibration system and the operational system should be one and the same. Unfortunately, this is seldom the case, and the scientific worker must endure the aforementioned scenario primarily because a carefully calibrated instrument is absolutely necessary for good research or development measurements. Several techniques which can be used to calibrate vacuum instrumentation are presented in this section. Detailed descriptions of these methods are provided in reference 2.

Static Volume-Expansion Technique

The static volume expansion simply involves pressurizing a very small volume and expanding that volume of gas into a much larger volume (ref. 34) to obtain a substantial reduction in pressure (Boyle's law). Figure 58(a) is a schematic of the technique. The small volume $\mathcal{V}_1$, typically a few cm^3, and the large volume $\mathcal{V}_2$, typically $>10^3$ cm^3, are initially cleaned and evacuated to the UHV range to minimize outgassing contributions to the signal. The small volume $\mathcal{V}_1$ is then normally pressurized to $p_1 = 10^{-2}$ or 10^{-1} torr (1.33 or 13.3 Pa) with the separation valve closed. The small-volume pressure p_1 is measured with a reference standard or a working standard such as a fused-quartz Bourdon tube, a capacitance manometer, or an SRG, and then the separation valve (which has a large-diameter bore) is fully opened. The equilibrium pressure then becomes

$$p_2 = \frac{\mathcal{V}_1 p_1}{\mathcal{V}_2 + \mathcal{V}_1} \tag{41}$$

Vacuum-chamber wall-pumping effects such as chemisorption and/or incorporation can be a serious problem, and several runs have to be made to saturate the walls and obtain repeatability. Furthermore, if hydrogen is the calibration gas, the walls may have to be significantly oxidized to inhibit the seemingly endless hydrogen incorporation. Another concern is gauge pumping. The ordinary ion gauge

at an emission current of ≈4 mA may have a pumping speed for N_2 of 0.1 liter/sec, which can have a substantial effect on the pressure diminution. Extrapolation techniques can be used to estimate the correct expanded pressure, but this is not a totally acceptable procedure. If wall effects and the gauge pumping are not serious problems, calibrations as low as 10^{-6} torr (1.33×10^{-4} Pa), depending on the gas, can be made. If the two volumes are initially cleaned to 10^{-10} torr (1.33×10^{-8} Pa), wall outgassing in the static system in $\mathcal{V}_2$ may increase the background pressure two decades to 10^{-8} torr (1.33×10^{-6} Pa) over the time of the individual measurement; thus, there is a 1-percent calibration gas uncertainty. In practice, the low-pressure calibration limit is probably 10^{-5} torr (1.33×10^{-3} Pa). This technique is not generally used because of the aforementioned effects and because of its one-decade (or less) range overlap with ionization-type instruments.

Pressure Rate-of-Rise Technique

A more desirable method of instrument calibration is a linear rate of rise of pressure in the measurement volume with which the instrument output is compared. The volume on the left $\mathcal{V}_1$ of figure 58(b) and the volume on the right $\mathcal{V}_2$, typically small, are initially cleaned and evacuated to the UHV range to minimize the outgassing contribution to the signal. The volume $\mathcal{V}_1$ is then pressurized to 1 to 1000 torr (133 to 1.33×10^5 Pa), which is measured by a reference standard such as a quartz Bourdon tube, capacitance gauge, or deadweight tester. The valve is then opened to the calibrated conductance C, which connects the two volumes. The resulting pressure rise in $\mathcal{V}_2$, which has been closed off from its pumps, is then compared with the instrument output, so that the change in pressure in $\mathcal{V}_2$ is given by

$$\mathcal{V}_2 \frac{dp_2}{dt} = C(p_1 - p_2) \tag{42}$$

Since $p_1 >> p_2$,

$$p_2(t) = \frac{p_1 C}{\mathcal{V}_2}\, t \tag{43}$$

where $p_2(t)$ is the pressure in $\mathcal{V}_2$ at any time t. The conductance C is usually selected to give a rate of rise that is fast enough to negate gauge pumping but slow enough so that instrument response is not a problem. Since $\mathcal{V}_2$ is small and exposure to the calibration gas for several cycles tends to minimize wall chemisorption and incorporation, wall effects are not a serious problem. Since C is also small enough that p_1 remains constant, the flow into $\mathcal{V}_2$ is assumed to be linear (after a few seconds). Furthermore, the low-pressure limit for this technique is probably an order of magnitude less than the static technique, since only a short time is spent in the low-pressure range (e.g., $\approx 10^{-7}$ torr (1.33×10^{-5} Pa)). The rate-of-rise technique has been studied and has been found to be an acceptable calibration method.

Orifice-Flow Technique

The orifice dynamic flow technique is the primary method used by the National Institute for Standards and Technology (NIST) for the calibration of ionization gauges and mass spectrometers (ref. 35), basically because it can extend the range of calibration several decades below the two methods previously discussed (i.e., from 5×10^{-5} to 5×10^{-10} torr (6.67×10^{-3} to 6.67×10^{-8} Pa)). The orifice-flow technique is a dynamic technique that uses a flowmeter to provide a known flow Q_1 into the first of two volumes which are pumped at known constant speeds (the two volumes have conductance-limiting orifices). The second volume, which is the second stage of pressure reduction, is where the instruments to be calibrated are located. Figure 58(c) is a diagram of the two-stage, ion- and sublimation-pumped, orifice calibration system. The entire system goes through a bakeout and is sufficiently degassed to achieve an ultimate pressure of $\approx 5 \times 10^{-12}$ torr or less in both volumes, although this low background pressure is not absolutely necessary in the first volume. A flow Q_1 is admitted into $\mathcal{V}_1$, and the steady-state pressure is

$$p_1 = \frac{Q_1 + S_1 p_{01}}{S_1} \approx \frac{Q_1}{S_1} \tag{44}$$

where S_1 is the conductance-limited orifice in $\mathcal{V}_1$ or $S_1 << S_{p1}$ and p_{01} is the pressure in pump 1. When the valve is opened to $\mathcal{V}_2$, the flow Q_2 into that volume is controlled by the calibrated conductance C and given by $Q_2 = C(p_1 - p_2)$. The steady-state pressure in $\mathcal{V}_2$ is

$$p_2 = \frac{CQ_1 + CS_1 p_{01} + S_1 S_2 p_{02}}{S_1 S_2 + CS_1} \tag{45}$$

where S_2 is the conductance-limited orifice in $\mathcal{V}_2$, or $S_2 << S_{p2}$, and p_{02} is the pressure in pump 2. (S_{p1} and S_{p2} are the intrinsic pumping speeds in pumps 1 and 2.)

The magnitude of Q_1 could be a value that permitted a steady-state pressure of the calibrated gas as low as 5×10^{-10} torr (6.67×10^{-8} Pa). Thus, the capability of a calibration from 5×10^{-5} to 5×10^{-10} torr (6.67×10^{-3} to 6.67×10^{-8} Pa), or a range of five decades, was provided.

The parameter of interest that characterizes the instrument over the calibration range is the sensitivity. The sensitivity of an ion gauge (shown as gauge constant) for N_2 as determined by an orifice system is presented in figure 59. The relative variation of this instrument approaches 5 percent. Similar calibrations could also be obtained for a mass spectrometer. In general, the conditions under which the calibrations are conducted should be nearly identical to those that the instrument would experience in the system where it is to be used. For example, it is recommended that gauges and mass spectrometers in the system have the same envelope around the instrument as in the calibration system, especially the ion source, because the electron density around the grid can be substantially different and result in errors exceeding 30 percent.

The total uncertainty of the calibration is governed primarily by three factors. First, there is the uncertainty in the standard input flow, which may be controlled to about 2 percent. Then there is an uncertainty in the conductances to the pumps in $\mathcal{V}_1$ and $\mathcal{V}_2$ as well as the conductance between the two volumes. Finally, there is a concern about the difference in gas composition in the pumps compared with the main volumes, but this should only be a minor concern.

NASA Langley Research Center
Hampton, VA 23665-5225
July 20, 1989

References

1. Boyle, Robert: *New Experiments—Physico-Mechanicall, Touching the Spring of the Air, and Its Effects, (Made, for the Most Part, in a New Pneumatical Engine).* Oxford Univ., 1660.
2. Berman, A.: *Total Pressure Measurements in Vacuum Technology.* Academic Press, Inc., 1985.
3. Redhead, P. A.; Hobson, J. P.; and Kornelsen, E. V.: *The Physical Basis of Ultrahigh Vacuum.* Chapman and Hall Ltd. (London), c.1968.
4. Roth, A.: *Vacuum Technology,* Second, Revised ed. North-Holland Publ. Co., 1982.
5. O'Hanlon, John F.: *A User's Guide to Vacuum Technology.* John Wiley & Sons, Inc., c.1980.
6. Beams, J. W.; Spitzer, D. M., Jr.; and Wade, J. P., Jr.: Spinning Rotor Pressure Gauge. *Review Sci. Instrum.,* vol. 33, no. 2, Feb. 1962, pp. 151–155.
7. Fremerey, J. K.: Spinning Rotor Gauge. *J. Vac. Sci. & Technol. A,* second ser., vol. 3, no. 3, pt. II, May/June 1985, pp. 1715–1720.
8. Alpert, D.; Matland, C. G.; and McCoubrey, A. O.: A Null-Reading Absolute Manometer. *Review Sci. Instrum.,* vol. 22, no. 6, June 1951, pp. 370–371.
9. Pirani, M. V.: Selbstzeigendes Vakuum-Mefsinstrument (Self-Indicating Vacuum Gauge). *Dtsch. Phys. Ges. Verh.,* vol. 8, no. 24, Dec. 30, 1906, pp. 686–694.
10. Buckley, O. E.: An Ionization Manometer. *Proc. Natl. Acad. Sci.,* vol. 2, 1916, pp. 683–685.
11. Nottingham, W. B.: *Proceedings of the 7th Annual Conference on Physical Electronics.* M.I.T., 1947.
12. Bayard, Robert T.; and Alpert, Daniel: Extension of the Low Pressure Range of the Ionization Gauge. *Review Sci. Instrum.,* vol. 21, no. 6, June 1950, pp. 571–572.
13. Schulz, G. J.; and Phelps, A. V.: Ionization Gauges for Measuring Pressures up to the Millimeter Range. *Review Sci. Instrum.,* vol. 28, no. 12, Dec. 1957, pp. 1051–1054.
14. Penning, F. M.: Ein Neues Manometer fur Niedrige Gasdrucke, Insbesondere Zwischen 10^{-3} und 10^{-5} mm. *Physica,* vol. IV, 1937, pp. 71–75.
15. Redhead, P. A.: The Magnetron Gauge: A Cold-Cathode Vacuum Gauge. *Canadian J. Phys.,* vol. 37, no. 11, Nov. 1959, pp. 1260–1271.
16. Redhead, P. A.: Modulated Bayard-Alpert Gauge. *Review Sci. Instrum.,* vol. 31, no. 3, Mar. 1960, pp. 343–344.
17. Schuemann, W. C.: Ionization Vacuum Gauge With Photocurrent Suppression. *Review Sci. Instrum.,* vol. 34, no. 6, June 1963, pp. 700–702.
18. Redhead, P. A.: New Hot-Filament Ionization Gauge With Low Residual Current. *J. Vac. Sci. & Technol.,* vol. 3, no. 4, July/Aug. 1966, pp. 173–180.
19. Helmer, J. C.; and Hayward, W. H.: Ion Gauge for Vacuum Pressure Measurements Below 1×10^{-10} Torr. *Review Sci. Instrum.,* vol. 37, no. 12, Dec. 1966, pp. 1652–1654.
20. Conn, G. K. T.; and Daglish, H. N.: A Thermionic Ionization Gauge of High Sensitivity Employing a Magnetic Field. *J. Sci. Instrum.,* vol. 31, Nov. 1954, pp. 412–416.
21. Lafferty, J. M.: Hot-Cathode Magnetron Ionization Gauge for the Measurement of Ultrahigh Vacua. *J. Appl. Phys.,* vol. 32, no. 3, Mar. 1961, pp. 424–434.
22. Redhead, P. A.: The Townsend Discharge in a Coaxial Diode With Axial Magnetic Field. *Canadian J. Phys.,* vol. 36, no. 3, Mar. 1958, pp. 255–270.
23. Herb, R. G.; Pauly, T.; and Fisher, K. J.: Electrostatic Electron Containment. *Bull. American Phys. Soc.,* ser. II, vol. 8, no. 1, 1963, p. 336.
24. Dempster, A. J.: New Method of Positive-Ray Analysis. *Phys. Review,* vol. 11, Apr. 1918, pp. 316–325.
25. Nier, Alfred O.: A Mass Spectrometer for Routine Isotope Abundance Measurements. *Review Sci. Instrum.,* vol. 11, no. 7, July 1940, pp. 212–216.
26. Sommer, H.; Thomas, H. A.; and Hipple, J. A.: The Measurement of e/M by Cyclotron Resonance. *Phys. Review,* ser. 2. vol. 82, no. 5, June 1, 1951, pp. 679–702.
27. Alpert, D.; and Buritz, R. S.: Ultra-High Vacuum. II. Limiting Factors on the Attainment of Very Low Pressures. *J. Appl. Phys.,* vol. 25, no. 2, Feb. 1954, pp. 202–209.
28. Cameron, A. E.; and Eggers, D. F., Jr.: An Ion "Velocitron." *Review Sci. Instrum.,* vol. 19, no. 9, Sept. 1948, pp. 605–607.

29. Paul, W.; Reinhard, H. P.; and Von Zahn, U.: Das Elektrische Massenfilter als Massenspektrometer und Isotopentrenner. *Z. Phys.*, Bd. 152, Heft 2, 1958, pp. 143–182.
30. McSharrafa, M.: Mass Spectrometry in Clinical and Medical Research. *Res. Dev.*, vol. 21, no. 3, Mar. 1970, pp. 24–28.
31. *RCA Photomultiplier Manual.* Tech. Ser. PT-61, RCA Corp., c.1970.
32. Kurz, Edward A.: Channel Electron Multipliers. *American Lab.*, vol. 11, no. 3, Mar. 1979, pp. 67–70, 72–74, 76–78, 81–82.
33. American Vacuum Socity Standard (Tentative) AVS 2.3—1972, Procedure for Calibrating Gas Analyzers of the Mass Spectrometer Type. *J. Vac. Sci. & Technol.*, vol. 9, no. 5, Sept./Oct. 1972, pp. 1260–1274.
34. Knudsen, M.: Determination of Molecular Weights of Small Quantities of Gas or Vapour. *Ann. Phys.*, vol. 44, no. 4, June 4, 1914, pp. 525–536.
35. Hayward, W. H.; and Jepsen, R. L.: A Simple High Vacuum Gauge Calibration System. *1962 Transactions of the Ninth National Vacuum Symposium of the American Vacuum Society*, George H. Bancroft, ed., Macmillan Co., c.1962, pp. 459–462.

Table I. Pressure Conversions

FROM \ TO	1 ATM (NORMAL)	2 ATM (TECH)	3 mm Hg (0° C)	4 cm Hg (0°C)	5 in Hg (32°F)	6 in Hg (60°F)	7 cm H_2O (4°C)	8 in H_2O (39.2°F)	9 in H_2O (60°F)	10 ft H_2O (39.2°F)	11 BAR	12 deci BAR	13 milli BAR	14 DYNE/cm²	15 gmf/cm²	16 Kgf/m²	17 Kgf/cm²	18 Kgf/mm²	19 KSI (kip/in²)	20 POUNDAL/ft²	21 POUND f/ft²	22 PSI	23 TORR	24 MICRON	25 PASCAL
1 ATM (NORMAL)	1	1.033227	7.60E2	7.60E1	2.992126 E1	3.000577 E1	1.033266 E3	4.067937 E2	4.071894 E2	3.389947 E1	1.013250*	1.013250* E1	1.013250* E3	1.013250* E6	1.033227 E3	1.033227 E4	1.033227	1.033227 E-2	1.469695 E-2	6.808725 E4	2.116217 E3	1.469695 E1	7.60E2	7.60E5	1.01325* 10^6
2 ATM (TECH)	9.678411 E-1	1	7.355592 E2	7.355592 E1	2.895903 E1	2.904082 E1	1.000028 E3	3.937116 E2	3.940946 E2	3.280930 E1	9.806650 E-1	9.806650	9.806650 E2	9.806650 E5	1.0E+3	1.0E+4	1.0	1.0E-2	1.422334 E-2	6.569764 E4	2.048161 E3	1.422334 E1	7.355592 E2	7.355592 E5	9.806650* E4
3 mm Hg (0°C)	1.315789 E-3	1.359510 E-3	1	10	3.937008 E-2	3.948128 E-2	1.359547	5.352548 E-1	5.357755 E-1	4.460457 E-2	1.333224 E-3	1.333224 E-2	1.333224	1.333224 E3	1.359510	1.359510 E1	1.359510 E-3	1.359510 E-5	1.933678 E-5	8.958849 E1	2.784495	1.933678 E-2	1.0	1.0 E3	1.333224 E2
4 cm Hg (0°C)	1.315789 E-2	1.359510 E-2	1.0 E1	1	3.937008 E-1	3.948128 E-1	1.359547 E1	5.352548	5.357755 E-1	4.460457 E-1	1.333224 E-2	1.333224 E-1	1.333224 E1	1.333224 E4	1.359510 E1	1.359510 E2	1.359510 E-2	1.359510 E-4	1.933678 E-4	8.958849 E2	2.784495 E1	1.933678 E-1	1.0 E1	1.0 E4	1.333224 E 3
5 in Hg (32°F)	3.342105 E-2	3.453155 E-2	2.540 E1	2.540	1	1.002825	3.453250 E1	1.359547 E1	1.360870 E1	1.132956	3.386388 E-2	3.386388 E-1	3.386388 E1	3.386388 E4	3.453155 E1	3.453155 E2	3.453155 E-2	3.453155 E-4	4.911541 E-4	2.275548 E3	7.072618 E1	4.911541 E-1	2.540 E1	2.540 E4	3.386388 E3
6 in Hg (60°F)	3.332692 E-2	3.443429 E-2	2.532846 E1	2.532846	9.971834 E-1	1	3.443524 E1	1.355718 E1	1.357037 E1	1.129765	3.376850 E-2	3.376850 E-1	3.376850 E1	3.376850 E4	3.443429 E1	3.443429 E2	3.443429 E-2	3.443429 E-4	4.897707 E-4	2.269138 E3	7.052698 E1	4.897707 E-1	2.532846 E1	2.532846 E4	3.37685 E3
7 cm H_2O (4°C)	9.678145 E-4	9.999725 E-4	7.355390 E-1	7.355390 E-2	2.895823 E-2	2.904002 E-2	1	3.937008 E-1	3.940837 E-1	3.280840 E-2	9.806360 E-4	9.806380 E-3	9.806380 E-1	9.806380 E2	9.999725 E-1	9.999725	9.999725 E-4	9.999725 E-6	1.422295 E-5	6.589583 E1	2.048105	1.422295 E-2	7.355390 E-1	7.355390 E2	9.80638 E1
8 in H_2O (39.2°F)	2.458249 E-3	2.539930 E-3	1.868269	1.868269 E-1	7.355390 E-2	7.376166 E-2	2.540	1	1.000973	8.333333 E-2	2.490820 E-3	2.490820 E-2	2.490820	2.490820 E3	2.539930	2.539930 E1	2.539930 E-3	2.539930 E-5	3.612630 E-5	1.673754 E2	5.202187	3.612630 E-2	1.868269	1.868269 E3	2.49082 E2
9 in H_2O (60°F)	2.455860 E-3	2.537462 E-3	1.866453	1.866453 E-1	7.348242 E-2	7.368898 E-2	2.537532	9.990282 E-1	1	8.325235 E-2	2.488400 E-3	2.488400 E-2	2.488400	2.488400 E3	2.537462	2.537462 E1	2.537462 E-3	2.537462 E-5	3.609119 E-5	1.672128 E2	5.197131	3.609119 E-2	1.866453	1.866453 E3	2.4884 E2
10 ft H_2O (39.2°F)	2.949898 E-2	3.047918 E-2	2.241923 E1	2.241923	8.826468 E-1	8.851399 E-1	3.048000 E1	1.20E1	1.201167 E1	1	2.988985 E-2	2.988985 E-1	2.988985 E1	2.988985 E4	3.047916 E1	3.047916 E2	3.047916 E-2	3.047916 E-4	4.335156 E-4	2.008508 E3	6.242624 E1	4.335156 E-1	2.241923 E1	2.241923 E4	2.988985 E3
11 BAR	9.869233 E-1	1.019716	7.500617 E2	7.500617 E1	2.952999 E1	2.961340 E1	1.019744 E3	4.014741 E2	4.018647 E2	3.345618 E1	1	1.0E1	1.0E3	1.0E6	1.019716 E3	1.019716 E4	1.019716	1.019716 E-2	1.019716 E-3	6.719689 E4	2.088543 E3	1.450377 E1	7.500617 E2	7.500617 E5	1.0E5
12 deci BAR	9.869233 E-2	1.019716 E-1	7.500617 E1	7.500617	2.952999	2.961340	1.019744 E2	4.014741 E1	4.018647 E1	3.345618	1.0E-1	1	1.0E2	1.0E5	1.019716 E2	1.019716 E3	1.019716 E-1	1.019716 E-3	1.450377 E-3	6.719689 E3	2.088543 E2	1.450377	7.500617 E1	7.500617 E4	1.0E4
13 milli BAR	9.869233 E-4	1.019716 E-3	7.500617 E-1	7.500617 E-2	2.952999 E-2	2.961340 E-2	1.019744	4.014741 E-1	4.018647 E-1	3.345618 E-2	1.0E-3	1.0E-2	1	1.0E3	1.019716	1.019716 E1	1.019716 E-3	1.019716 E-5	1.450377 E-5	6.719689 E1	2.088543	1.450377 E-2	7.500617 E-1	7.500617 E2	1.0E2
14 DYNE/cm²	9.869233 E-7	1.019716 E-6	7.500617 E-4	7.500617 E-5	2.952999 E-5	2.961340 E-5	1.019744 E-3	4.014741 E-4	4.018647 E-4	3.345618 E-5	1.0E-6	1.0E-5	1.0E-3	1	1.019716 E-3	1.019716 E-2	1.019716 E-6	1.019716 E-8	1.450377 E-8	6.719689 E-2	2.088543 E-3	1.450377 E-5	7.500617 E-4	7.500617 E-1	1.0E-1
15 gmf/cm²	9.678411 E-4	1.0E-3	7.355592 E-1	7.355592 E-2	2.895903 E-2	2.904082 E-2	1.000028	3.937116 E-1	3.940946 E-1	3.280930 E-2	9.806650 E-4	9.806650 E-3	9.806650 E-1	9.806650 E2	1	1.0E1	1.0E-3	1.0E-5	1.422334 E-5	6.589764 E1	2.048161	1.422334 E-2	7.355592 E-1	7.355592 E2	9.806650* E1
16 Kgf/M²	9.678411 E-5	1.0E-4	7.355592 E-2	7.355592 E-3	2.895903 E-3	2.904082 E-3	1.000028 E-1	3.937116 E-2	3.940946 E-2	3.280930 E-3	9.806650 E-5	9.806650 E-4	9.806650 E-2	9.806650 E1	1.0E-1	1	1.0E-4	1.0E-6	1.422334 E-6	6.589764	2.048161 E-1	1.422334 E-3	7.355592 E-2	7.355592 E1	9.806650*
17 Kgf/cm²	9.678411 E-1	1.0	7.355592 E1	7.355592 E1	2.895903 E1	2.904082 E1	1.000028 E3	3.937116 E2	3.940946 E2	3.280930 E1	9.806650 E-1	9.806650	9.806650 E2	9.806650 E5	1.0E3	1.0E4	1	1.0E-2	1.422334 E-2	6.589764 E4	2.048161 E3	1.422334 E1	7.355592 E2	7.355592 E5	9.806650* E4
18 Kgf/mm²	9.678411 E+1	1.0E2	7.355592 E4	7.355592 E3	2.895903 E3	2.904082 E3	1.000028 E5	3.937116 E4	3.940946 E4	3.280930 E3	9.806650 E1	9.806650 E2	9.806650 E4	9.806650 E7	1.0E 5	1.0E6	1.0E2	1	1.422334	6.589764 E6	2.048161 E5	1.422334 E3	7.355592 E4	7.355592 E7	9.806650* E6
19 KSI (kip/in²)	6.804598 E1	7.030695 E1	5.171493 E4	5.171493 E3	2.036021 E3	2.041772 E3	7.030889 E4	2.768067 E4	2.770759 E4	2.306722 E3	6.894757 E1	6.894757 E2	6.894757 E4	6.894757 E7	7.030695 E4	7.030695 E5	7.030695 E1	7.030695 E-1	1	4.633063 E6	1.440 E5	1.0E3	5.171493 E4	5.171493 E7	6.894757 E6
20 POUNDAL ft²	1.488704 E-5	1.517505 E-5	1.116215 E-2	1.116215 E-3	4.394548 E-4	4.406959 E-4	1.517547 E-2	5.974594 E-3	5.980405 E-3	4.978828 E-4	1.488164 E-5	1.488164 E-4	1.488164 E-2	1.488164 E1	1.517505 E-2	1.517505 E-1	1.517505 E-5	1.517505 E-7	2.158399 E-7	1	3.108095 E-2	2.158399 E-4	1.116215 E-2	1.116215 E1	1.488164
21 POUND f/ft²	4.725414 E-4	4.882428 E-4	3.591315 E-1	3.591315 E-2	1.413904 E-2	1.417897 E-2	4.882562 E-1	1.922289 E-1	1.924138 E-1	1.601890 E-2	4.788026 E-4	4.788026 E-3	4.788026 E-1	4.788026 E2	4.882428 E-1	4.882428	4.882428 E-4	4.882428 E-6	6.944445 E-6	3.217405 E1	1	6.944445 E-3	3.591315 E-1	3.591315 E2	4.788026 E1
22 PSI	6.804596 E-2	7.030695 E-2	5.171493 E1	5.171493	2.036021	2.041772	7.030889 E1	2.768067 E1	2.770759 E1	2.306722	6.894757 E-2	6.894757 E-1	6.894757 E1	6.894757 E4	7.030695 E1	7.030695 E2	7.030695 E-2	7.030695 E-4	1.0E-3	4.633063 E3	1.440 E2	1	5.171493 E1	5.171493 E4	6.894757 E3
23 TORR	1.315789 E-3	1.359510 E-3	1.0	1.0E-1	3.937008 E-2	3.948128 E-2	1.359547	5.352548 E-1	5.357755 E-1	4.460457 E-2	1.333224 E-3	1.333224 E-2	1.333224	1.333224 E3	1.359510	1.359510 E1	1.359510 E-3	1.359510 E-5	1.933678 E-5	8.958849 E1	2.784495	1.933678 E-2	1	1.0E-3	1.333224 E2
24 MICRON	1.315789 E-6	1.359510 E-6	1.0E-3	1.0E-4	3.937008 E-5	3.948128 E-5	1.359547 E-3	5.352548 E-4	5.357755 E-4	4.460457 E-5	1.333224 E-6	1.333224 E-5	1.333224 E-3	1.333224	1.359510 E-3	1.359510 E-2	1.359510 E-3	1.359510 E-8	1.933678 E-8	8.958849 E-2	2.784495 E-3	1.933678 E-5	1.0 E-3	1	1.333224 E-1
25 PASCAL	9.869233 E-6	1.019716 E-5	7.500617 E-3	7.500617 E-4	2.952999 E-4	2.961340 E-4	1.019744 E-2	4.014741 E-3	4.018647 E-3	3.345618 E-4	1.0E-5	1.0E-4	1.0E-2	1.0E1	1.019716 E-2	1.019716 E-1	1.019716 E-5	1.019716 E-7	1.450377 E-7	6.719689 E-1	2.088543 E-2	1.450377 E-4	7.500617 E-3	7.500617	1

* EXACT

· BY DEFINITION

Table II. Vacuum Ranges

Vacuum range	Pressure units	
	Torr	Pa
Low	25 to 760	3.3×10^3 to 10^5
Medium	7.5×10^{-3} to 25	10^{-1} to 3.3×10^3
High	7.5×10^{-7} to 7.5×10^{-4}	10^{-4} to 10^{-1}
Very high	7.5×10^{-10} to 7.5×10^{-7}	10^{-7} to 10^{-4}
Ultrahigh	7.5×10^{-13} to 7.5×10^{-10}	10^{-10} to 10^{-7}
Extreme ultrahigh	$p < 7.5 \times 10^{-13}$	$p < 10^{-10}$

Table III. Relative Ionization Gauge Sensitivities

[$S(x)$ is gauge sensitivity for x]

x	$\frac{S(x)}{S(\mathrm{Ar})}$
Ar	1.00
He	.16
Ne	.20
Kr	1.60
Xe	2.30
H_2	.37
N_2	.80
O_2	.90
Hg	2.50
Air	.80
CO	.90
CO_2	1.20
H_2O	.80
Organics	2–5

Table IV. Gauge Pumping Speed For Various Gases (Reprinted With Permission From Chapman and Hall Ltd., London; *The Physical Basis of Ultrahigh Vacuum*, 1968)

Gauge	Pumping speed, liters/sec								
	He	Ne	Ar	Kr	Xe	H_2	N_2	O_2	CO
Bayard-Alpert	10^{-2}						1×10^{-1}		
	4×10^{-3}								
	6.2×10^{-3}	7.0×10^{-3}	1.7×10^{-2}	5.2×10^{-2}	6.05×10^{-2}				
	1.1×10^{-2}	1.2×10^{-2}	2.9×10^{-2}	6.9×10^{-2}	9.1×10^{-2}				
	1.18×10^{-2}								
	1.7×10^{-3}		7.2×10^{-3}	1.2×10^{-2}					
	6×10^{-5}		6×10^{-4}	1×10^{-3}					
							1.8×10^{-1}		
							5×10^{-1}		
							3×10^{-1}	2.5	
							2		
							2.5×10^{-1}		
							8×10^{-1}		30
							20		
						8×10^{-1}			
						2.5×10^{-1}			
Magnetron	1.7×10^{-1}		1.7			2.0	2.5		
Magnetron	2×10^{-1}						1.4×10^{-1}	1.5×10^{-1}	
Magnetron	1×10^{-1}						1×10^{-1}	1.2×10^{-1}	
Inverted magnetron	3×10^{-2}		2.5×10^{-1}				7.5×10^{-1}		

Table V. Ionization Gauge Characteristics (Reprinted With Permission From American Institute of Physics, New York, N.Y.; *The History of Vacuum Science and Technology,* 1984)

[All pressures are equivalent nitrogen; p = Pressure; I = Current]

Gauge	Pressure range[a], torr	I, A[b]	Sensitivity
Hot cathode:			
Bayard-Alpert (BAG)	10^{-4} to 4×10^{-12}	4×10^{-3}	[c]42
Modulated BAG	10^{-4} to 10^{-13}	4×10^{-3}	[c]42
Extractor	2×10^{-4} to 1.5×10^{-12} 10^{-5} to 10^{-16}[d]	1.85×10^{-3}	[c]6
Bent beam	10^{-5} to 3×10^{-14} 10^{-5} to 10^{-16}[d]	3×10^{-3}	[c]40
Hot-cathode magnetron	10^{-6} to 10^{-18}[d]	3.5×10^{-9}	[c]10^4
Cold cathode:			
Inverted magnetron	10^{-4} to 3×10^{-12}		[e]0.31
Magnetron	10^{-5} to 5×10^{-13}		[e]3.0

[a]Range of linear pressure versus ion-current response.
[b]Electron emission, A.
[c]Sensitivity factor for nitrogen, $torr^{-1}$.
[d]Electron multiplier used.
[e]Sensitivity factor for nitrogen, $A\text{-}torr^{-1}$.

Table VI. Representative Fragmentation Patterns, UTI Model 100C (Reprinted With Permission From Uthe Technology, Inc., Milpitas, Calif.)

[Electron energy = 70 V; Ion energy = 15 V; Focus = −20 V; Filament emission = 2.5 mA; Resolution potential = 5.00]

amu	Hydrogen (H_2)	Methane (CH_4)	Acetylene (C_2H_4)	Ethylene (C_2H_4)	Carbon monoxide (CO)	Nitrogen (N_2)	Diborane (B_2H_6)	Ethane (C_2H_6)	Silane (SiH_4)	Oxygen (O_2)	Phosphine (PH_3)	Argon (Ar)
1	2.7	3.8	3.8	6.4			21.1	3.2				
2	100	0.64	1.2	1.1			134.7	0.93				
3	0.31	0.0068	0.0017	0.022			0.347	0.15				
4												
5												
6		0.00029	0.00061	0.00022	0.0008							
7		0.0013		0.0018		0.00056				0.0013		
8					0.0001							
9												
10							9.72					
11							39.4					
12		2.1	4.5	2.3	3.5		26.4	0.47				
13		7.4	7.6	4.0			34.9	1.1				
14		15	0.86	8.1	1.4	9.0	2.23	3.4	0.4			
14.5								0.24	0.5			
15		83				0.026		5.7	0.4			
15.5									0.1		0.229	
16		100			1.4			0.53		14	0.619	
16.5											0.133	
17		1.3								0.0052	0.476	
18										0.028		0.071
19												0.016
20							0.223					5.0
21							1.85					
22							11.8					
23							48.5					
24			7.1	3.2			94.0	0.52				
25			23	12			57.7	3.5				
26			100	61			100	24				
27			2.5	59			95.2	33				
28				100	100	100	16.7	100	28			
29				2.8	1.2	0.71		21	32			
30					0.20	0.0014		24	100			
31								0.54	80		26.7	
32									7.3	100	100	
33									1.5	0.074	25.2	
34									0.2	0.38	76.7	
35												
36										0.0023		0.36
37												
38												0.068
39												
40												100

Table VI. Concluded

amu	Carbon dioxide (CO_2)	Methyl mercapton (CH_3SH)	Cyclo-propane (C_3H_6)	Cis, trans 2-butene (C_4H_8)	n-butane (n-C_4H_{10})	1-butane (1-C_4H_{10})	Carbonyl sulfide (COS)	Disilane (Si_2H_6)	Diphosphine (P_2H_4)	Arsine (AsH_3)	Krypton (Kr)	n-hexane (n-C_6H_{14})
1		47	1.4	0.71	1.4	1.1						0.93
2		43	32	20	0.62	0.40						42
3		0.32	0.096	0.032	0.025	0.016						0.036
4												
5												
6	0.0005	0.00072	0.000037	0.000031			0.0013					0.00007
7		0.0016	0.000049	0.000031								0.000075
8	0.00046											
9												
10												
11												
12	6.3	7.3	0.85	0.28	0.13	0.13	19					0.26
13	0.063	13	1.6	0.32	0.26	0.27						0.28
14		29	5.6	1.5	1.1	1.3	3.2					0.17
15		100	8.1	4.9	7.8	8.7						7.6
16	13	92	2.0	2.3	0.49	0.65	6.5					3.4
17			0.073	0.22								0.34
18	0.0088											
19			2.7	0.017								
19.5			1.3	0.0054	0.0086	0.013						
20			2.3	0.18								
20.5			0.68	0.0028	0.0058	0.011						0.0051
21												0.0044
22	0.52						0.047					
22.5	0.0047	0.099										
23	0.0012											
23.5		0.27										
24		0.21	0.35	0.12	0.0062	0.035						0.11
25			2.1	1.3	0.35	0.17						0.44
26			17	14	7.8	3.3						6.1
27			46	38	55	4.1						56
28	15		18	52	47	4.4	100					30
29	0.15		11	23	61	8.9	0.83					77
30	0.029		0.29	0.57	1.3	0.20	2.9					2.0
31												0.056
32		7.6					55					
32.5												0.013
33		7.8										0.025
33.5												0.0087
34		4.1					2.1					0.0062
34.5												0.0012
35		7.0										0.00084
36		3.8	1.4	0.15	0.033	0.057						0.028
37		0.77	11	2.3	0.99	1.4						0.44
38			15	4.2	2.3	3.3						1.6
39			69	40	18	23						25
40			80	9.9	2.3	3.3					0.078	2.0
41			100	100	39	55					0.50	100
41.5											2.6	
42			90	3.4	16	39					2.6	46
43			18	0.51	100	100					12	76
44	100	6.3		0.26	3.3	3.2	8.7				3.6	2.6
45	1.2	38		0.0058			0.11					0.029
46	0.38	8.0					0.15					
47	0.0034	57										0.0034
48	0.00054	45		0.18	0.022	0.016						0.039
49	0.000043	3.4		1.4	0.26	0.18						0.69
50		2.1		5.7	1.2	0.84						

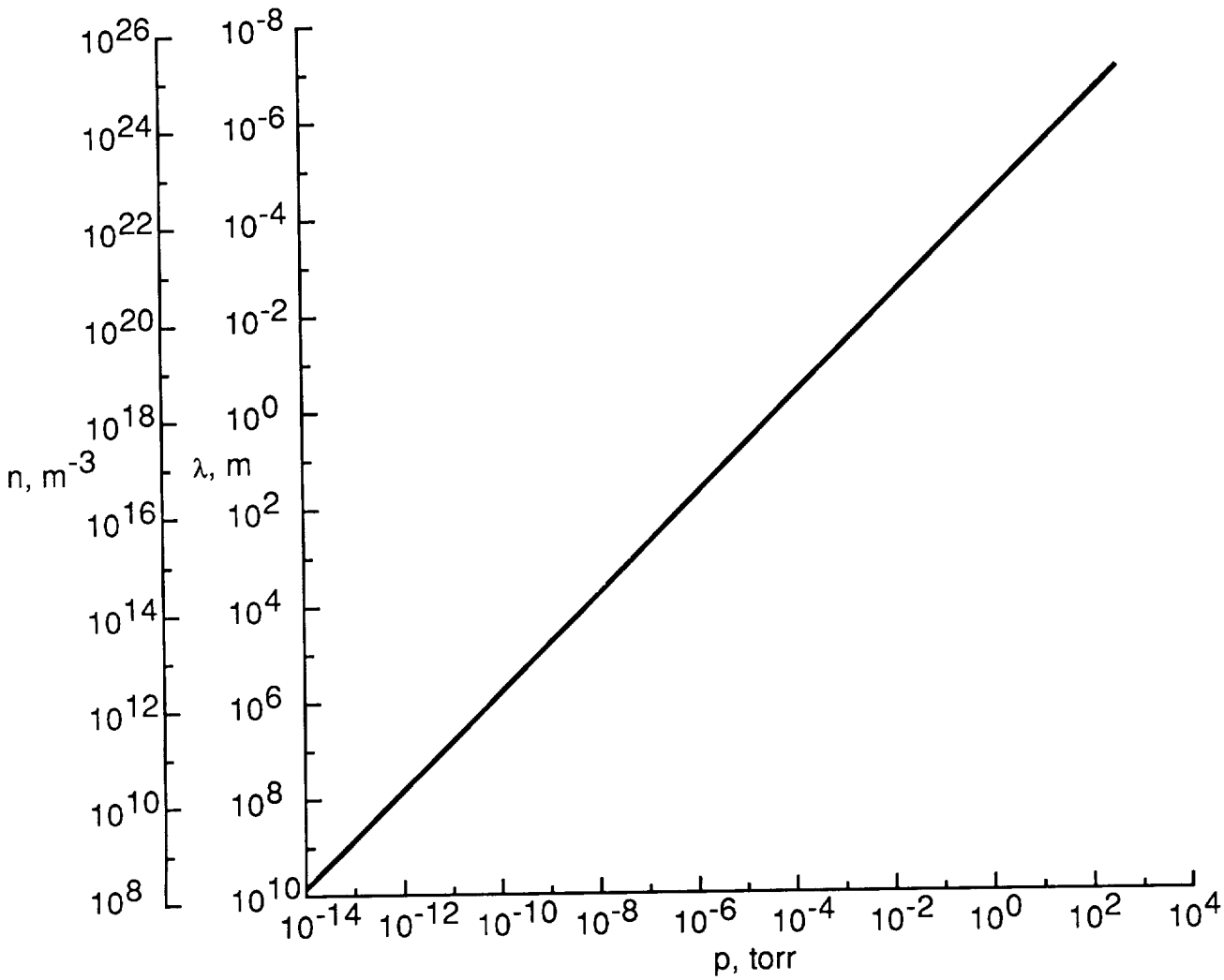

Figure 1. Number density and mean-free path as a function of pressure.

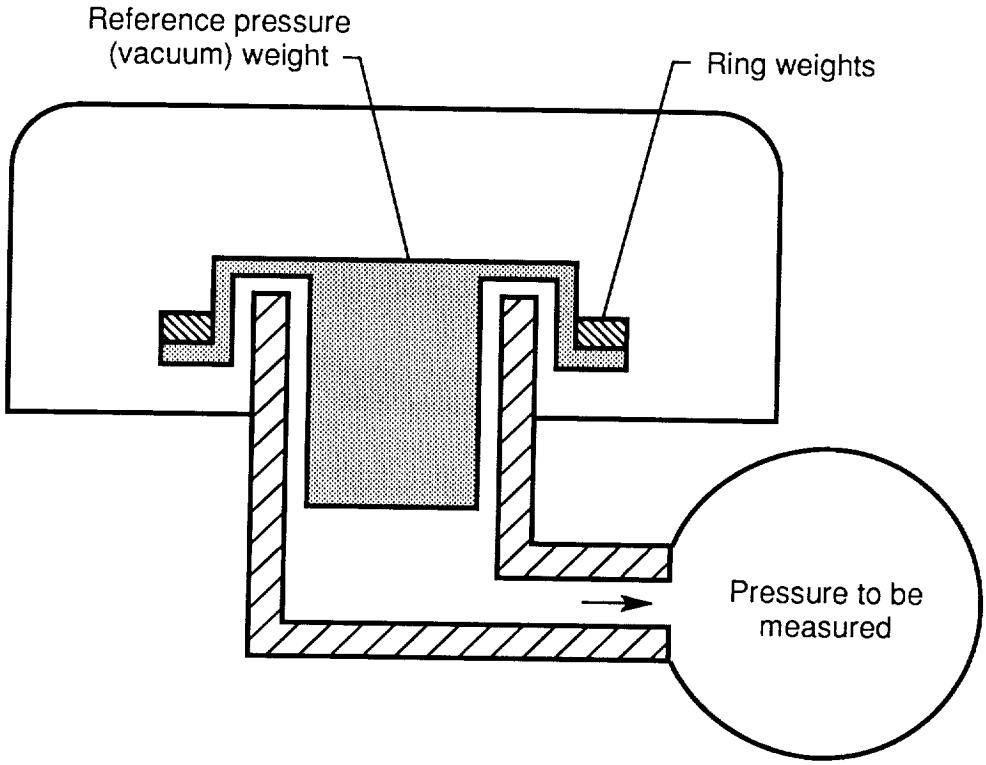

Figure 2. Deadweight tester.

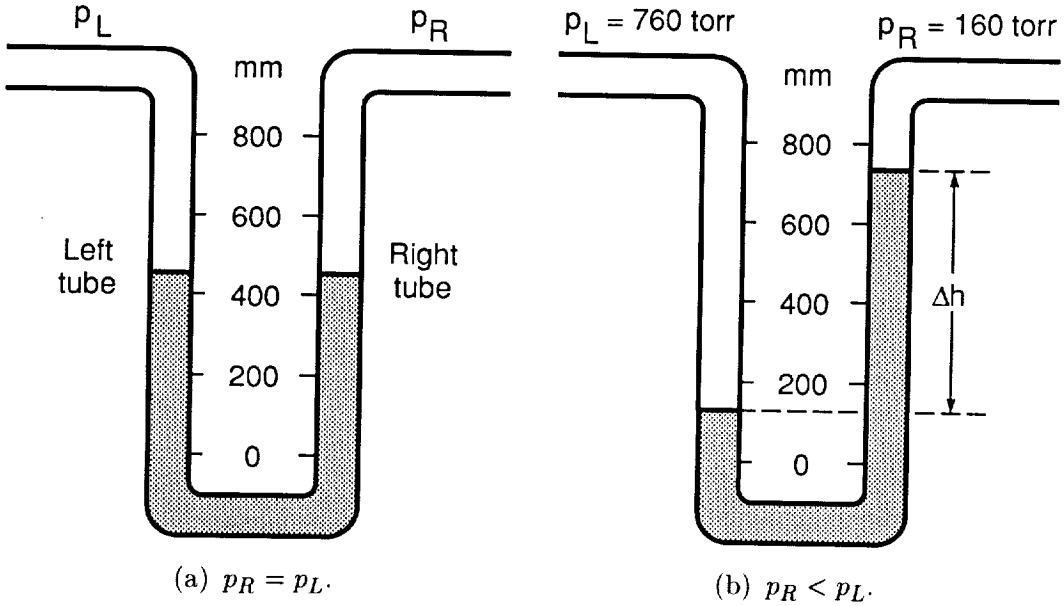

(a) $p_R = p_L$.

(b) $p_R < p_L$.

Figure 3. U-tube manometer.

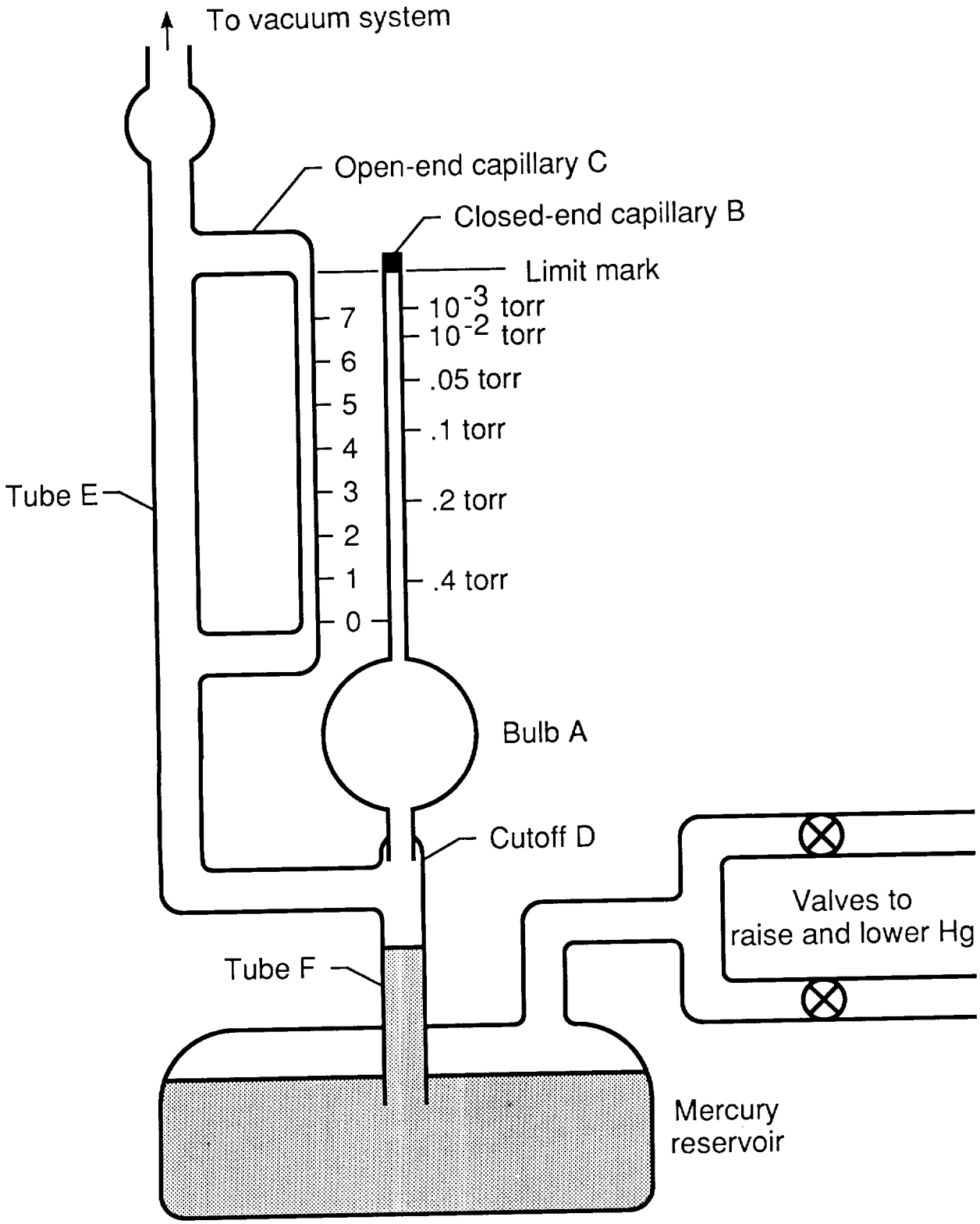

(a) In equilibrium with unknown pressure.

Figure 4. McLeod gauge.

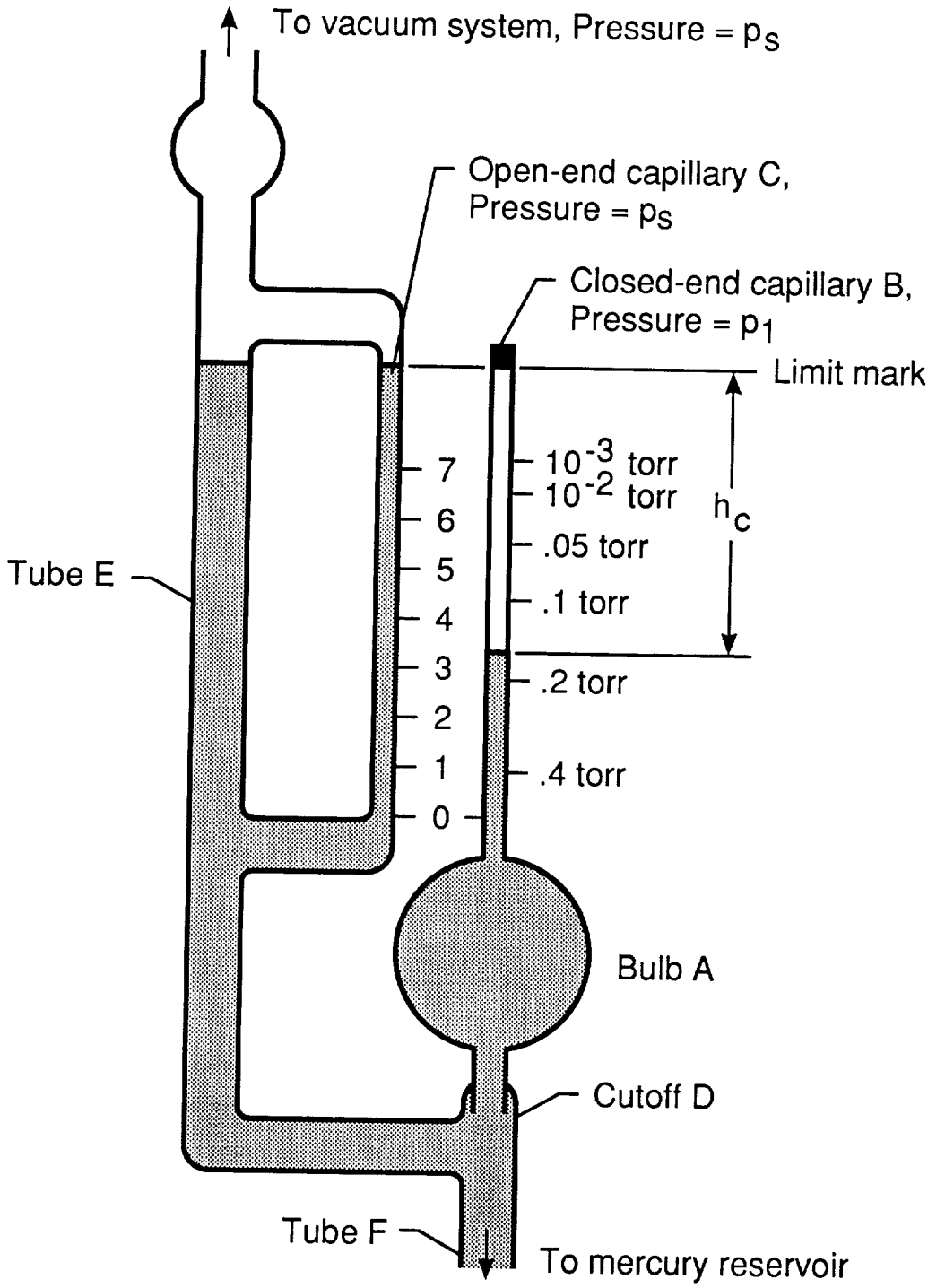

(b) Raised mercury level during measurement.

Figure 4. Concluded.

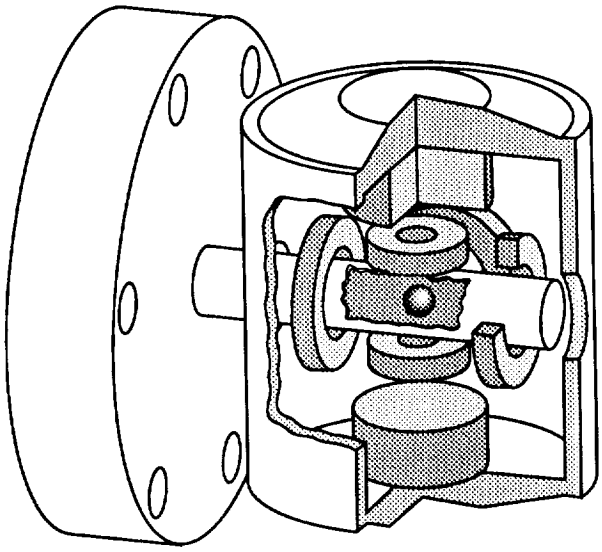

(a) Assembly.

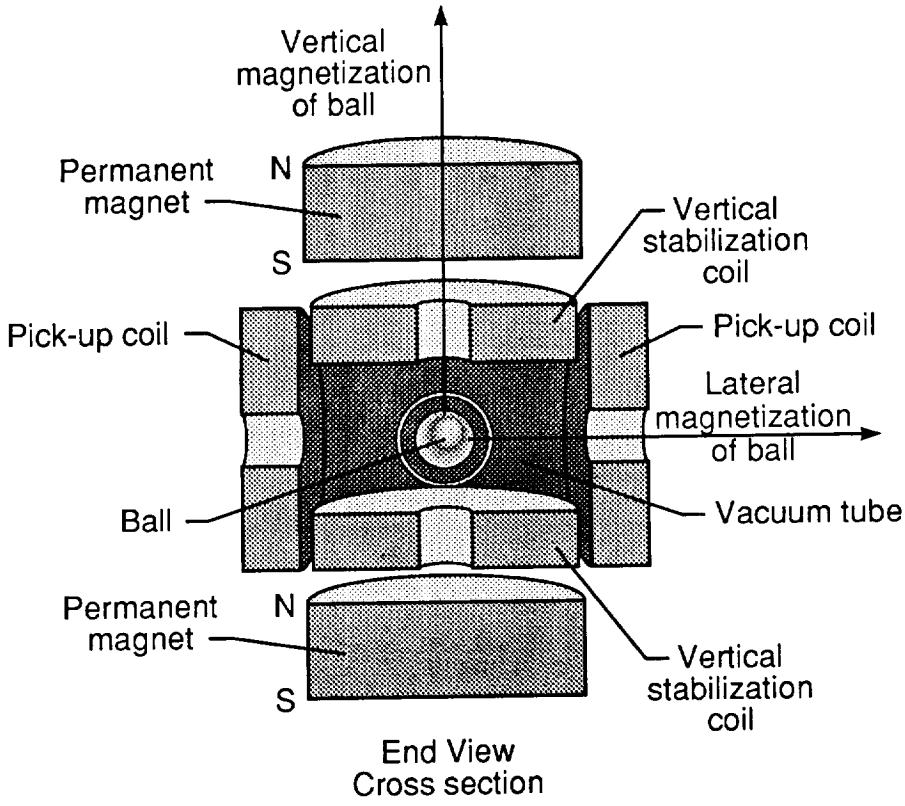

(b) Cross section.

Figure 5. Spinning-rotor gauge. (Reprinted with permission from MKS Instruments, Inc., Burlington, Mass.)

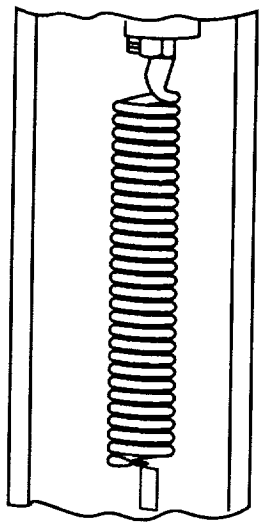

(a) Quartz element.

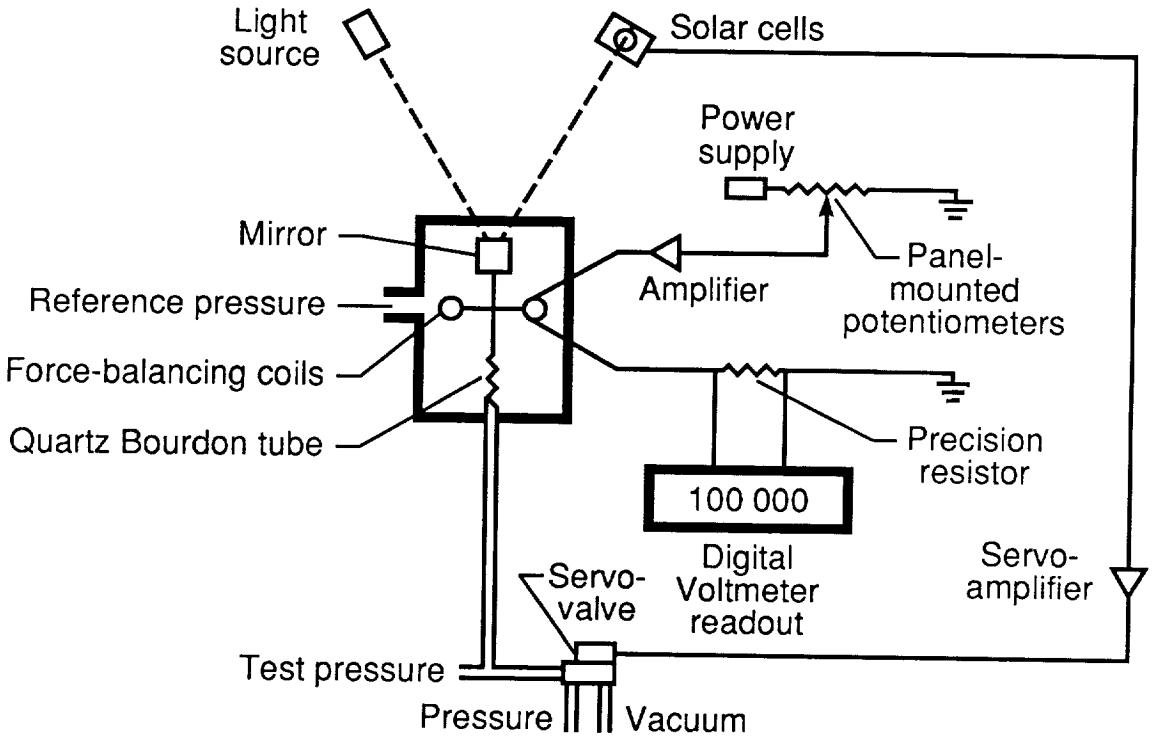

(b) Instrument schematic.

Figure 6. Quartz Bourdon tube.

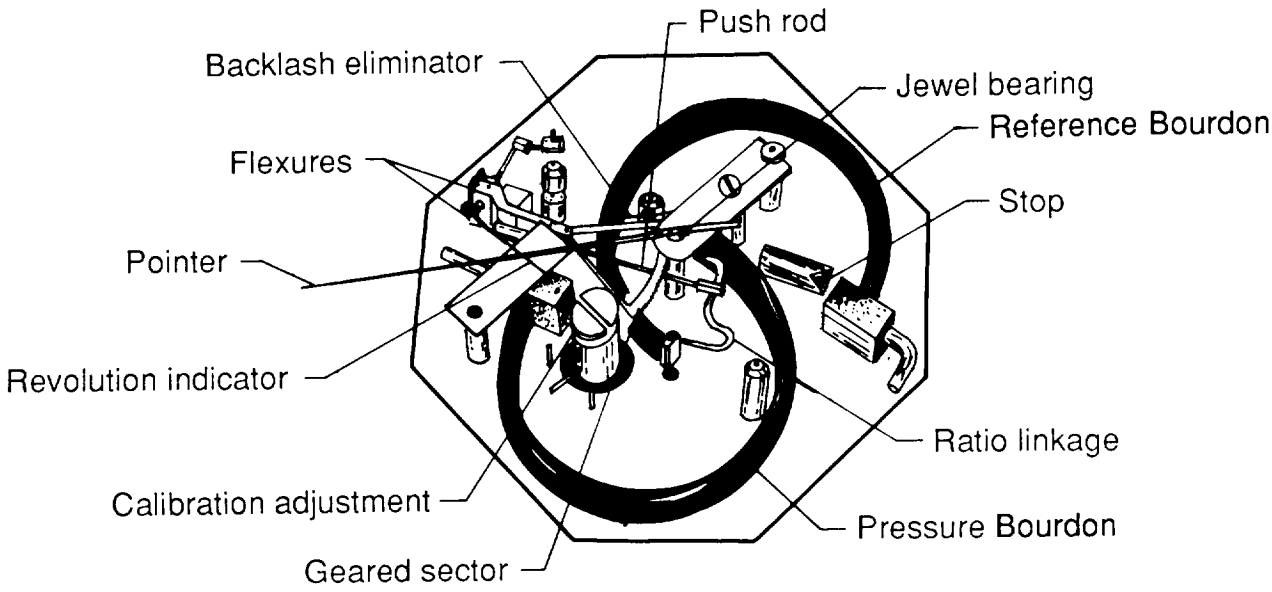

Figure 7. Bourdon tube mechanism for absolute pressure measurement. (Reprinted with permission from the Wallace and Tiernan Division, Belleville. N.J.)

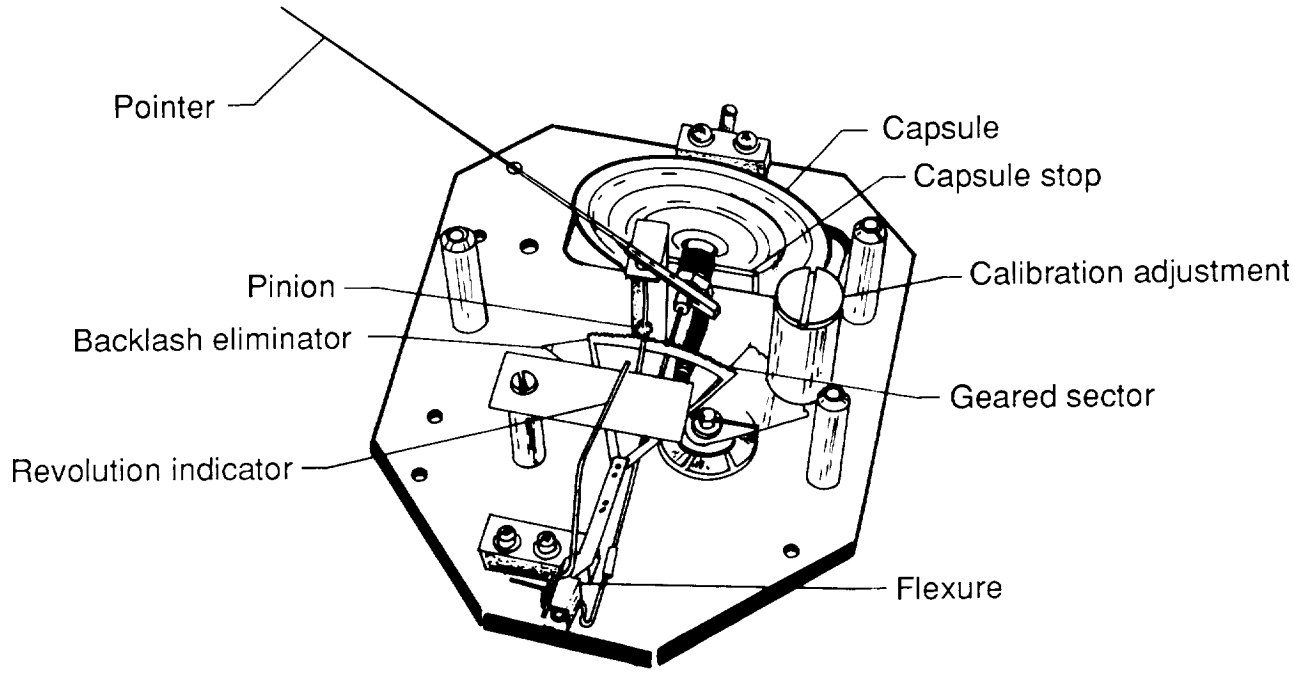

Figure 8. Diaphragm mechanism for absolute pressure measurement. (Reprinted with permission from the Wallace and Tiernan Division, Belleville, N.J.)

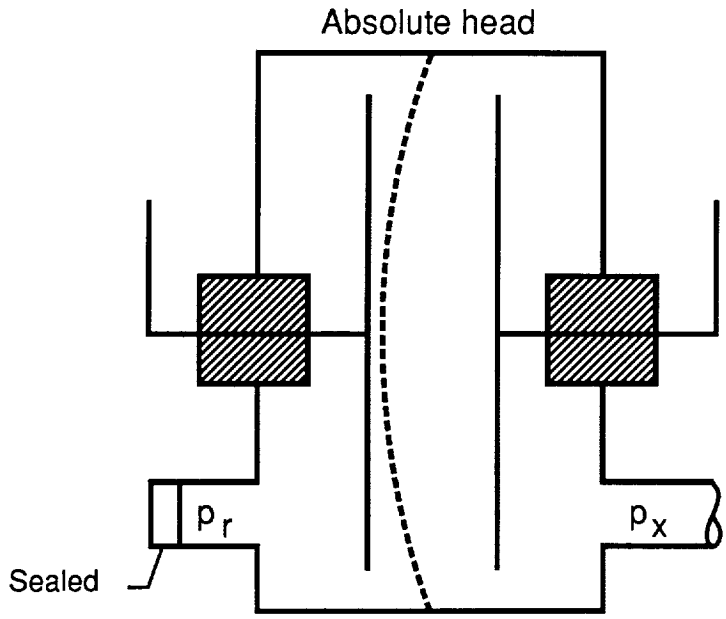

(a) $p_r << p_x$.

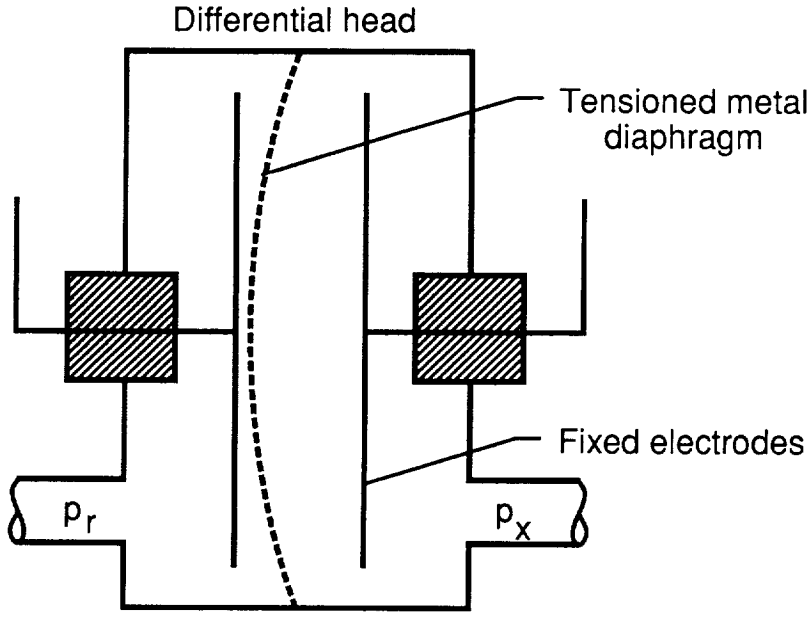

(b) $p_r < p_x$.

Figure 9. Schematic of capacitance manometers. p_r = Reference pressure; p_x = Unknown pressure.

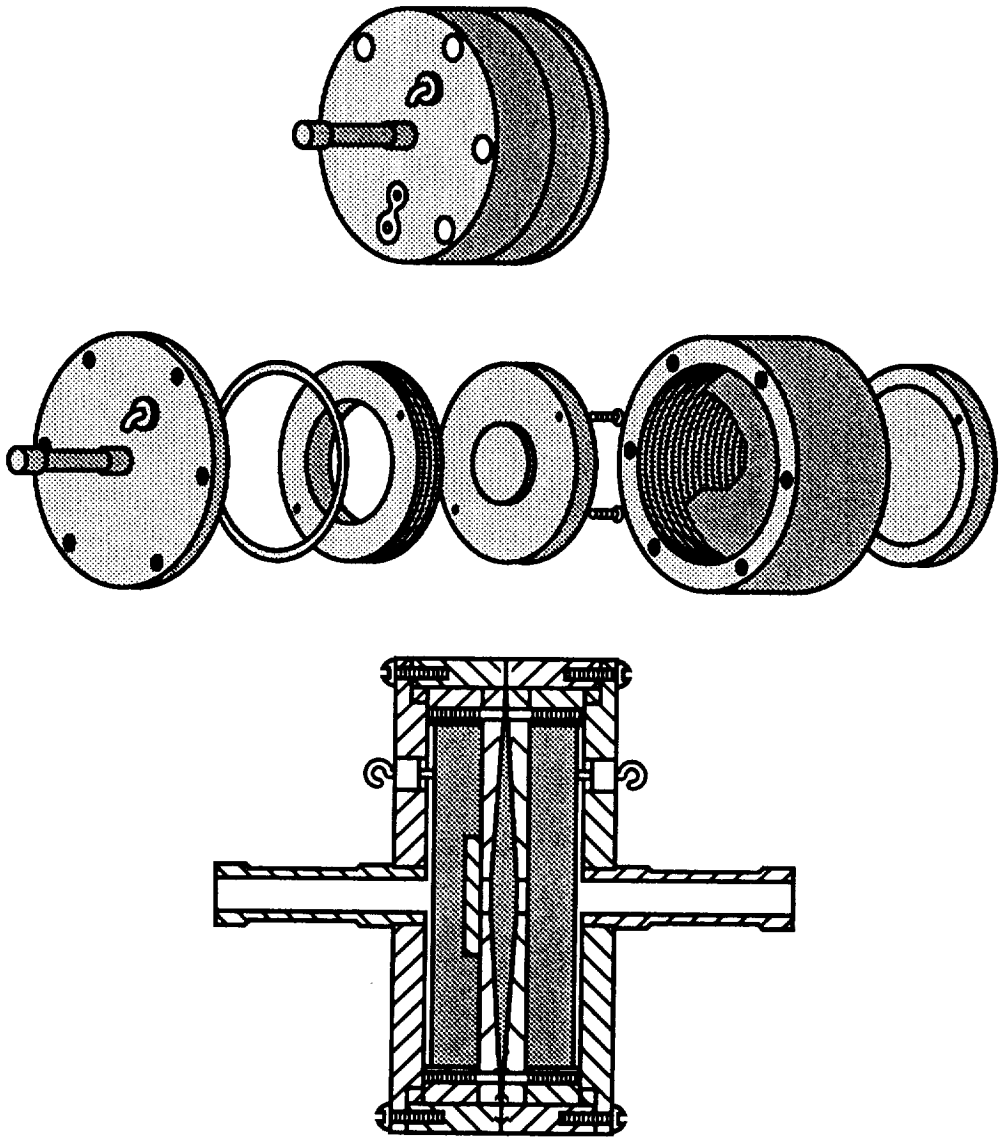

Figure 10. Partially welded double-sided sensor. (Reprinted with permission from MKS Instruments, Inc., Burlington, Mass.)

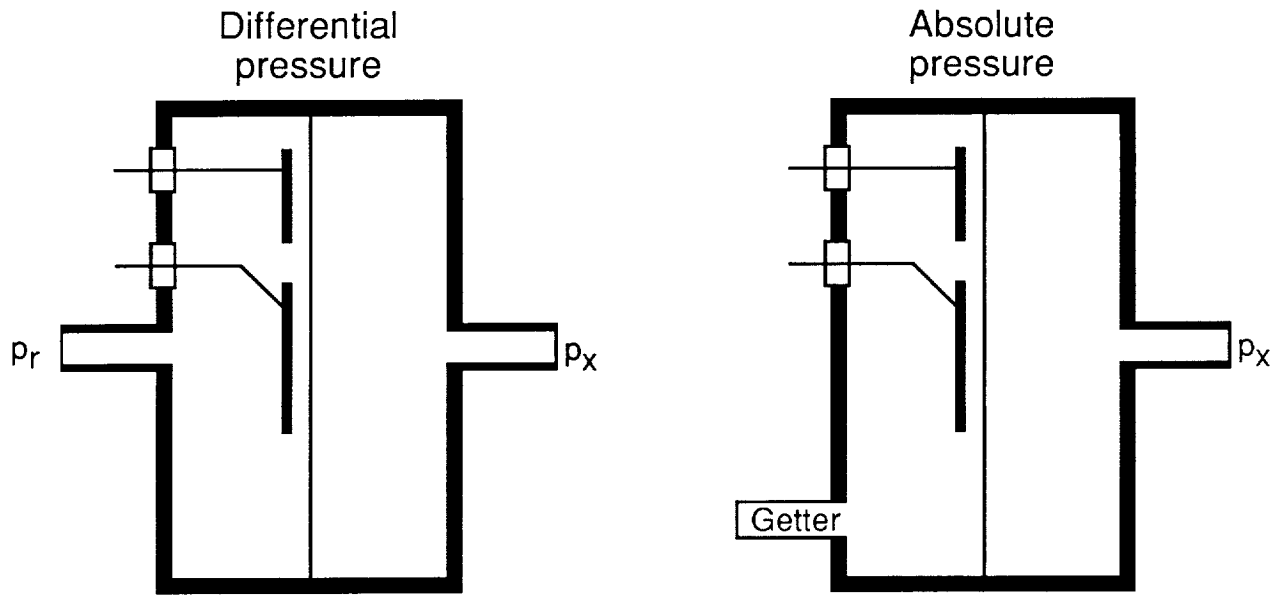

Figure 11. Single-sided dual-electrode capacitance manometer. p_r = Reference pressure; p_x = Unknown pressure. (Reprinted with permission from MKS Instruments, Inc., Burlington, Mass.)

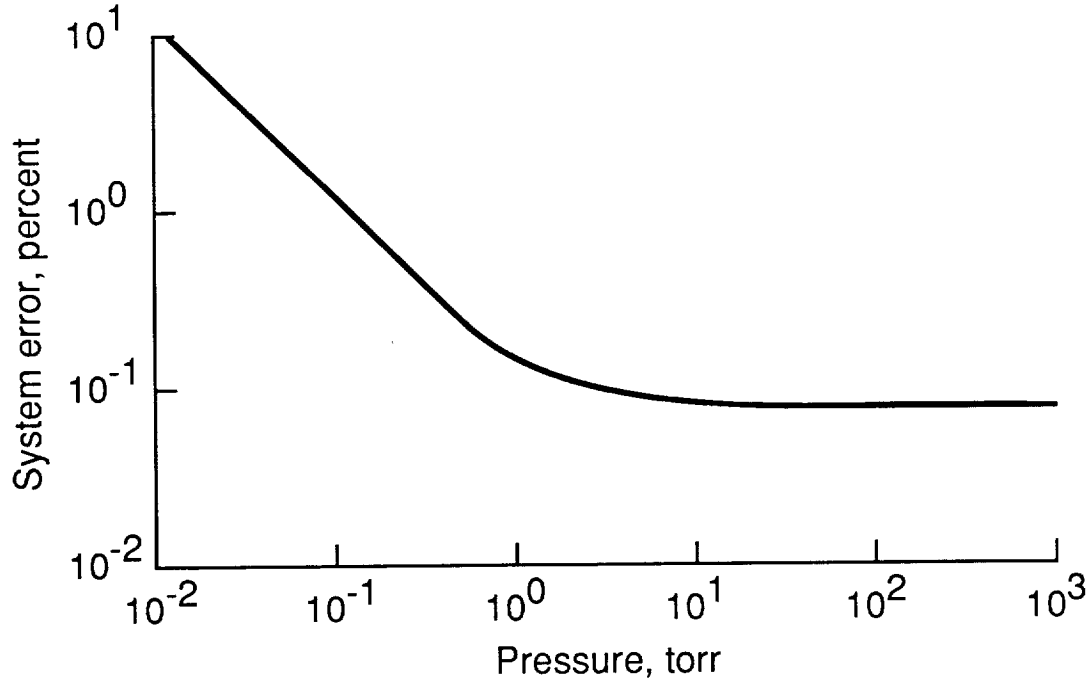

Figure 12. Capacitance manometer measurement error. (Reprinted with permission from R&D, January 1976.)

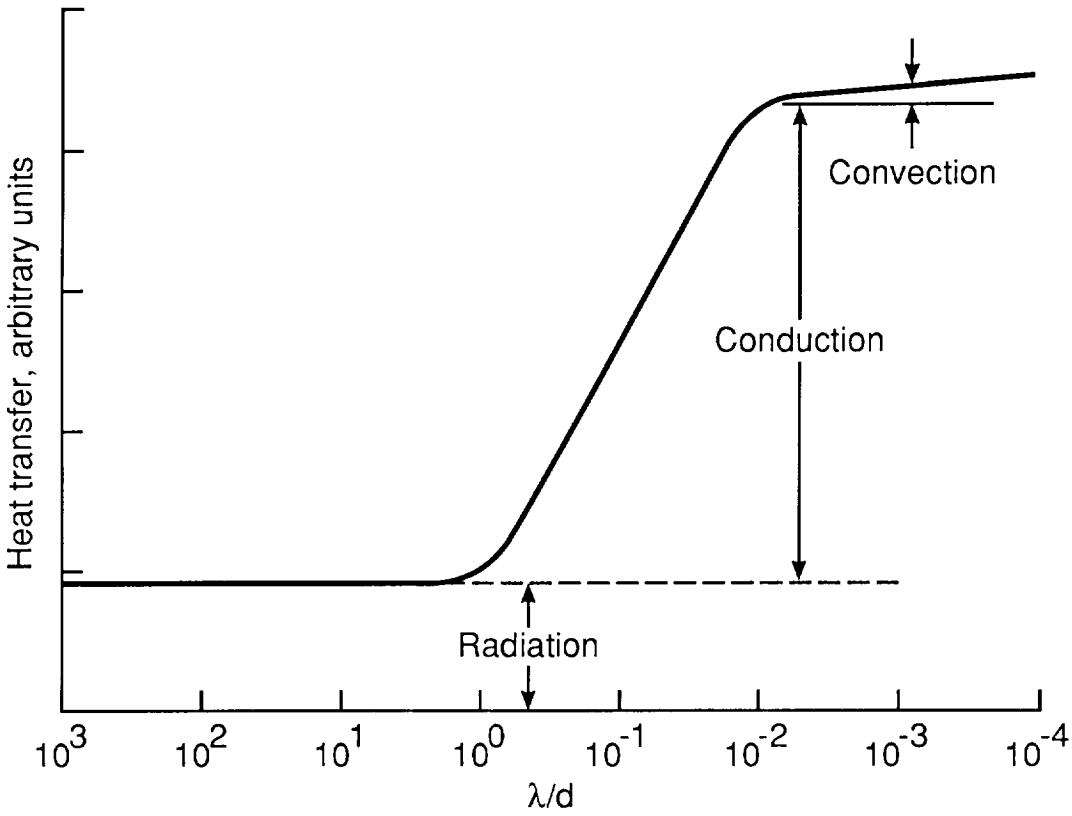

Figure 13. Knudsen number as a function of heat-transfer regime.

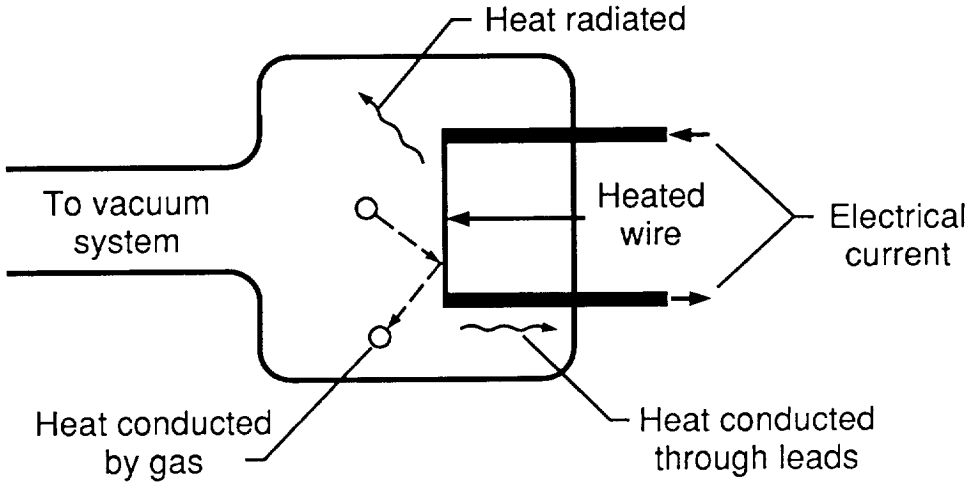

Figure 14. Thermoconductivity gauge.

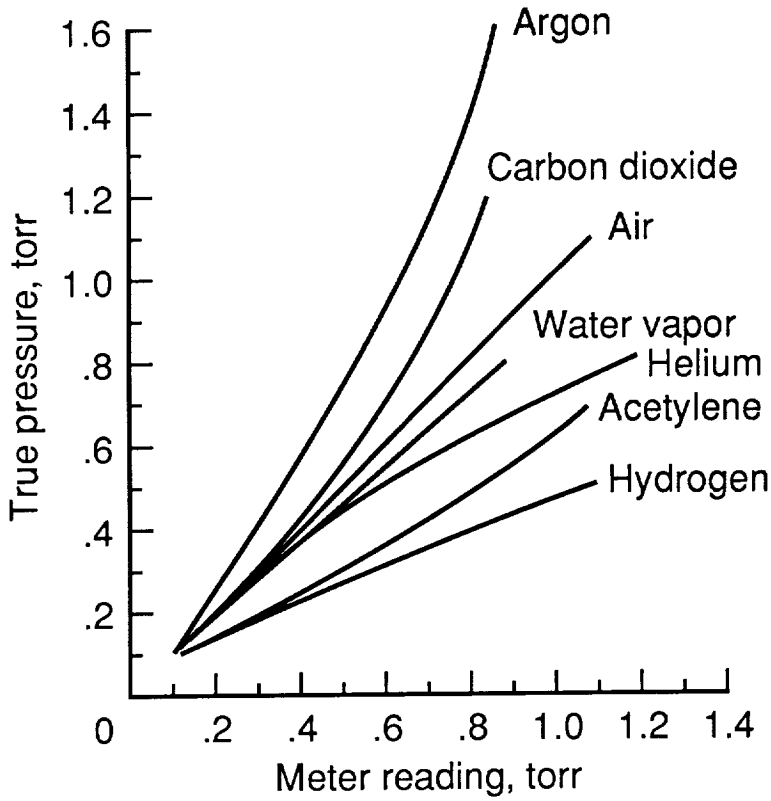

Figure 15. Gas sensitivity of thermal-conductivity gauge. (Reprinted with permission from Teledyne-Hastings-Raydist, Hampton, Va.)

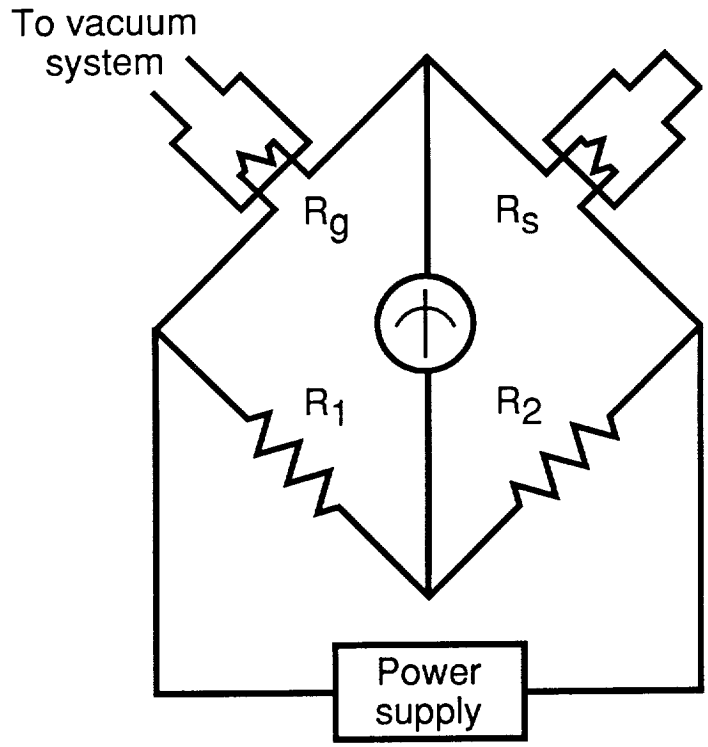

Figure 16. Wheatstone bridge circuit for thermal-conductivity gauge. R_g = Gauge resistance; R_s = Standard resistance to compensate for changes in ambient temperature.

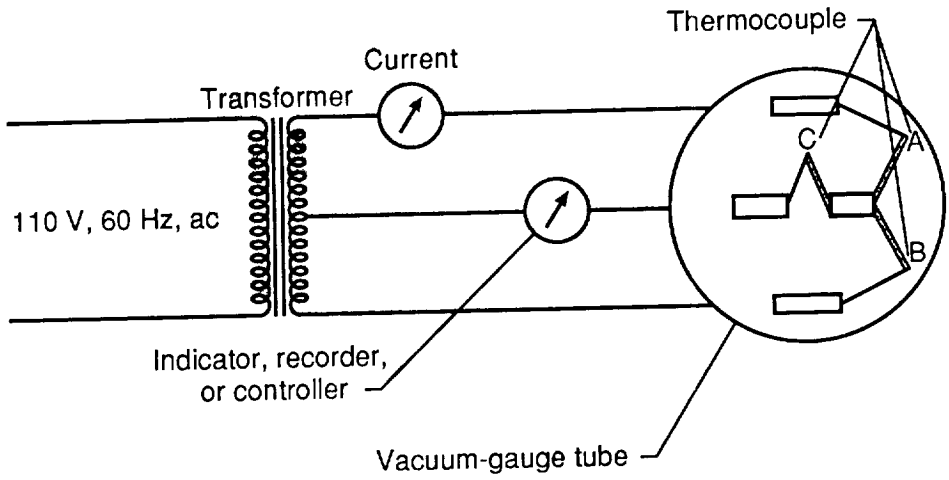

Figure 17. Thermocouple gauge.

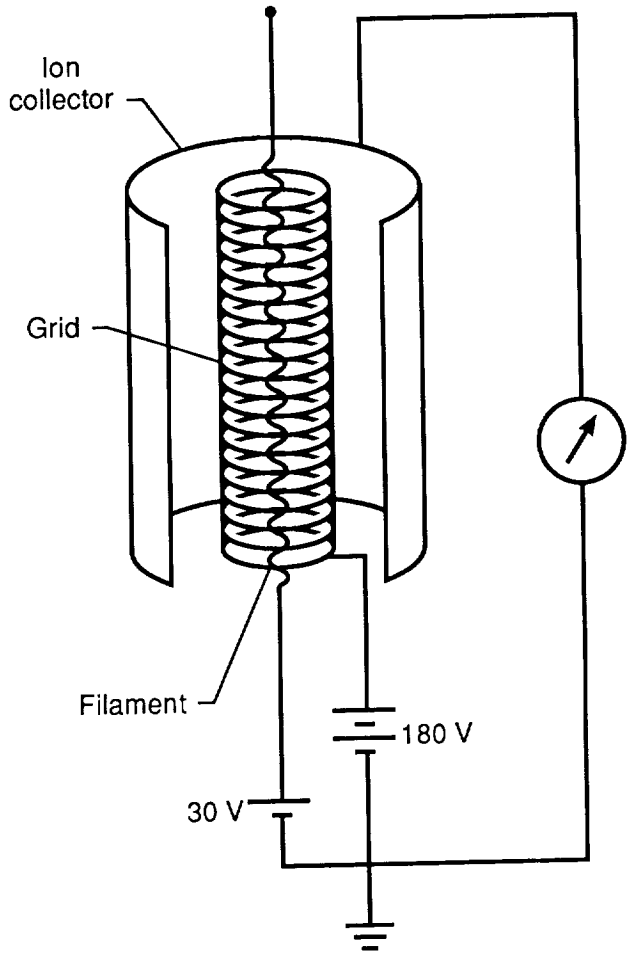

Figure 18. Ionization gauge, normal triode configuration.

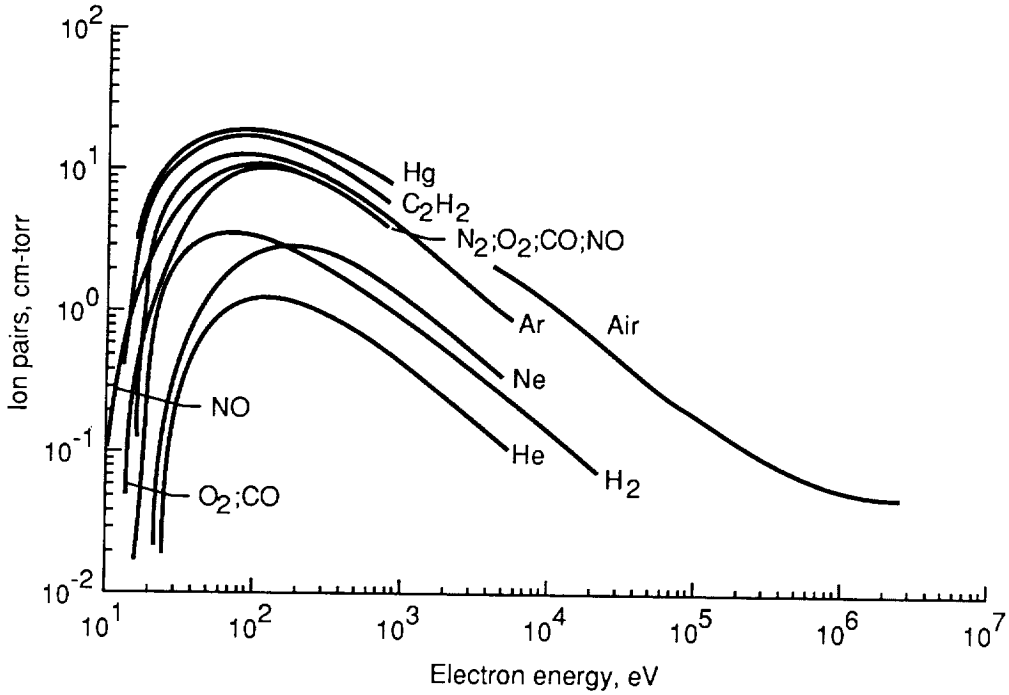

Figure 19. Ionization efficiency curve for inorganic gases.

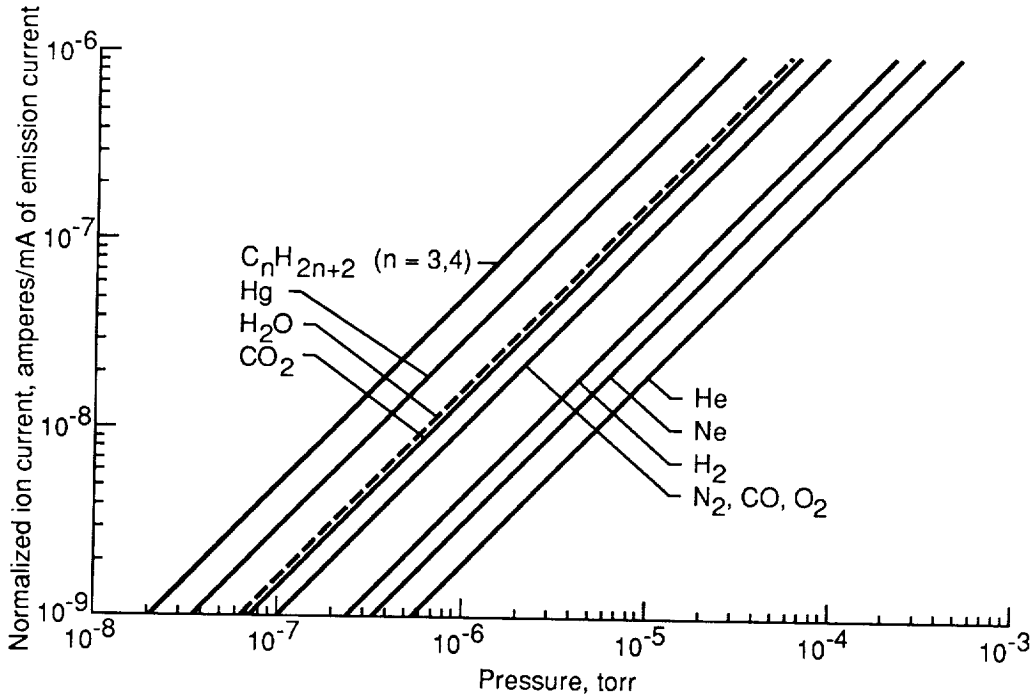

Figure 20. Gas sensitivity of ionization gauges.

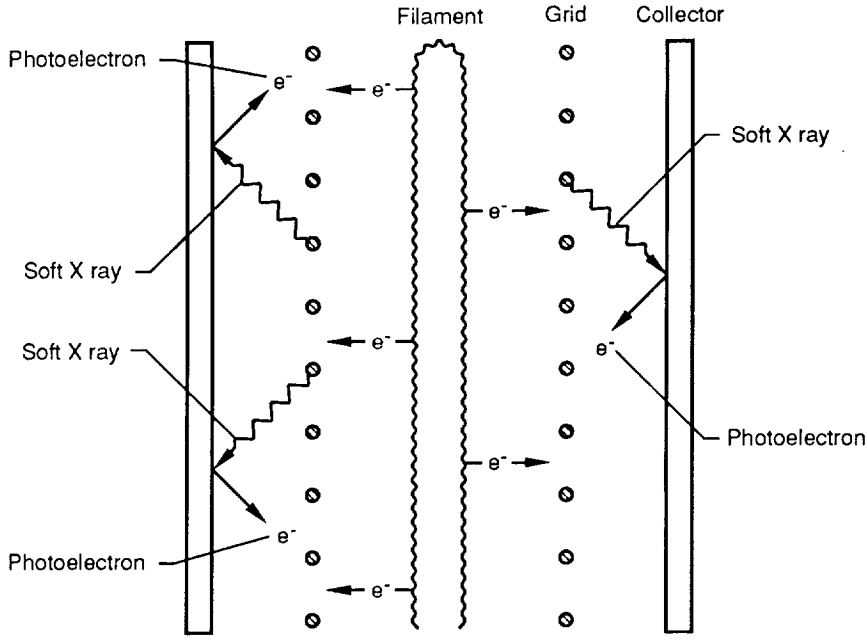

Figure 21. Triode gauge X-ray limit, $\approx 10^{-8}$ torr.

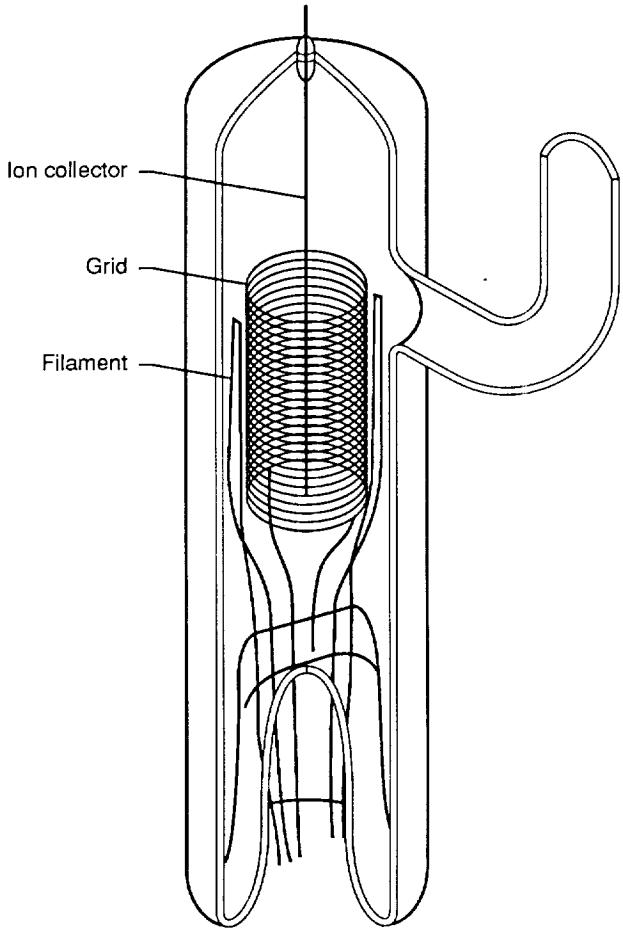

Figure 22. Original form of Bayard-Alpert ionization gauge with filament, grid, and ion collector. (Reprinted with permission from *American Institute of Physics, Review Sci. Instrum.*, vol. 21, no. 6, 1950, p. 571.)

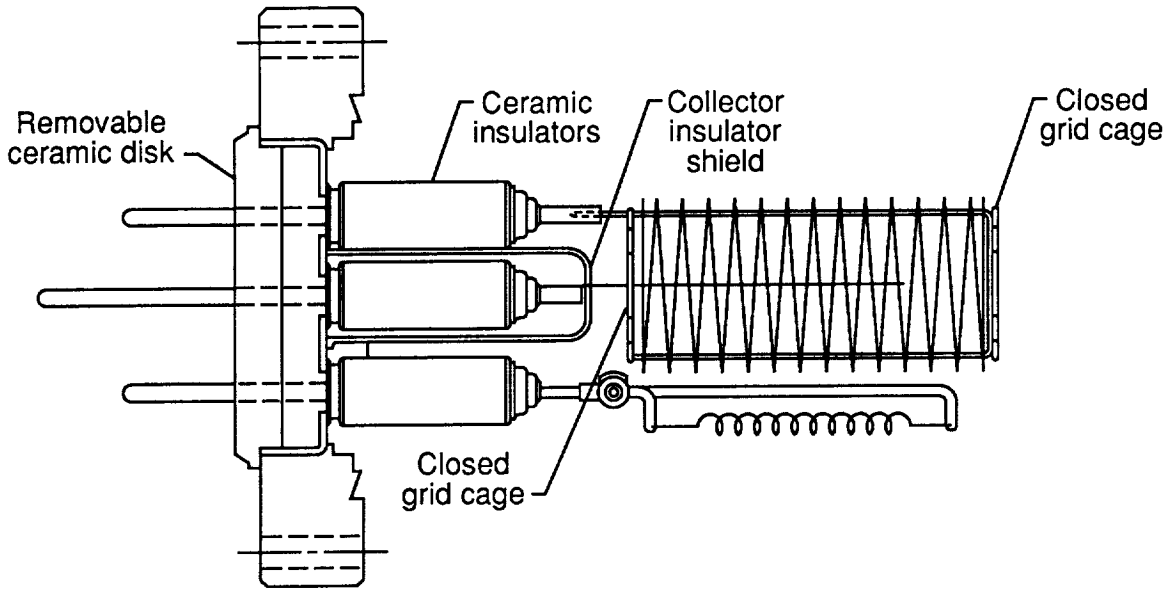

Figure 23. Nude Bayard-Alpert ionization gauge with closed grid cage.

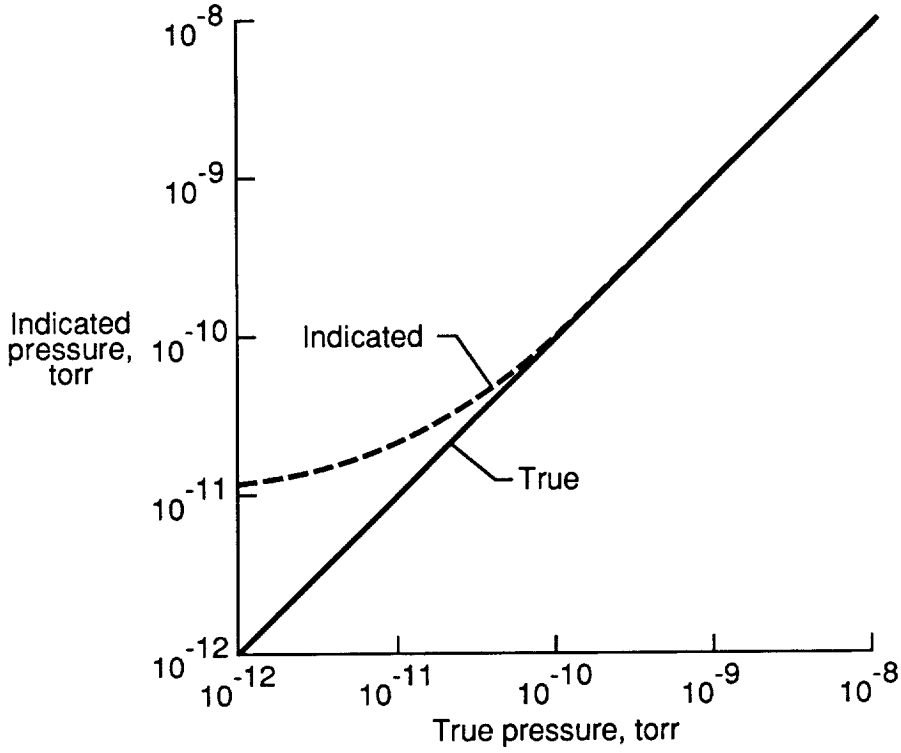

Figure 24. X-ray limit of nude ionization gauge shown in figure 23.

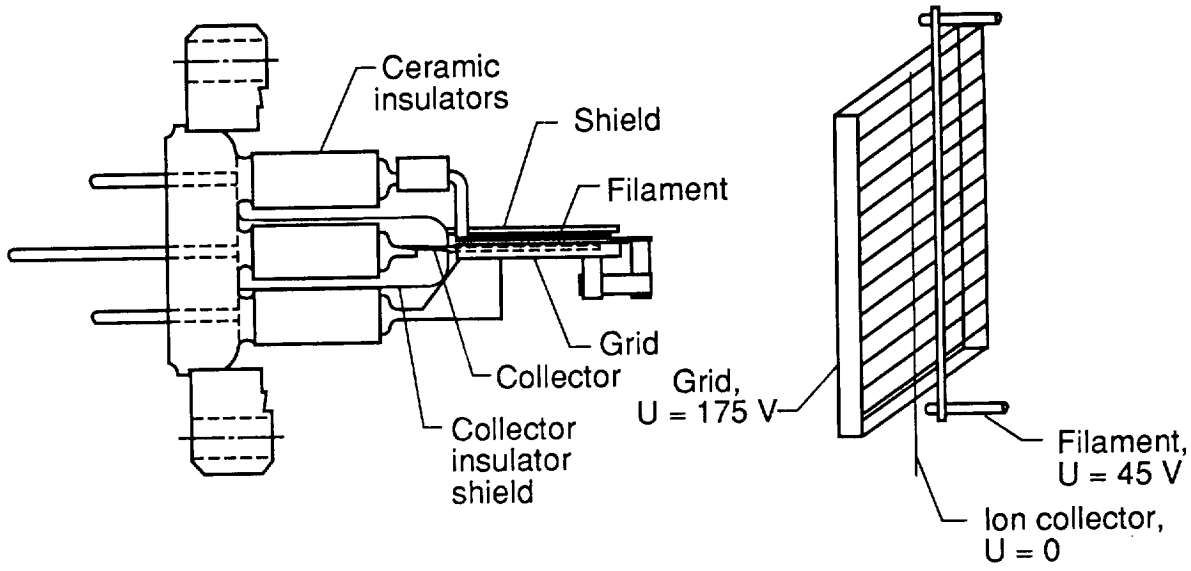

Figure 25. Schultz-Phelps ionization gauge. (Reprinted with permission from Varian Associates, Inc., Lexington, Mass.)

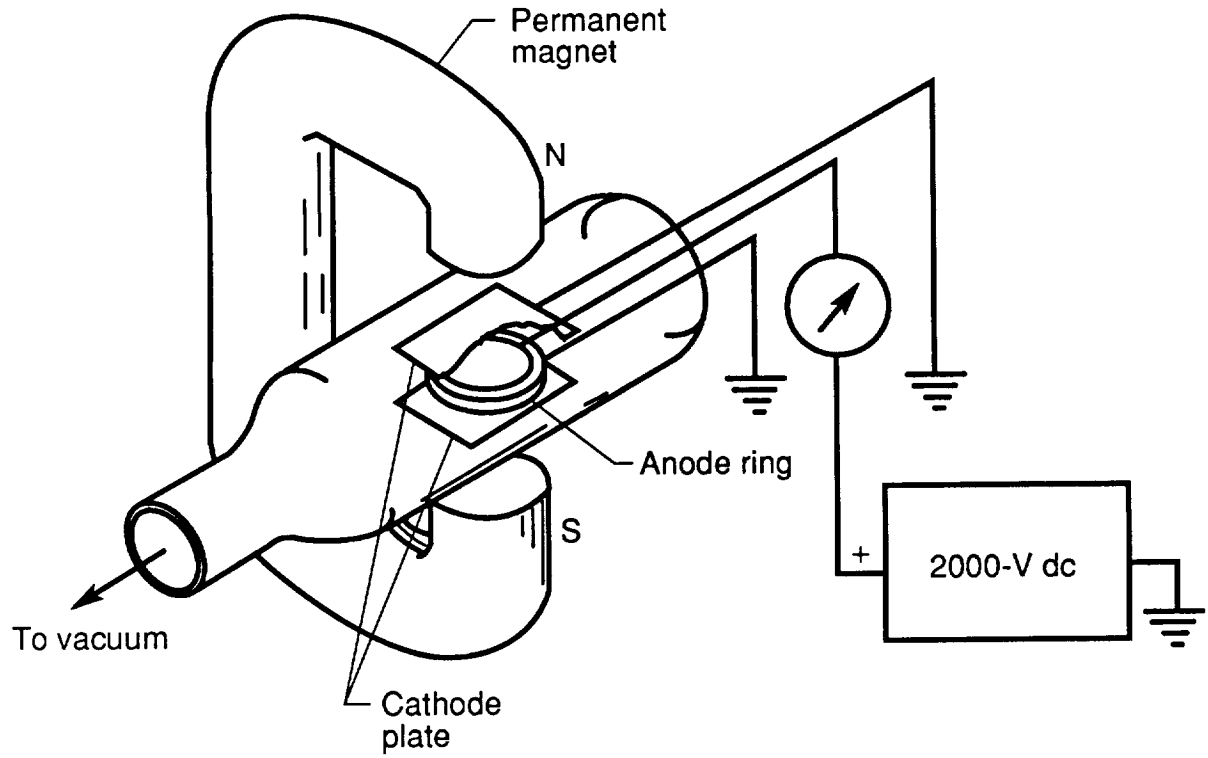

Figure 26. Penning cold-cathode ionization gauge.

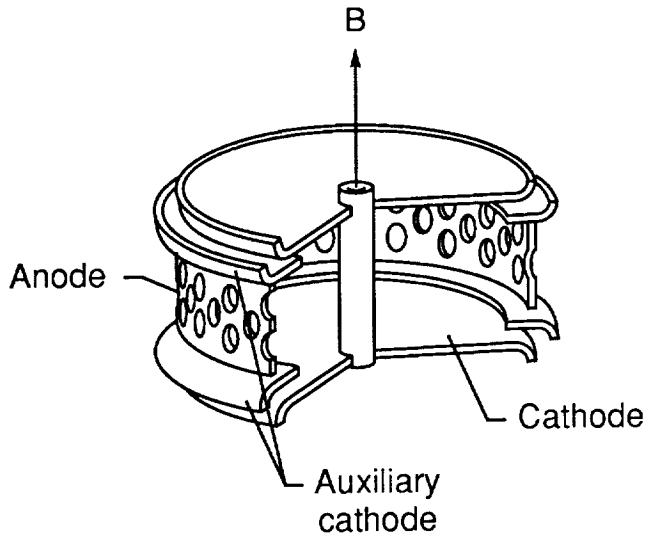

(a) Schematic of magnetron elements.

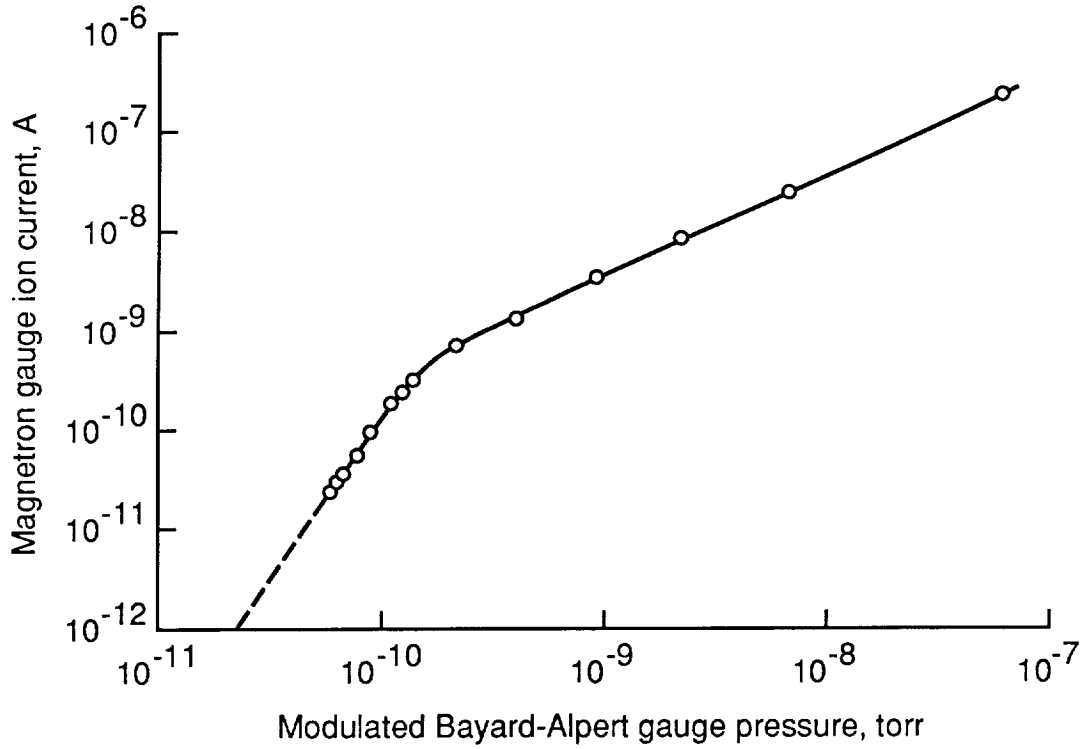

(b) Nonlinear response of gauge.

Figure 27. Redhead magnetron gauge. Anode voltage = 4800 V; Magnetic field = 1050 gauss; Modulated Bayard-Alpert gauge emission = 3 mA.

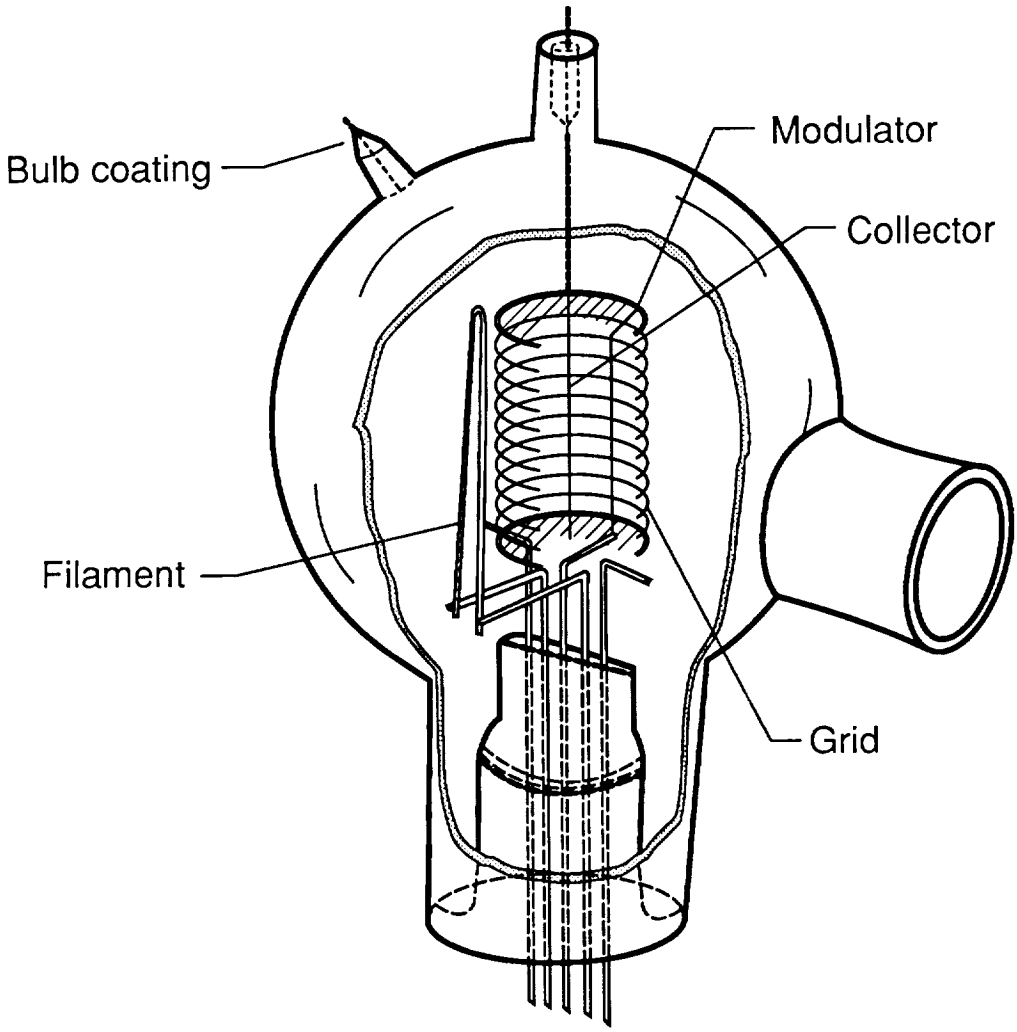

Figure 28. Schematic of modulated Bayard-Alpert gauge.

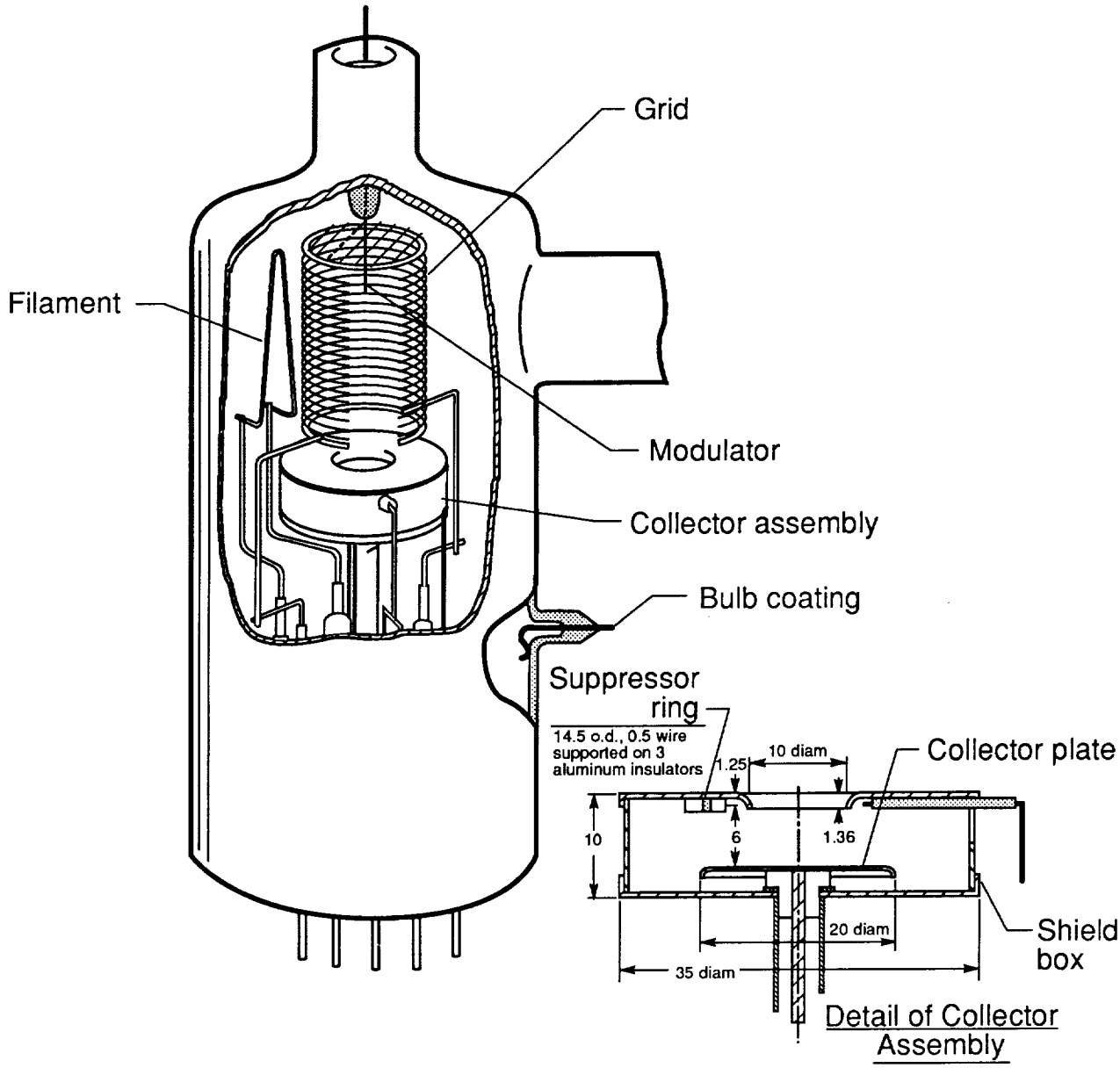

Figure 29. Suppressor-type ionization gauge. All dimensions in mm. (From ref. 3.)

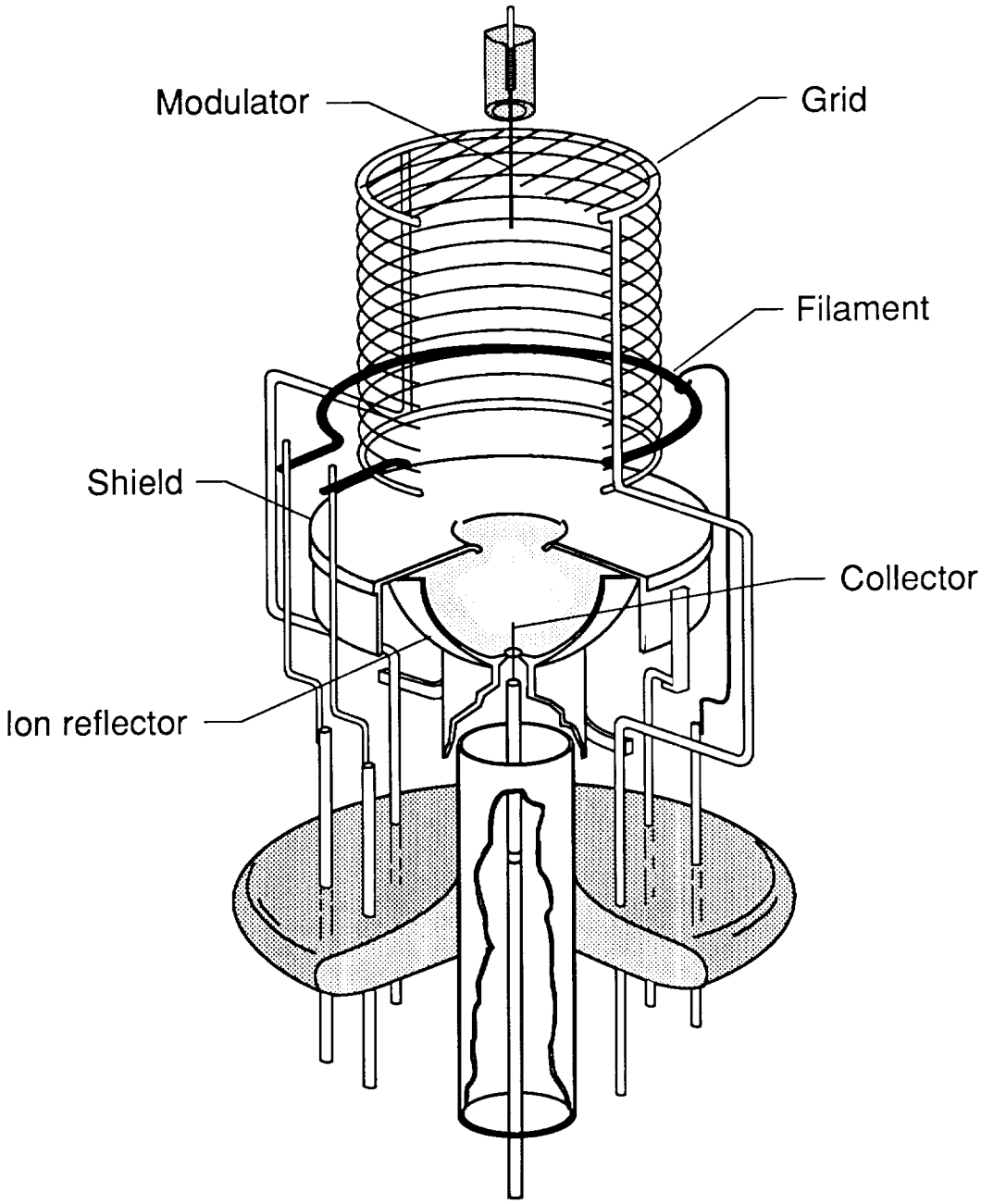

Figure 30. Redhead extractor ionization gauge. (From ref. 3.)

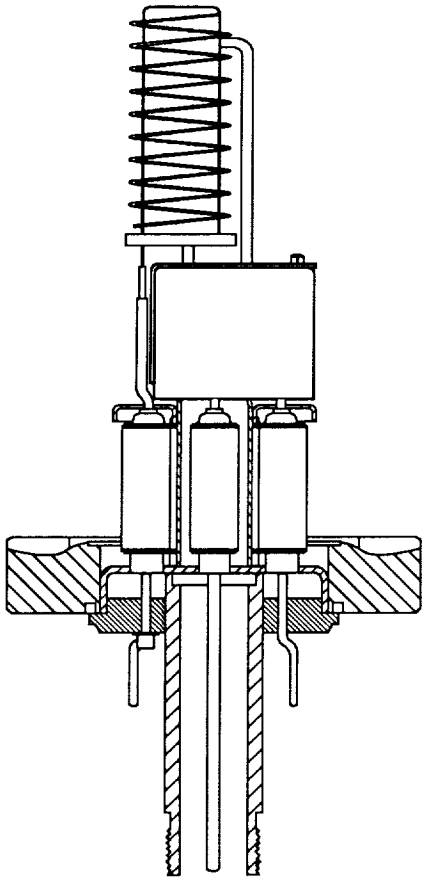

(a) Gauge tube geometry.

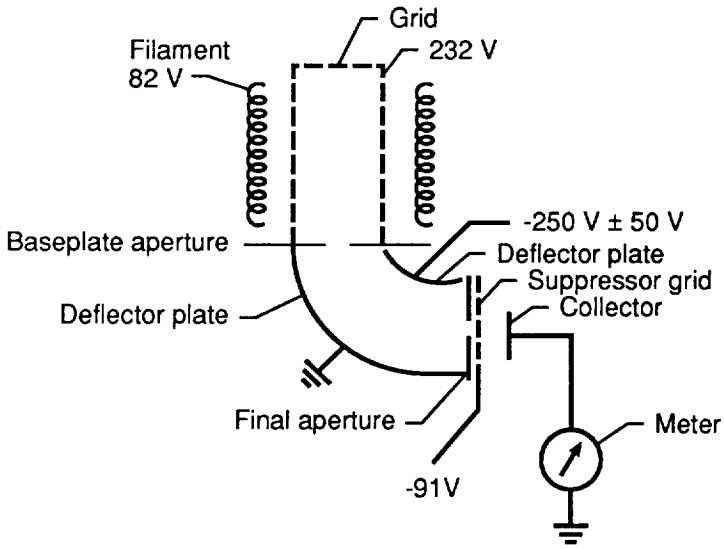

(b) Instrument schematic. (Reprinted with permission from Varian Associates, Inc., Lexington, Mass.)

Figure 31. Helmer ionization gauge.

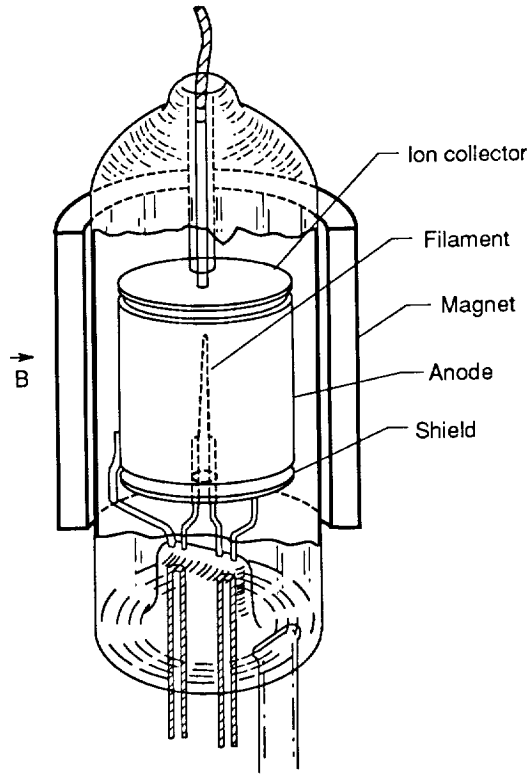

Figure 32. Lafferty ionization gauge. (From ref. 3.)

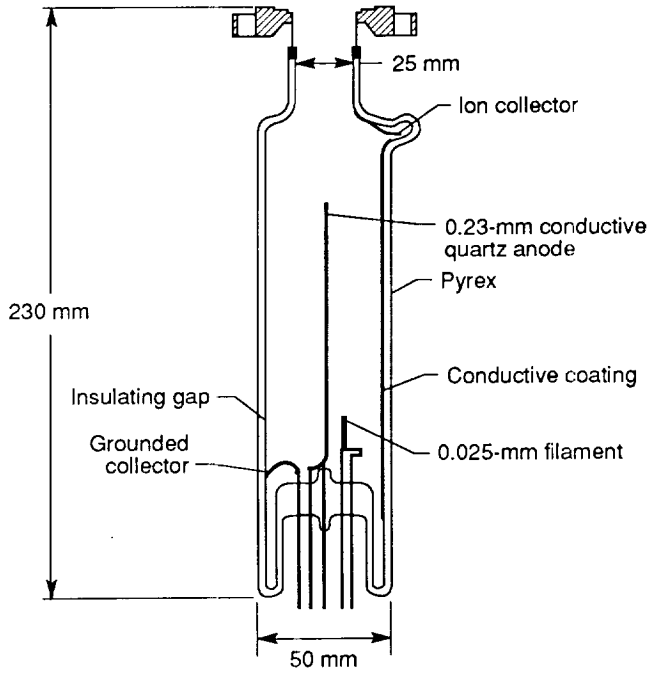

Figure 33. Orbitron ionization gauge. (From ref. 3.)

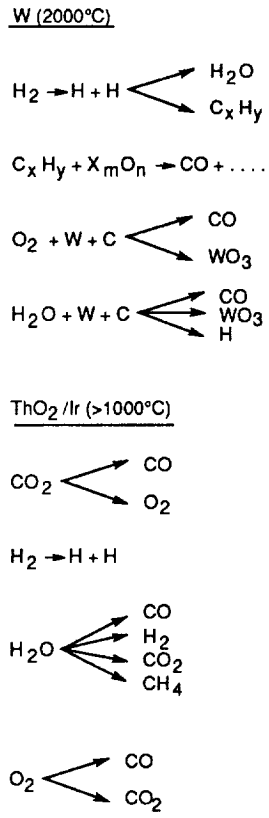

Figure 34. Possible gas interactions at hot-filament surfaces.

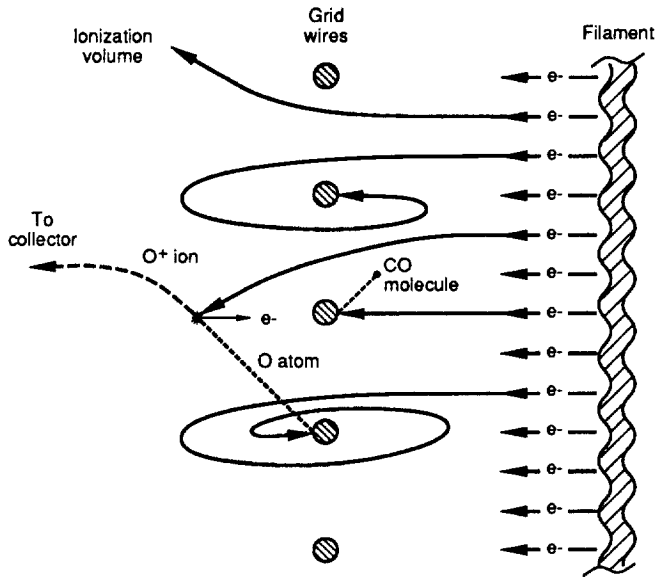

Figure 35. Electron stimulated desorption mechanism.

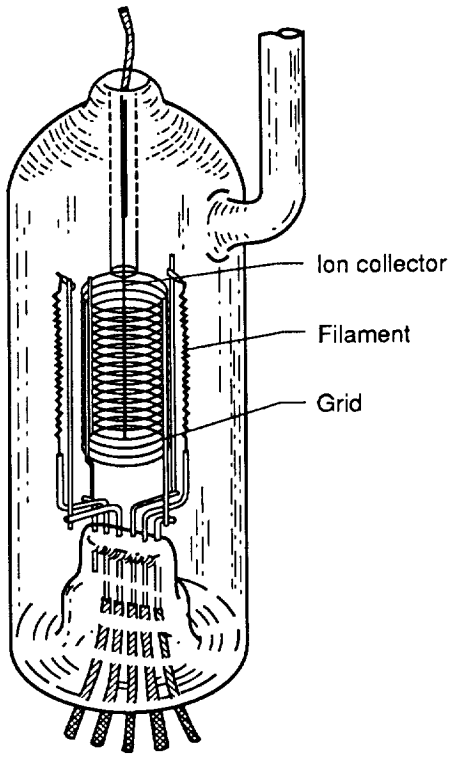

Figure 36. Ionization gauge with glass envelope.

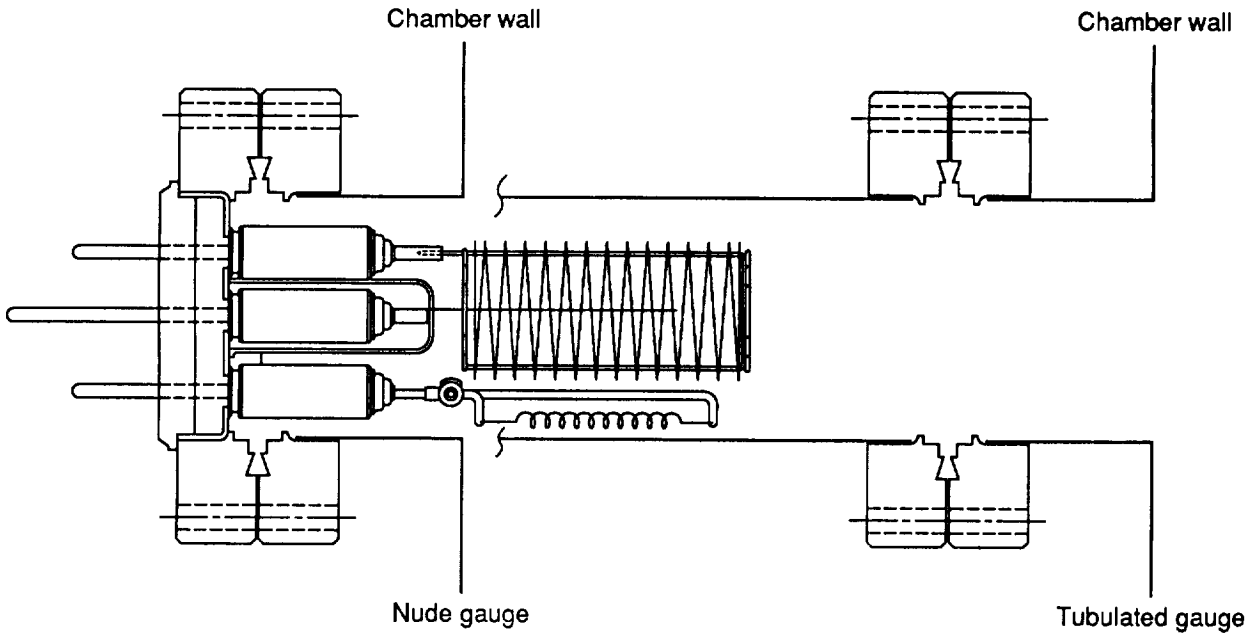

Figure 37. Nude ionization gauge with and without metal envelope.

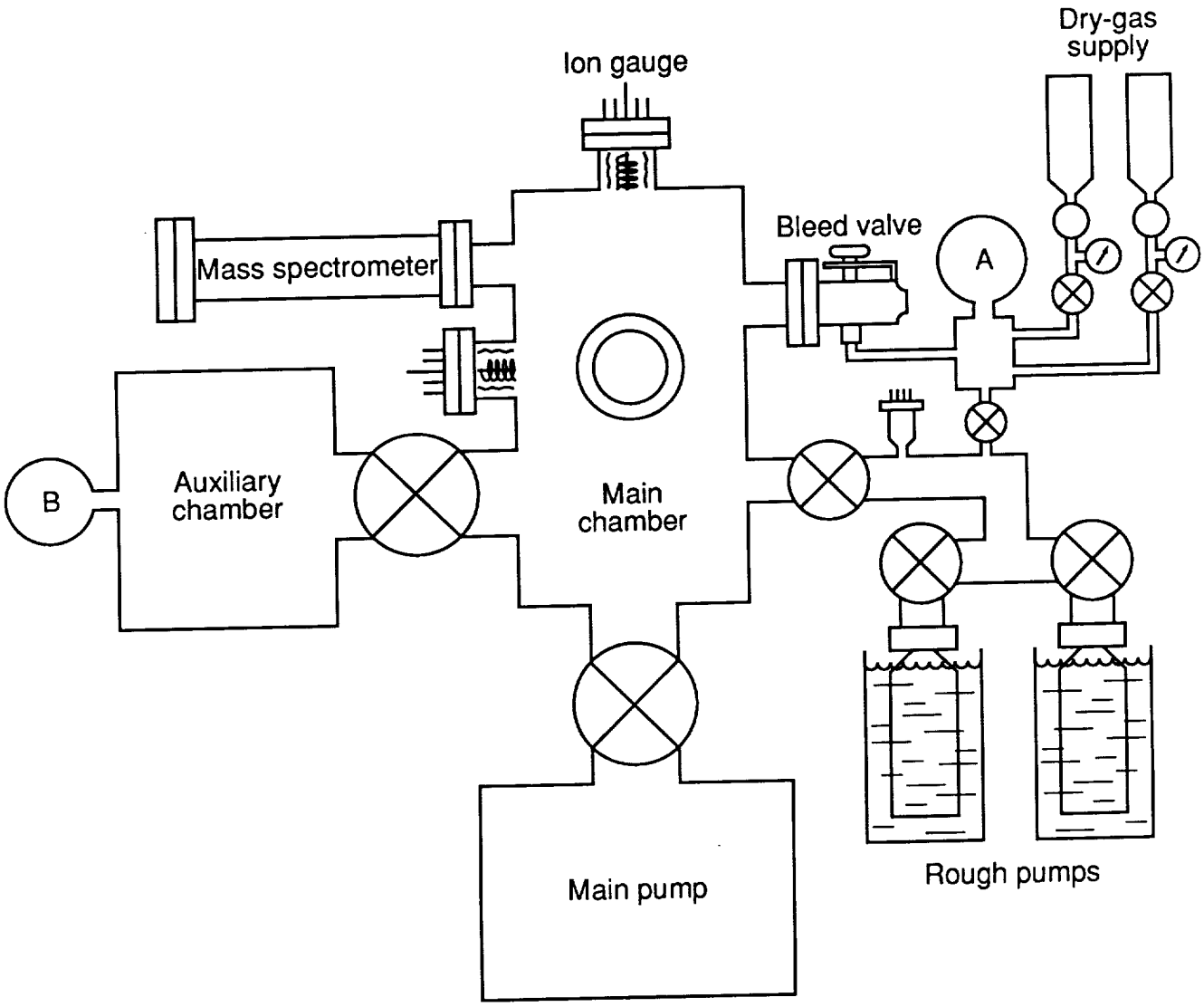

Figure 38. Vacuum instrument location. A and B are other measurement areas.

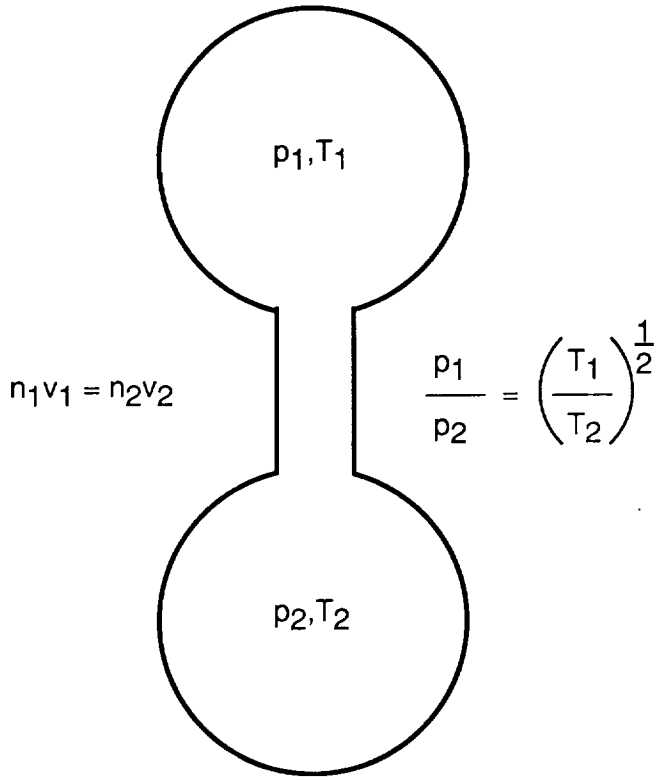

Figure 39. Thermal transpiration. p = Pressure; T = Temperature; n = Number density; v = Velocity.

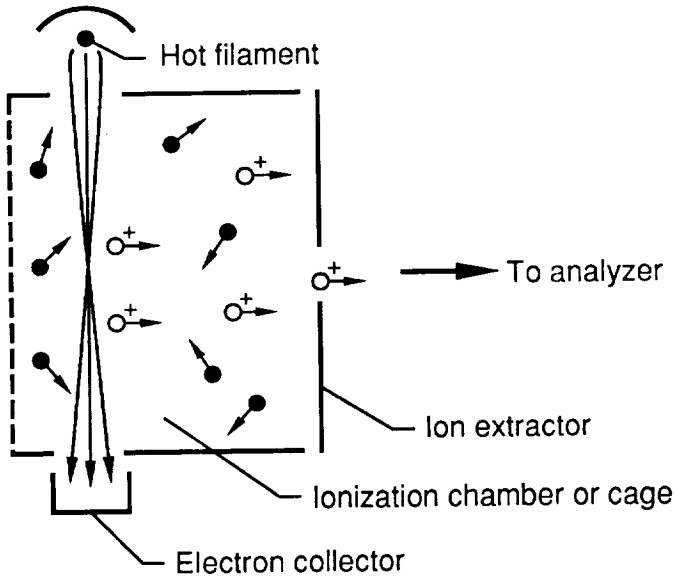

Figure 40. Electron bombardment ionizer.

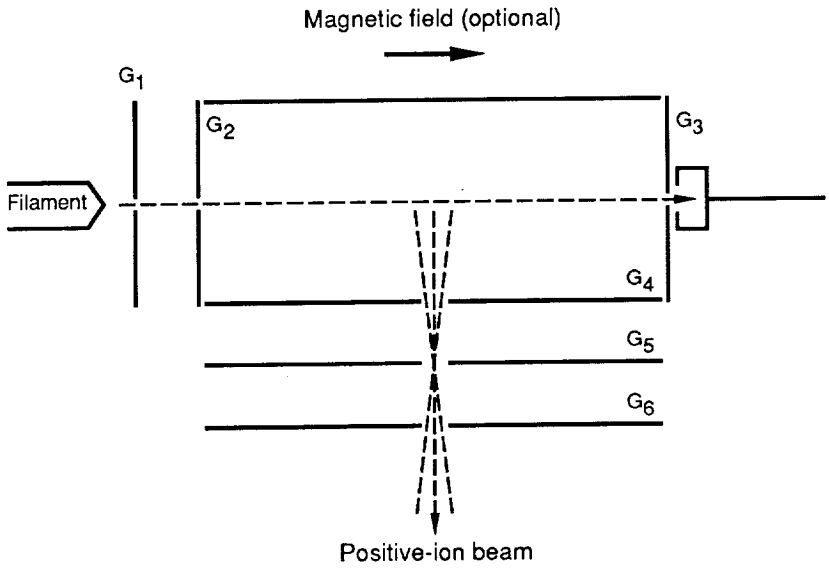

Figure 41. Nier ionization source. G_1 to G_6 are grids.

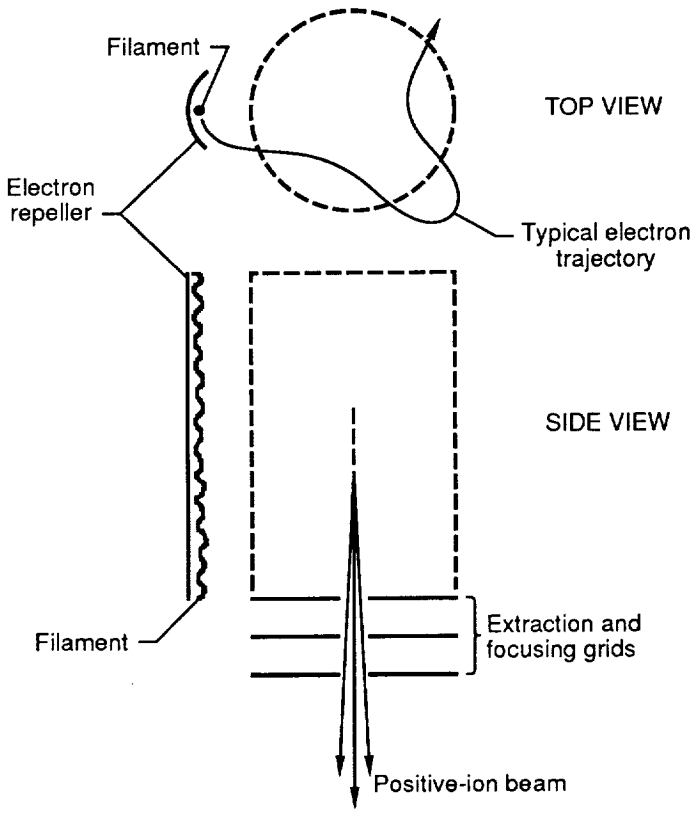

Figure 42. Axial ionization source.

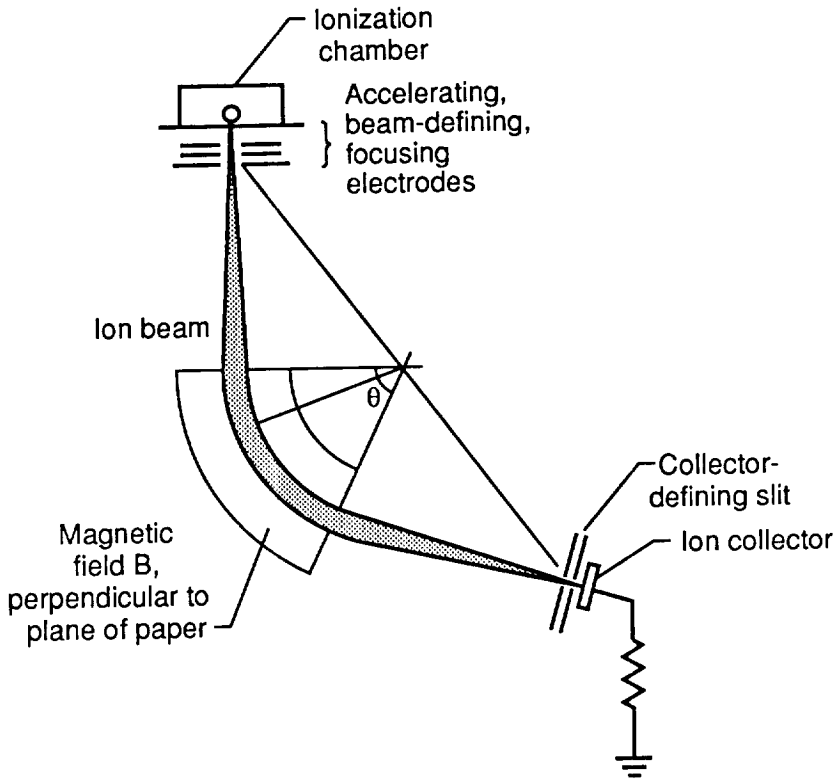

Figure 43. Schematic of magnetic-sector mass spectrometer.

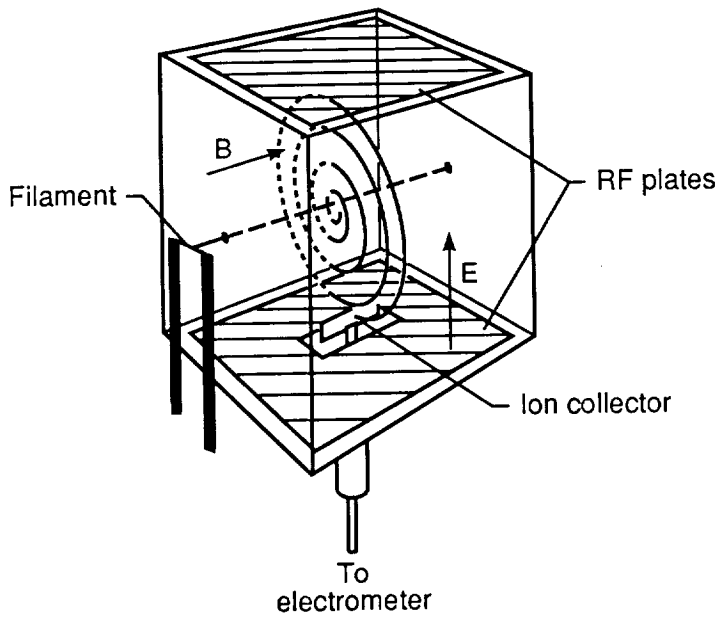

Figure 44. Schematic of omegatron mass spectrometer where B and E are magnetic and electric fields.

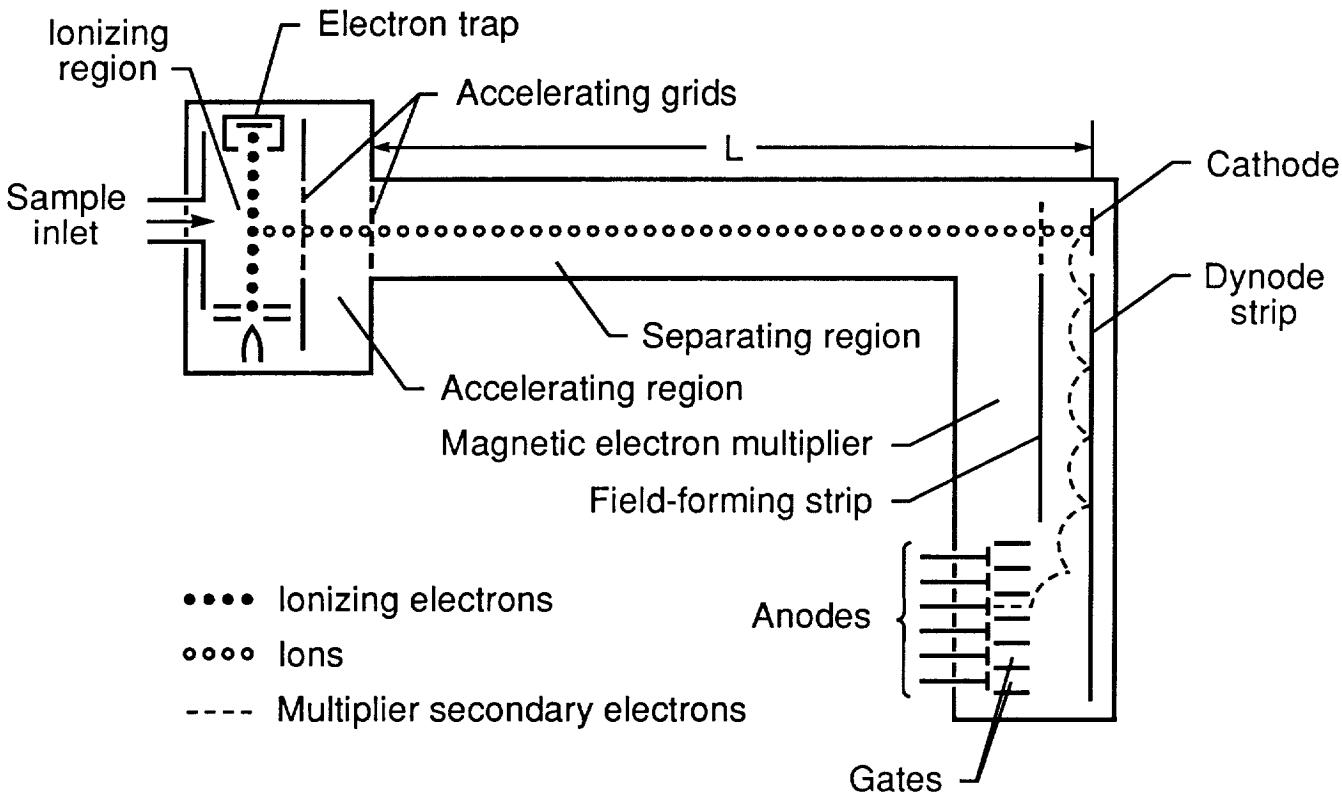

Figure 45. Time-of-flight mass spectrometer with electron multiplier.

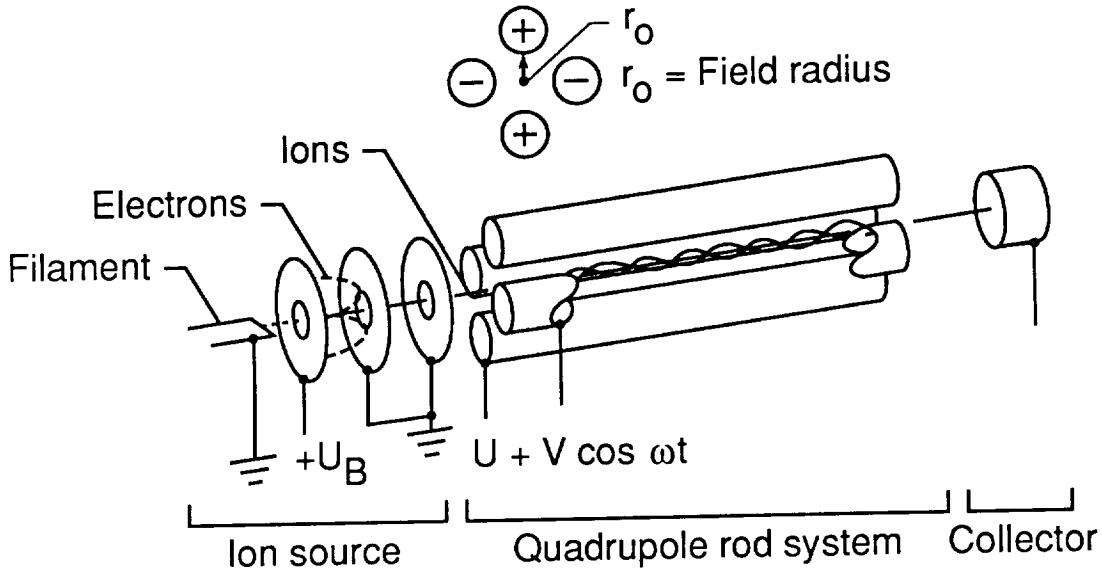

(a) Schematic of instrument.

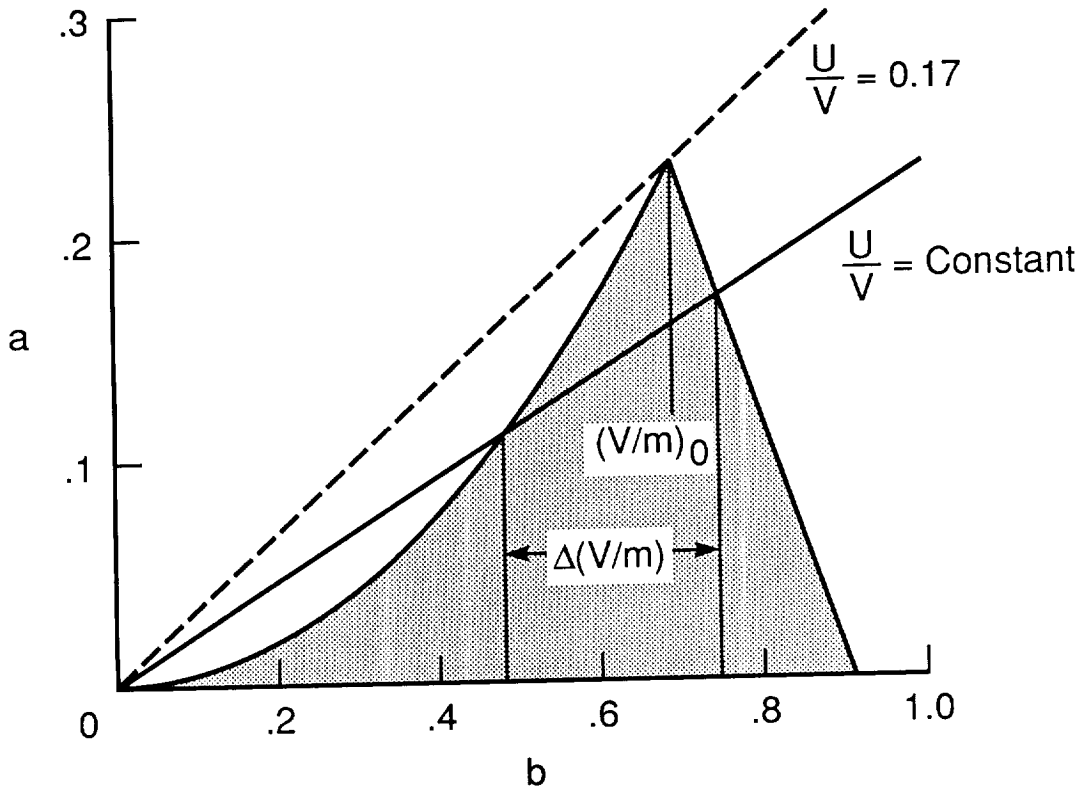

(b) Quadrupole operation: stable paths (transmitted) for ions in shaded area.

Figure 46. Quadrupole mass spectrometer.

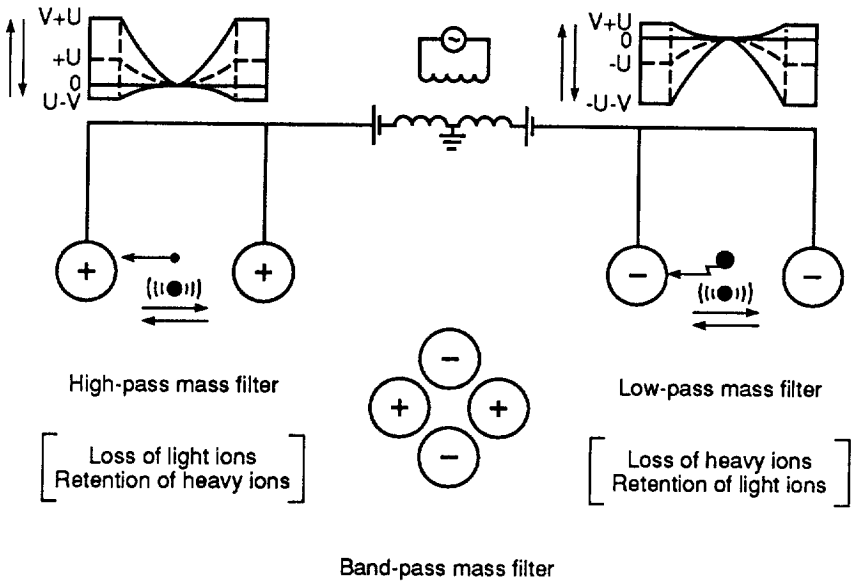

Figure 47. Superimposed RF and dc fields on quadrupole rods. (Reprinted with permission from R&D, March 1970.)

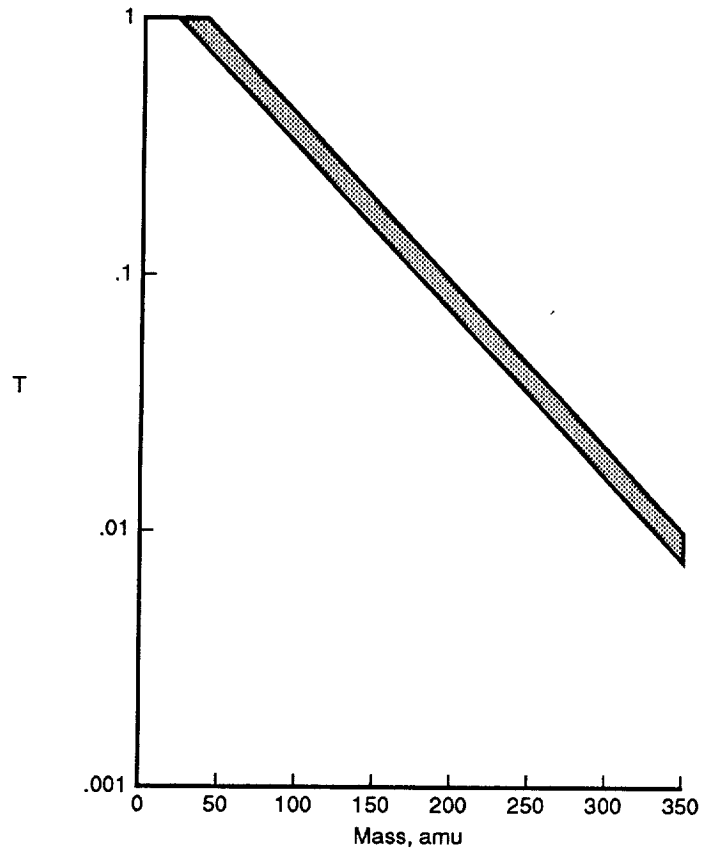

Figure 48. Relative transmission T versus mass.

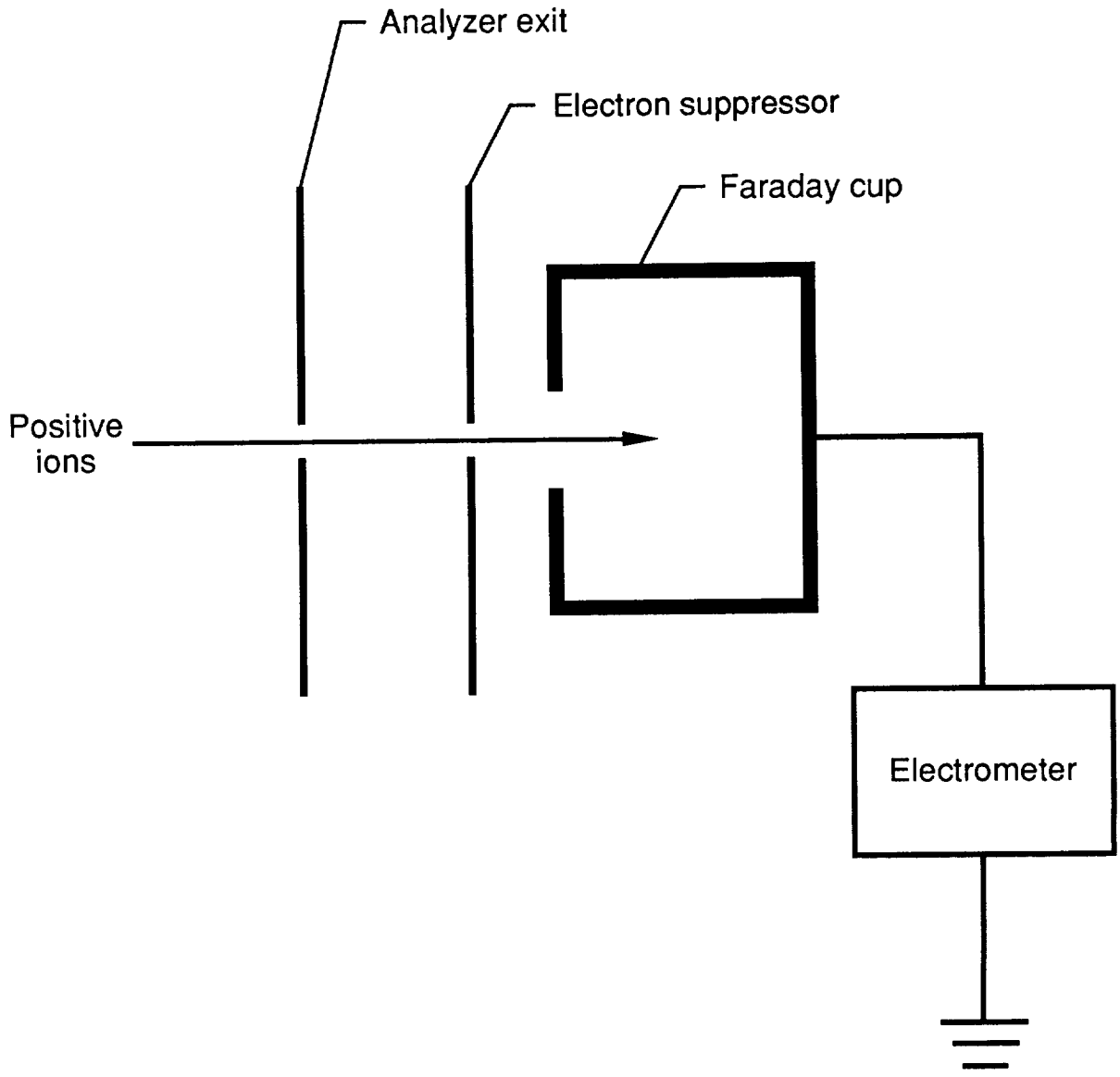

Figure 49. Faraday cup detector.

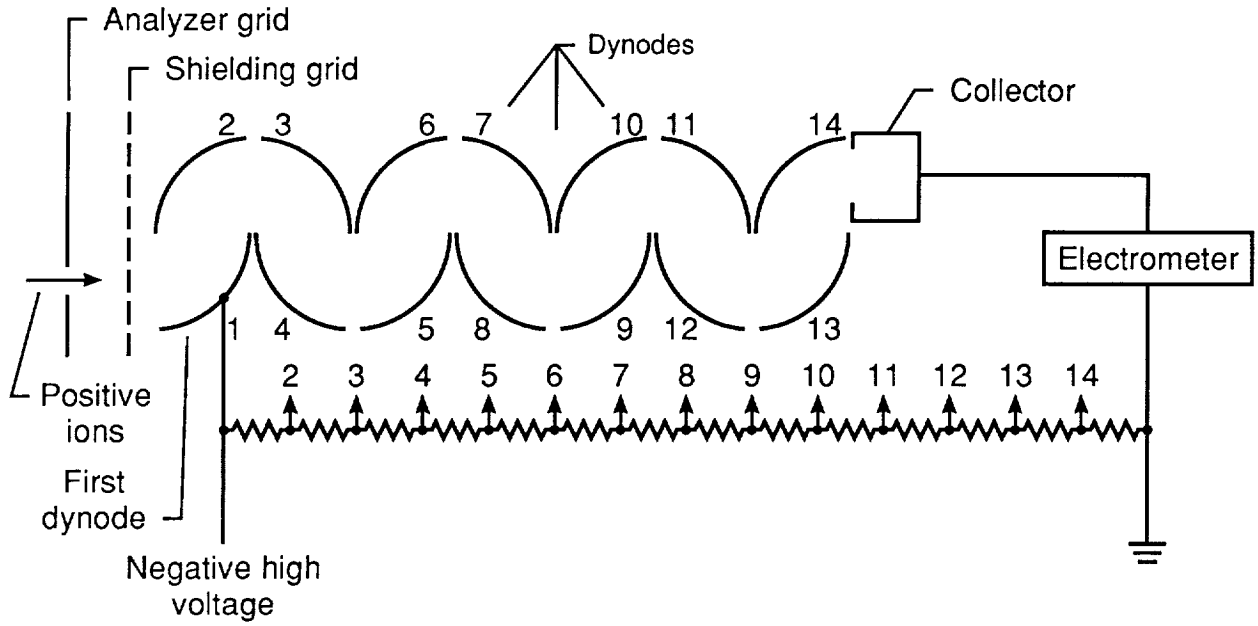

(a) Cu 2–4% Be discrete stage.

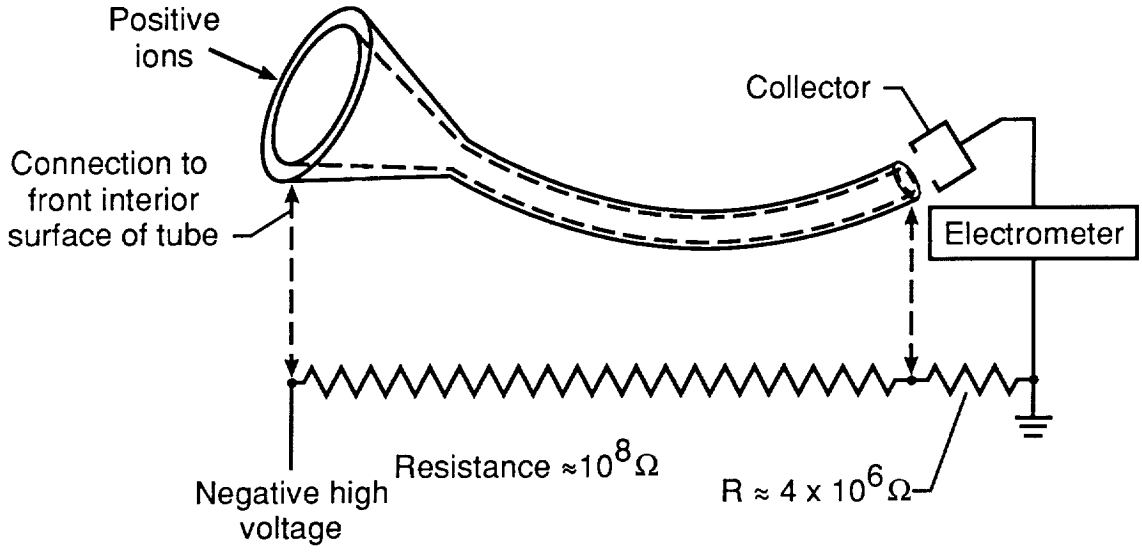

(b) Channeltron continuous dynode.

Figure 50. Electron multipliers.

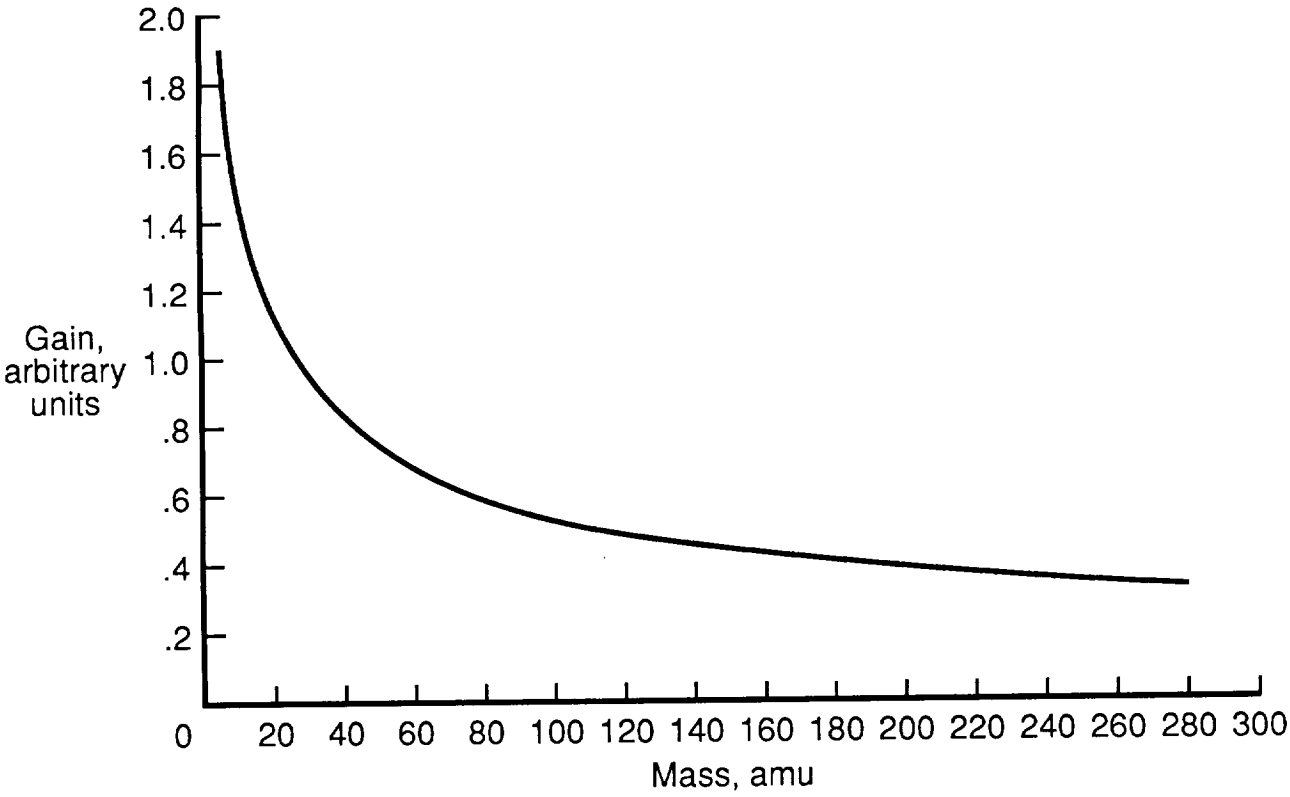

Figure 51. Electron multiplier gains versus mass.

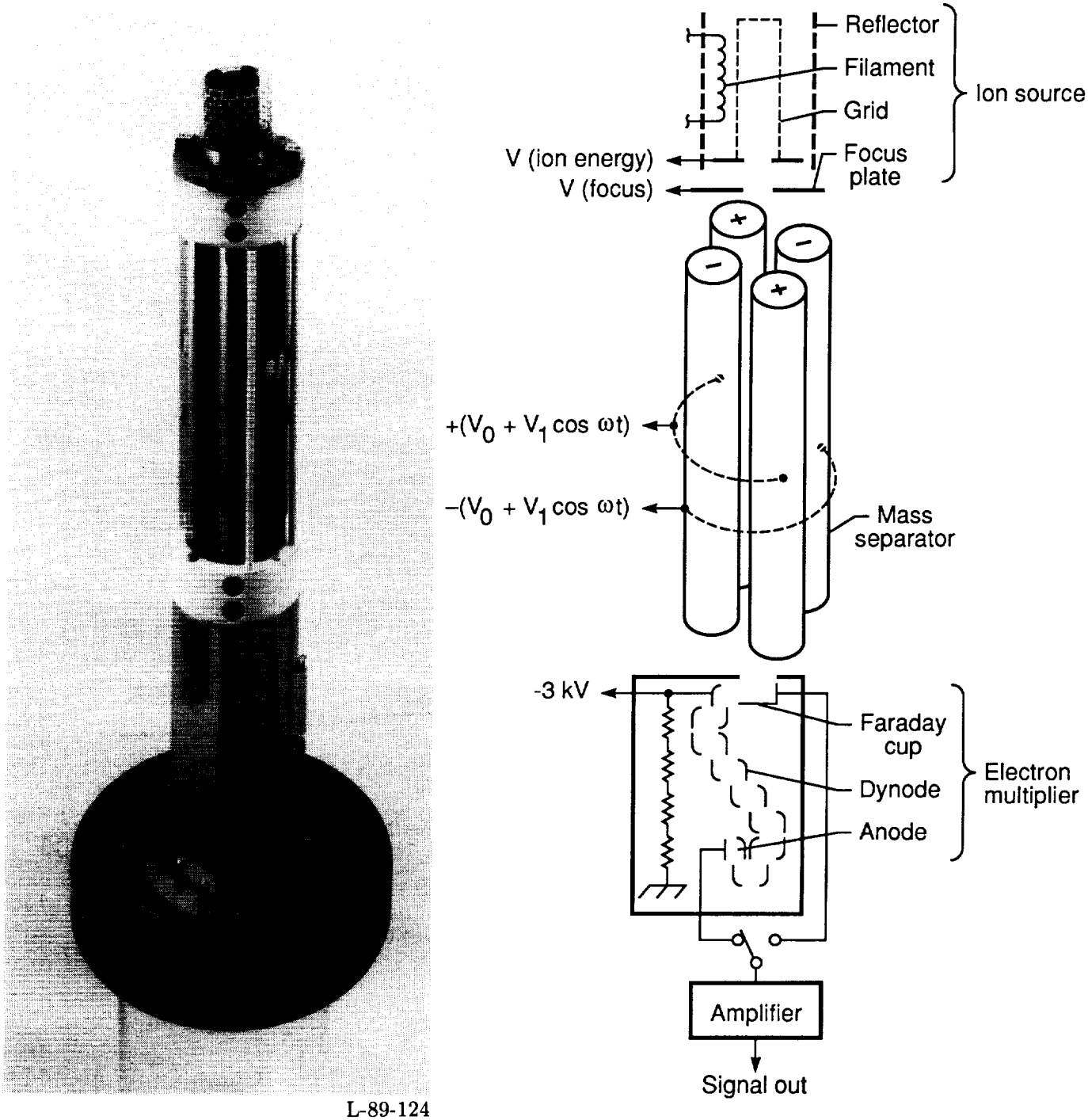

L-89-124

Figure 52. Assembly and schematic of quadrupole mass spectrometer. (Reprinted with permission from Uthe Technology, Inc., Milpitas, Calif.)

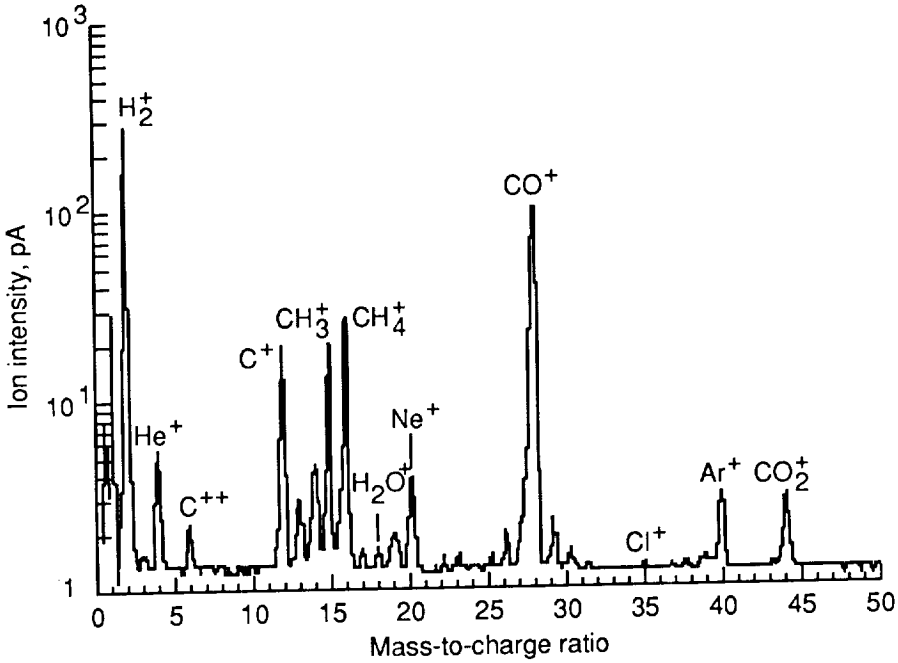

Figure 53. Mass spectrum for total pressure of 1.5×10^{-10} torr.

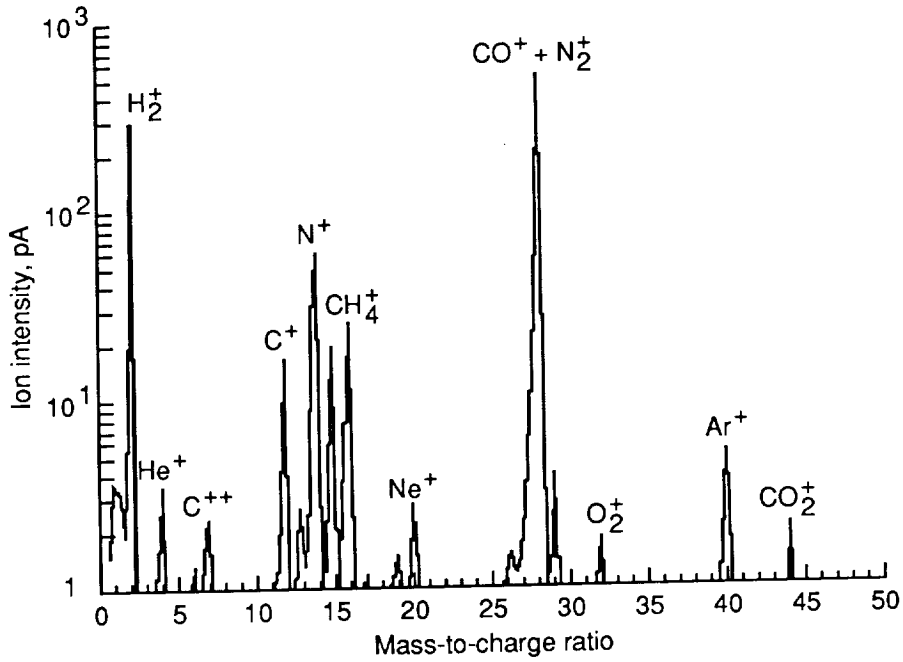

Figure 54. Mass spectrum for small leak for total pressure of 3.2×10^{-10} torr.

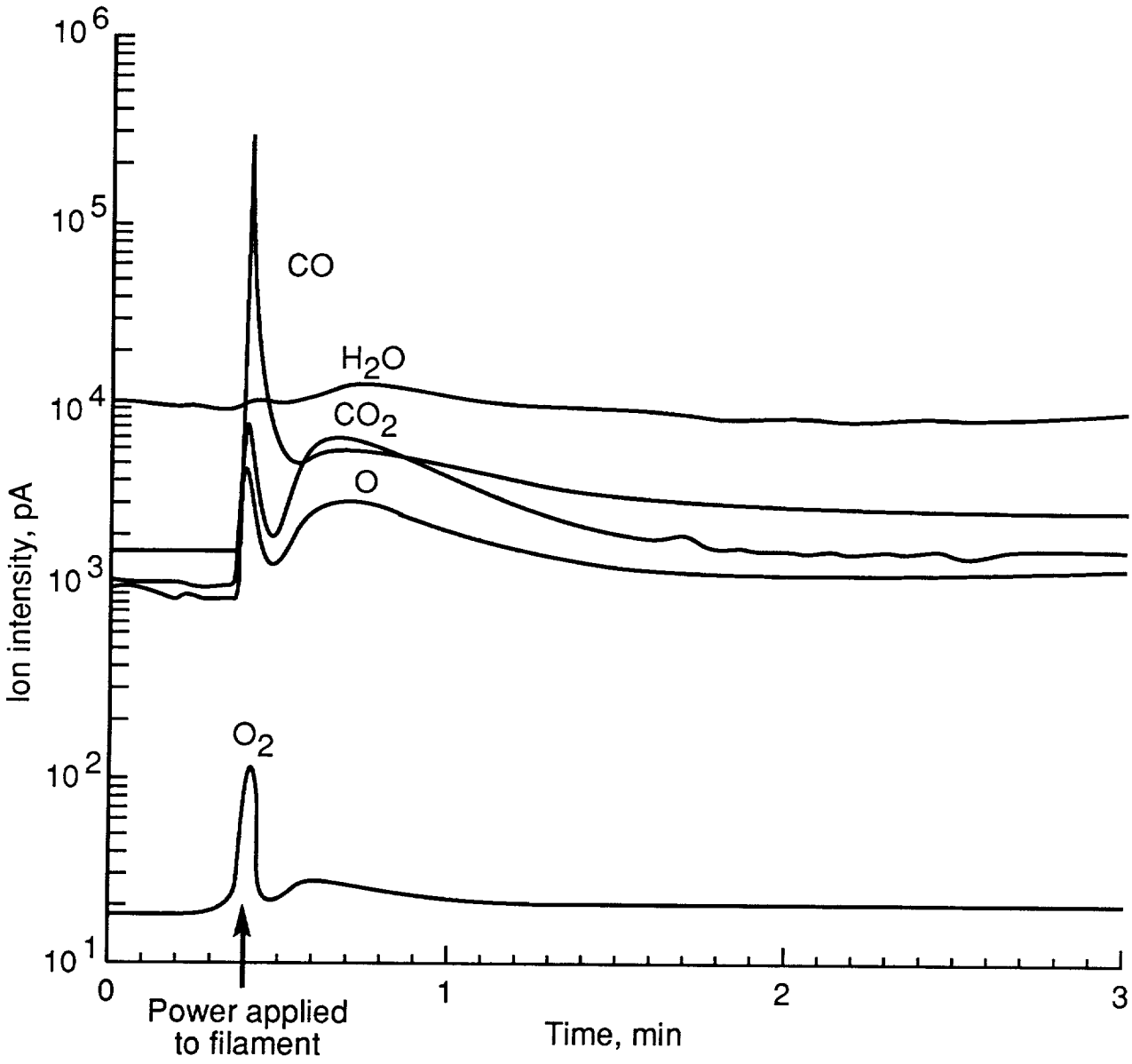

Figure 55. Desorption spectra of Re filament.

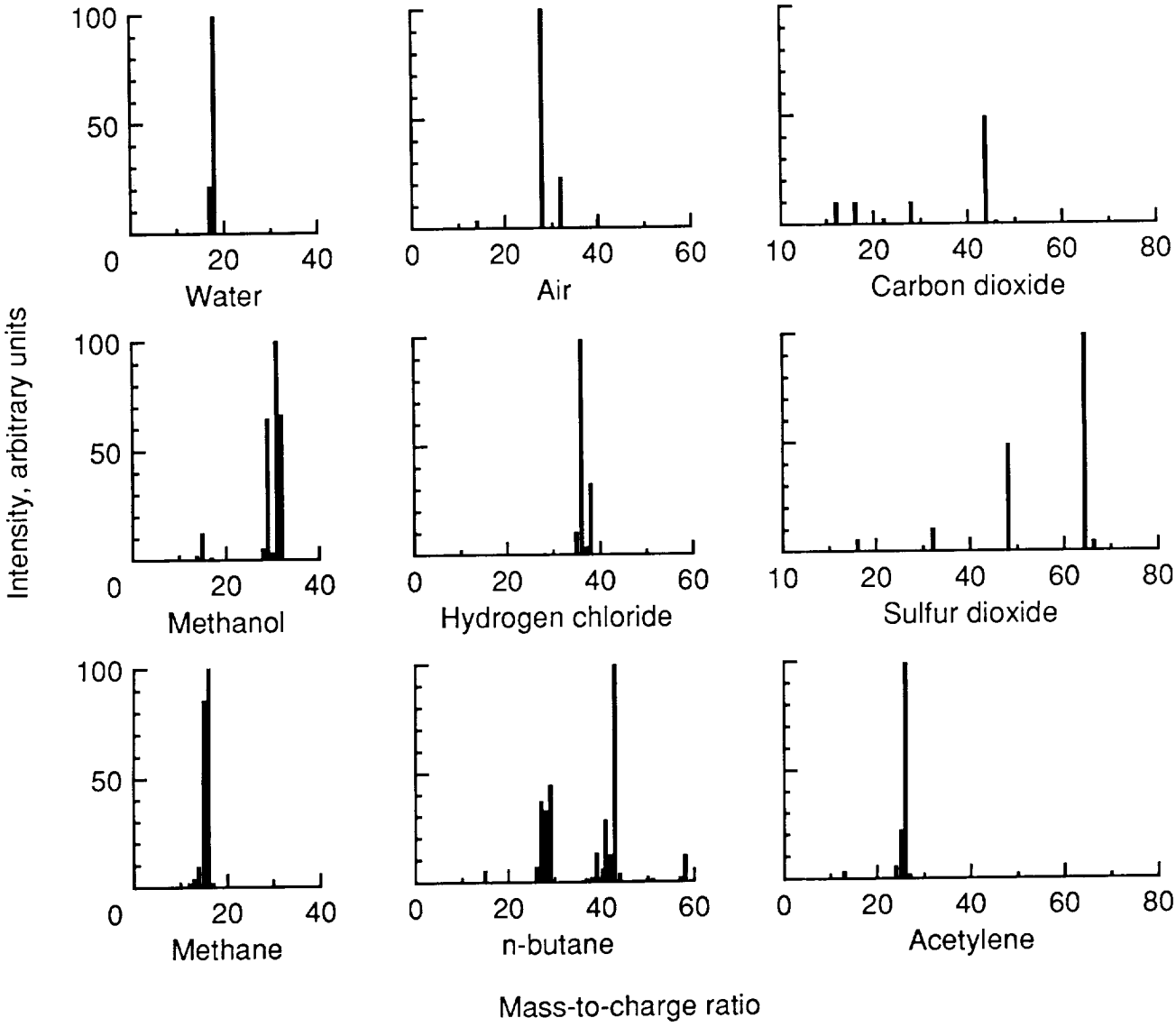

Figure 56. Examples of mass fragmentation spectra. (Reprinted with permission from Uthe Technology, Inc., Milpitas, Calif.)

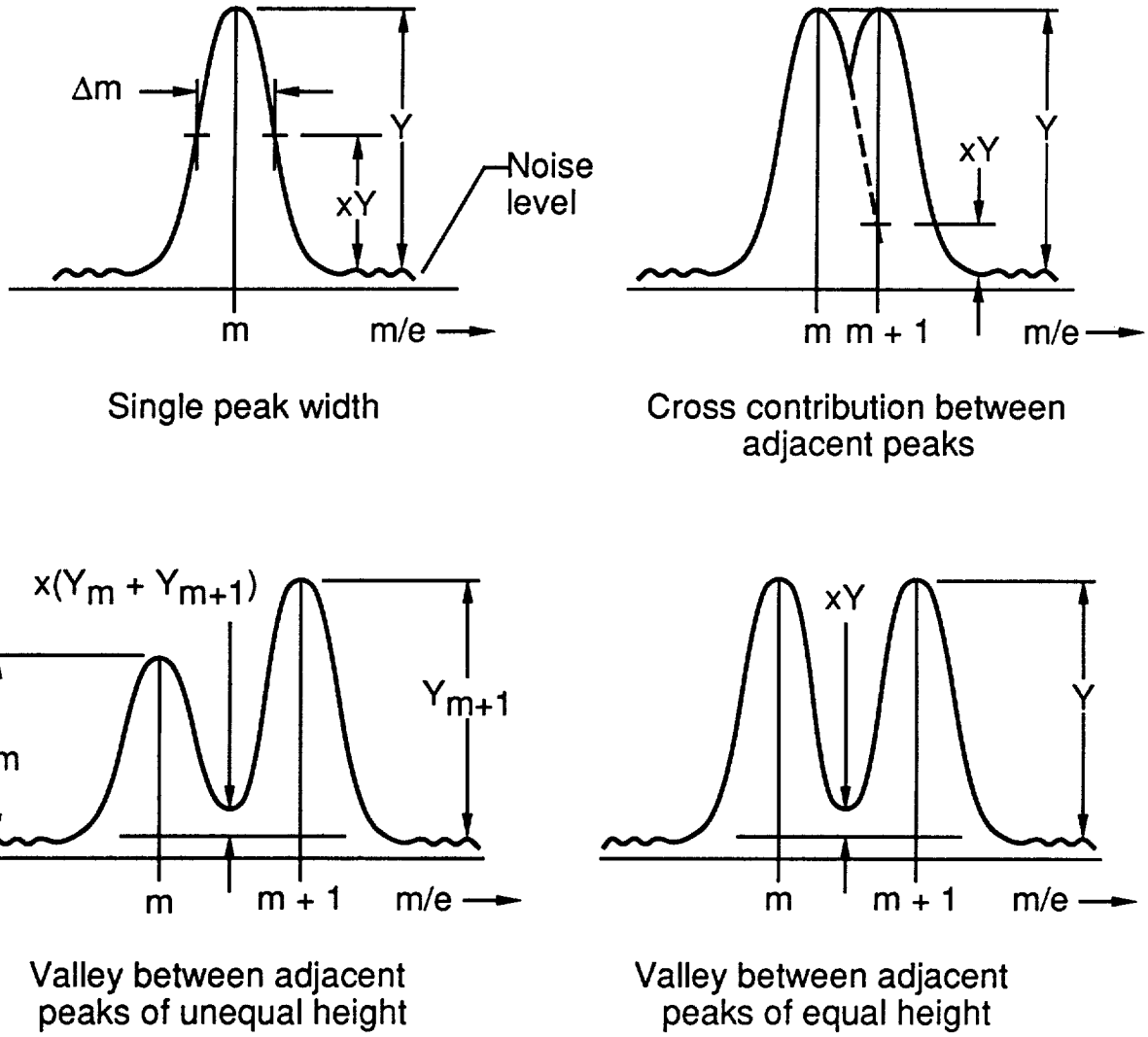

Figure 57. Examples of resolution measurement. x is a multiplicative factor.

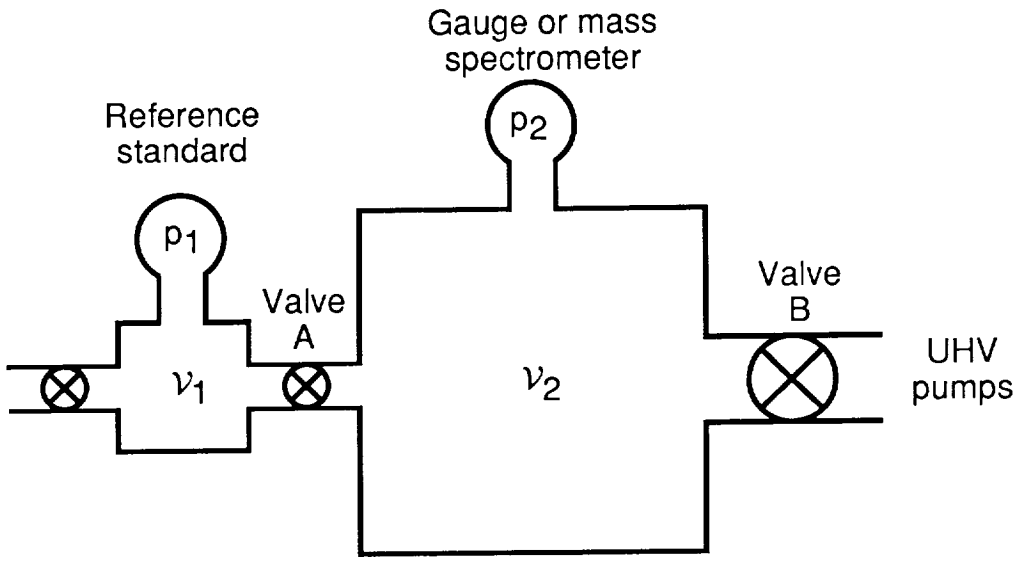

(a) Volume expansion.

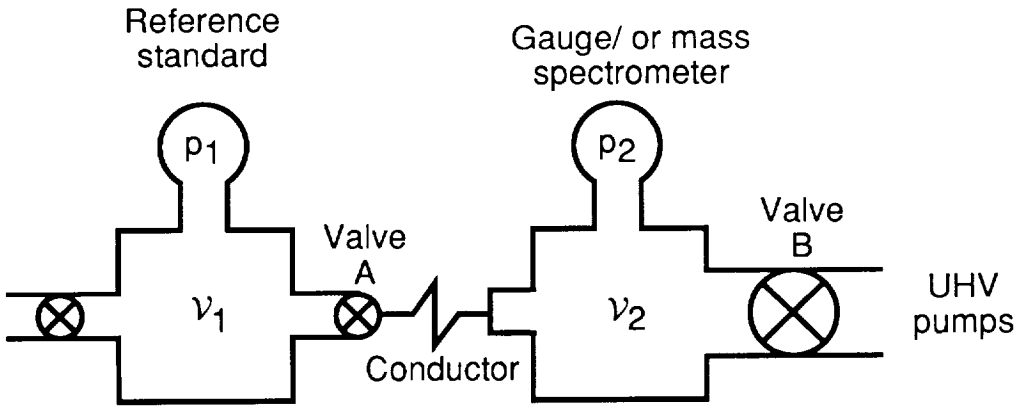

(b) Rate of rise.

Figure 58. Calibration methods.

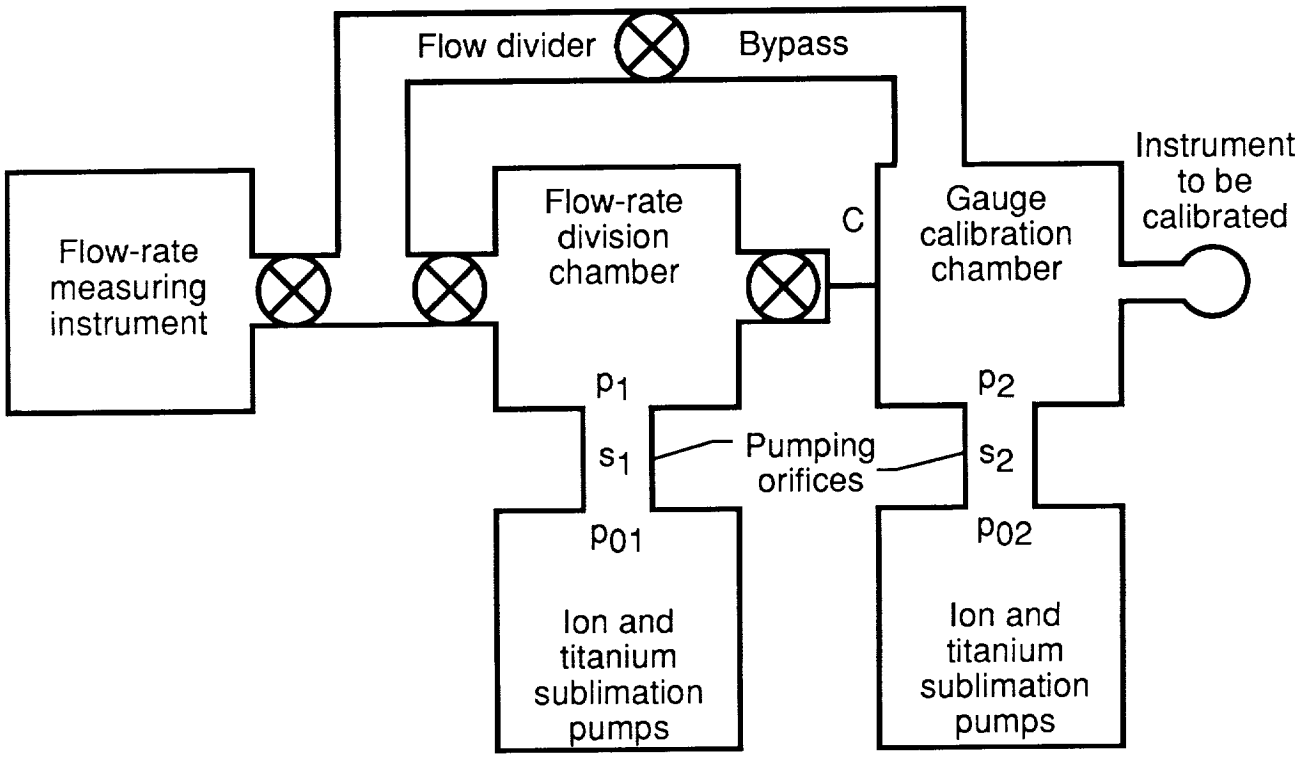

(c) Orifice flow.

Figure 58. Concluded.

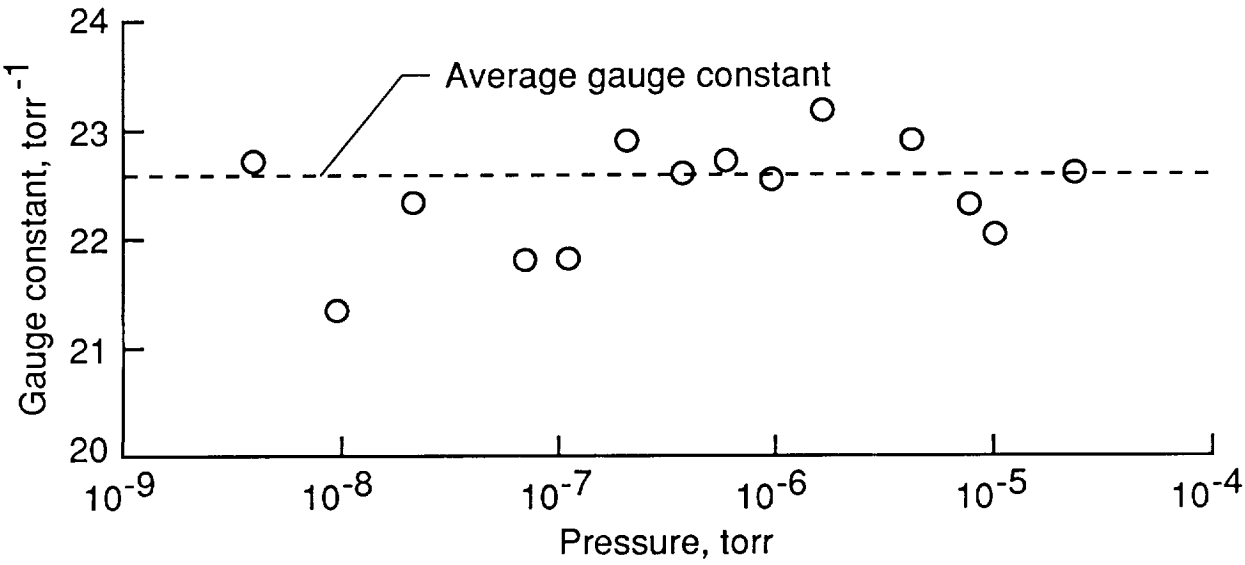

Figure 59. Calibration of nude Bayard-Alpert gauge. Emission current = 4.0 mA; Grid voltage = 135 V; Collector voltage = 45 V; N_2 calibration gas.

NASA
National Aeronautics and Space Administration

Report Documentation Page

1. Report No.	2. Government Accession No.	3. Recipient's Catalog No.
NASA RP-1219		

4. Title and Subtitle	5. Report Date
Introduction to Total- and Partial-Pressure Measurements in Vacuum Systems	November 1989
	6. Performing Organization Code
7. Author(s)	8. Performing Organization Report No.
R. A. Outlaw and F. A. Kern	L-16494
9. Performing Organization Name and Address	10. Work Unit No.
NASA Langley Research Center Hampton, VA 23665-5225	307-51-08-04
	11. Contract or Grant No.
12. Sponsoring Agency Name and Address	13. Type of Report and Period Covered
National Aeronautics and Space Administration Washington, DC 20546-0001	Reference Publication
	14. Sponsoring Agency Code

15. Supplementary Notes

16. Abstract

An introduction to the fundamentals of total- and partial-pressure measurement in the vacuum regime (760 to 10^{-16} torr (10^5 to 1.33×10^{-14} Pa)) is presented. The instruments most often used in scientific fields that require vacuum measurement are discussed, and special emphasis is placed on ionization-type gauges and quadrupole mass spectrometers. Some attention is also given to potential errors in measurement and to calibration techniques.

17. Key Words (Suggested by Authors(s))	18. Distribution Statement
Vacuum technology Pressure measurement Mass spectrometer	Unclassified– Unlimited Subject Category 35

19. Security Classif. (of this report)	20. Security Classif. (of this page)	21. No. of Pages	22. Price
Unclassified	Unclassified	72	A04

NASA FORM 1626 OCT 86

NASA-Langley, 1989

For sale by the National Technical Information Service, Springfield, Virginia 22161-2171